Regulation of cellular dormancy in disseminated breast cancer cells

Dissertation

zur Erlangung des Doktorgrades der Naturwissenschaften (Dr. rer. nat.)
der Fakultät für Biologie und Vorklinische Medizin der
Universität Regensburg

vorgelegt von

Ana Grujovic

aus Kragujevac, Serbien

2019

Das Promotionsgesuch wurde eingereicht am

29.04.2019

Die Arbeit wurde angeleitet von

Herr Prof. Dr. Christoph A. Klein

Untershrift:

Table of Contents

1 Introduction

1.1 Mammary gland development and cellular organization

Mammary gland is a very specific organ which distinguishes mammals from all other animals due to unique anatomical structure that enables production and secretion of the milk for the nourishment of the offspring. Adult human breast consists of the parenchyma, which originates from the ectoderm and the stroma, which develops from mesodermal elements (Figure 1). The parenchyma is a system of branching ducts and acini, while the stroma mainly consists of adipose tissue (Forsyth, 1991; Javed and Lteif, 2013; Medina, 1996). The mammary gland reaches its final development late after birth, during pregnancy (Inman et al., 2015; Macias and Hinck, 2012) which facilitates studying its developmental process. Most of the knowledge about embryonal development of the mammary gland arises from studies in rodents.

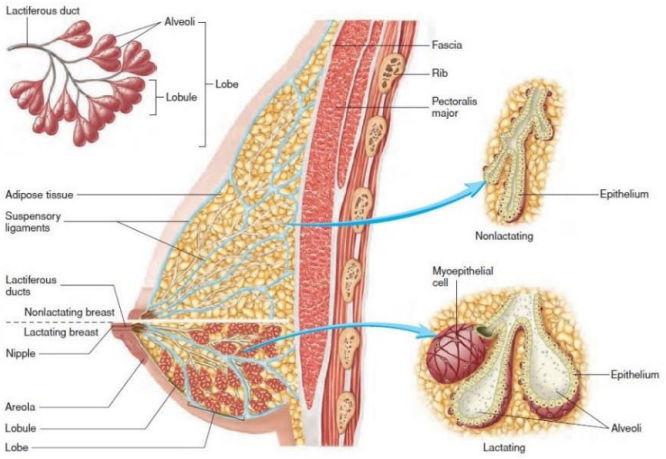

Figure 1: Anatomy of the human mammary gland. Each lactiferous duct in the mammary gland starts from the nipple and branches into ducts that end with the acini (in a non-lactating breast) or alveoli (in a lactating breast). Therefore the alveoli in a lactating breast occupy more space than in a non-lactating one, on the cost of adipose stromal tissue. Picture modified from https://theanatomybody.com/mammary-gland-anatomy/

The stadium of the embryonal development comprises of two phases: (1) formation of the primary mammary bud and (2) development of a rudimentary mammary gland (Hughes, 1950; Inman et al., 2015). Once the mammary sprout reaches the fat pad, its further sprouting is initiated to form a rudimentary ductal tree. The ductal tree consists of epithelial and myoepithelial cells forming 15-20 secondary branches, each containing a lactiferous duct which finally leads to a nipple and enables collection and directing of the milk stream. At the time of birth, the nipple is formed from epidermal cells overlying the bud, while the rudimentary ductal tree protrudes into the surrounding fat pad. (Hens and Wysolmerski, 2005; Hogg et al., 1983; Macias and Hinck, 2012; Sakakura et al., 1976).

In the period from birth until the age of two, not many changes occur, mostly maturation of the ducts and sprouting of the vasculature. From the third year until puberty, the mammary gland remains quiescent and its development continues with the beginning of sex hormone secretion (Anbazhagan et al., 1991; Naccarato et al., 2000). Under their influence, extensive proliferation occurs which results in filling the fat pad and formation of mammary lobes. The mammary lobe comprises of the mammary

ducts which end with the terminal end buds (TEB) (Hinck and Silberstein, 2005; Macias and Hinck, 2012; Paine and Lewis, 2017). Cap cells of the TEBs differentiate into myoepithelial cells, forming the outer layer, and the inner layer consist of the luminal cells (Williams and Daniel, 1983). During puberty, before pregnancy, the ends of the mammary tree are blind-ended ducts, called acini (Howard and Gusterson, 2000). These acini protrude in the fat pad, and consist of predominantly adipocytes, but also endothelial cells (which form a vascular net), fibroblasts and immune cells (Macias and Hinck, 2012; Sheffield, 1988). At the time of puberty, estrogen secretion starts and together with the pituitary growth hormone and insulin-like growth factor-1 (IGF-1) initiates further events in the mammary gland development (Kleinberg and Ruan, 2008). Those processes involve formation of the breast bud with elevation of the nipple and enlargement of the diameter of the areola around the nipple (Marshall and Tanner, 1969). Constant increase in the size of the mammary gland during puberty is a result of changes in both, parenchymal and stromal tissue (Howard and Gusterson, 2000), with first preparation of the surrounding fibrous and fatty tissue which then enables further elongation and sprouting of the parenchymal mammary ducts (Howard and Gusterson, 2000; Russo and Russo, 2004)

Intensive growth and changing during puberty results in formation of the final structure of a double layered ducto-alveolar net in mammary parenchyma. The outer layer of cells consists of myoepithelial cells, responsible for the contraction and the guidance of milk that is produced by alveolar cells from inner layer. The alveolar cells form the inner layer together with luminal cells, lining the lumen of ducts and alveoli (Tiede and Kang, 2011; Watson and Khaled, 2008). During each menstrual cycle, upon a complex effect of hormones, the number and size of the alveoli increase, while significant increase is only seen when pregnancy occurs (Monaghan et al., 1990; Russo and Russo, 2004). All these processes are dictated mainly by the female sex hormones secreted by the ovaries, such as estrogen (inducing ductal elongation) and progesterone (responsible for side branching) (Brisken et al., 1998). Mammary ducts are branching to smaller ducts and further to very small ductuli ending with acini. All the acini arising from one terminal duct together with the surrounding stroma form the functional unit of the breast called the terminal duct lobular unit (TDLU) (Howard and Gusterson, 2000; Javed and Lteif, 2013). Again, most information about mammary growth during pregnancy and involution came from studies in mice. During pregnancy numerous changes occur in the mammary gland under the influence of progesterone and prolactin. Intensive branching of secondary and tertiary ducts is followed by alveolar development, when epithelial cells forming alveolar buds start proliferating and differentiating into milk-secreting lobules. The growth of mammary ducts and alveoli continues on a cost of stromal adipose tissue, which is reduced and disappears. Simultaneously the vascular net is branching and by late pregnancy every functional alveolus is surrounded by a capillary network (Baillo et al., 2011). A functionally mature gland is then fully developed and prepared for milk production and secretion.

The involution process starts with the weaning. At the weaning phase the produced milk is retained in the mammary epithelium, the branched mammary tree is removed and milk-producing epithelial cells

are disappearing. This process starts with a reversible phase of alveolar cells detachment, their accumulation in the lumen and apoptosis inducing engorgement of the alveoli. After this phase, the alveoli start to collapse, and milk supply is lost. As of that moment involution becomes an irreversible process. In this phase, tissue remodeling is most prominent while activation of matrix metalloproteinases (MMP) induces degradation of extracellular matrix (ECM) and an intensive apoptotic wave in mammary epithelial cells. As a result, the mammary gland is anatomically very similar to the original mammary gland before pregnancy, but interestingly the pattern of gene expression differs (Balogh et al., 2006; D'Cruz et al., 2002). The mammary development processes with all described phases is depicted in the Figure 2.

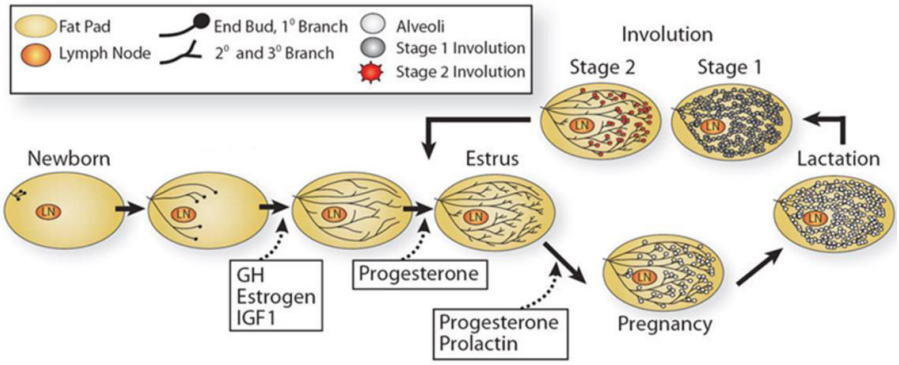

Figure 2: The stages of postnatal mammary gland development. At birth, the mammary epithelium is rudimentary, consisting of only a few small ducts. At the onset of puberty, expansive growth that fills the fat pad with the epithelial mammary tree happens. This growth is influenced by the growth hormones (GH), estrogen, and insulin-like growth factor-1 (IGF1). When pregnancy begins, sprouting and further branching of the existing branches continues and alveologenesis occurs under the influence of progesterone and prolactin. Prolactin stimulation continues during the stage of lactogenesis, culminating in milk production that continues until involution, the process of mammary gland remodeling back to its original adult state before pregnancy. Picture modified from (Macias and Hinck, 2012).

1.2 Stem cell hierarchy during mammary gland development

All the changes that the mammary gland undergoes during maturation and during the described cyclic differentiation process, are based on the function of undifferentiated stem cells (Stingl et al., 2006). In a first step division and differentiation of the mammary stem cells give rise to self-renewed stem cells and mammary progenitor cells. These progenitor cells continue to divide and further differentiate into matured mammary cells, while self-renewed stem cells persist and wait for another activation signal to divide again. Hence, in the parenchyma of the mammary gland, among undifferentiated stem and differentiated mature cells also progenitors reside, which are in between these two populations in regard of their differentiation status.

Early gland development is based on the expansion of the bipotent fetal mammary stem cells (fMaSCs) (Spike et al., 2012). Repeated cycles of expansion and involution of mammary glands during menstrual cycles and pregnancies clearly indicate the existence of the adult counterparts to fMaSC that are able to

expand and give the progeny of different lineages. These cells named adult mammary stem cells (aMaSCs) are much less abundant than fMaSC, with 1/50 and 1/14 cells in corresponding tissues respectively (Spike et al., 2012). These cells are slow cycling cells waiting for internal and external signals to activate them, renew and give the progeny instructions to develop all the changes in the adult gland (Guo, 2014; Pasic et al., 2011; Zeng and Nusse, 2010). A hierarchy of mammary cells is maintained in the adult mammary gland which, beside stem cells comprise of progenitors and differentiated mammary cells.

Thus, the mammary gland is a hierarchically structured organ (Stingl et al., 2006). The proof of pluripotency of adult mammary stem cells (MaSC) was provided in the work of Shakelton and colleagues who succeeded to reconstitute the whole mouse mammary gland upon transplantation of a single cell (Shackleton et al., 2006). Transplantation of pieces of a human mammary gland resulted in engraftment and mammary gland reconstitution in immunodeficient mice (Kuperwasser et al., 2004). All different processes during mammary gland development are strictly controlled by growth factors and hormones and disruption of that signaling composition can lead to increased growth of the mammary gland and breast cancer (Martin, 2003). In line with the evidence that changes in the mammary gland are driven by growth and division of mammary stem cells, a corresponding subpopulation of mammary cancer stem cells (MaCSC) are believed to initiate breast cancer (Luo et al., 2015; Morrison et al., 2008).

In line with the stem cell theory that proposes that all cells in the mammary gland originate from a small proportion of stem cells, cancer stem cell theory proposes that among all cancer cell pool only a few of them act as so-called cancer stem cells (CSC), which reproduce themselves and sustain the cancer, much like normal stem cells renew and sustain organs and tissues (Yoo and Hatfield, 2008). New data, showing that the majority of malignant cells, rather than only CSCs can sustain tumors questions the stem cell theory, emphasizing it must be reevaluated. (Yoo and Hatfield, 2008). In accordance with previously stated, albeit still under controversy, nowadays both stem and progenitor cells are candidate cells-of-origin in tumorigenesis (Chen et al., 2017). Besides the theories that aberrations in less differentiated (stem and progenitors) cells cause cancer, some clues indicate that also differentiated cells, which sustain neoplastic transformation can acquire properties of less differentiated stem or progenitors and become the founders of malignancies (Bjerkvig et al., 2005). Cancer cells that leave the primary site and home to distant organs can i) undergo cell death; ii) proliferate and give rise to metastasis or iii) lodge and stay quiescent for a certain period (Aguirre-Ghiso, 2007; Goss and Chambers, 2010; Reymond et al., 2013). Such outcome we exactly see in our stem cell model where majority of cells undergo anoikis, few of them start immediate proliferation and give rise to mammospheres and rest stay quiescent but retain the potential to be reactivated. Some data show that all the cells that extravasate to distant organs first undergo the same state of dormancy (Paez et al., 2012) or proliferation (Wang et al., 2015a). The nature of the cells that acquire the ability to disseminate

from the primary tumor is still under investigation. It is also unknown which population in the hierarchy of mammary epithelial cells is capable to leave the primary site and lodge to distant organs.

Cellular heterogeneity and hierarchical organization present in the mammary gland are also found within mammary tumors (Bliss et al., 2018; Hassiotou et al., 2013). In line with MaSCs, MaCSCs are less differentiated cells in the cell hierarchy of mammary tumors, able to give rise to more differentiated progeny, like non-cancer stem cells (non-CSCs). Although they are not numerous, CSCs exert a very important and potent function in breast tumors. CSCs possess the features of both cancer cells and stem cells, hence they have the ability to seed tumors when transplanted into an animal host (Clarke et al., 2006). They also possess the capacity for self-renewal and the ability to differentiate into diverse specialized cell types. A pool of undifferentiated multipotent stem cells is maintained through the self-renewal process (Yu et al., 2012). Analysis of the gene expression profiles of different cell populations isolated from the mammary gland based on the expression of surface markers revealed similarities to specific subtypes of breast cancer, with CSCs being closest to claudin-low breast cancer, progenitors to basal-like breast cancer, and luminal A and luminal B showing most similarities to differentiated mammary cells (Figure 3) (da Silveira et al., 2017). The frequency of detected tumors of a certain type increases in the direction from less to more differentiated cells, but the aggressiveness of the tumors is inversely correlated (Figure 3) (da Silveira et al., 2017).

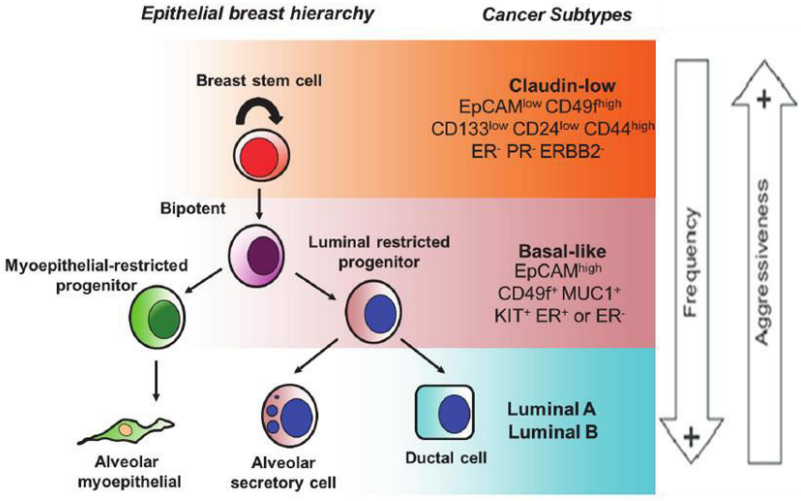

Figure 3: Connection between stem cell hierarchy and breast cancer subtypes. The mammary stem cell (MaSC) may give rise to a "committed progenitor", which further differentiates into luminal and myoepithelial cells. MaSC profile corresponds to most aggressive claudin-low (triple-negative) breast cancer. Less aggressive basal-like breast cancers have profiles most similar to progenitor cells, while luminal breast cancers result from more differentiated cells. BC – breast cancer. Picture adapted from (da Silveira et al., 2017).

1.3 Breast cancer

Breast cancer is the most frequent type of cancer among women, with 2.09 million new cases and 627000 deaths in 2018 worldwide. In 2012 the number of newly diagnosed cases was 1.7 million and these numbers are constantly increasing (WHO, 2018). Breast cancer includes numerous cancer types, which are most frequently systematized using TNM (Tumor, Node, Metastasis) staging. Classification of the tumors depends on the size of the primary tumor (T), the number of the nearby lymph nodes positive for the presence of tumor cells (N), and presence of distant metastasis (M) (Roland et al., 2016). Besides TNM staging, the histological grade of the tumors is determined. Although histological grade does not correlate to the overall survival of the patients, it can generate important information related to the clinical behavior of breast cancers (Rakha et al., 2010). The result of the histological grading of the tumor is grade 1 to 3 and is determined as a result of the three variables: 1) the frequency of mitotic cells; 2) formation of the tubular gland structures, and 3) how closely tumor cells resemble normal breast cells (nuclear grade) (Elston and Ellis, 1991). Grade 1 tumors comprise of the small tubules and cords (for ductal cancer or lobular cancer, respectively) with slowly growing, well differentiated cells. These tumors give the best prognosis for the patient. Grade 2 tumors are moderately differentiated and based on all parameters lie in between tumors of grades 1 and 3. The worst prognosis have the patients with tumor grade 3, that is characterized with poorly differentiated cells that lack normal organization and grow rapidly, resulting in a faster spread than in tumors of lower grades (Rakha et al., 2010). In the last decades, a new approach was developed for breast cancer classification, based on the systemic investigation of expression patterns of thousands of genes using cDNA microarrays (Sorlie et al., 2001) in collectives of breast cancer samples, classified to following groups using immunohistological staining, with non-transformed mammary tissue as healthy controls. Hierarchical clustering separated the analyzed cohorts into two main branches, basal-like/estrogen receptor (ER)- and luminal/ER+ groups. ER- branch comprised of basal-like, Her2-like and normal breast-like mammary tumors, while ER+ cells comprised of several types of luminal-like tumors. Both, overall and relapse-free survival analysis showed a highly significant difference between ER- and ER+ groups, with the basal-like and Her2+ subtypes being associated with the shortest survival times (Sorlie et al., 2001; Sotiriou et al., 2003). So far, irrespective of the subtype, for the majority of the breast cancers the first line therapy is surgery followed by chemotherapy and radiation therapy, that kill the cancer cells that eventually were not seen and removed during surgery (Dhankhar et al., 2010). In some cases neoadjuvant therapy is given before the surgery to shrink tumor bulk and increase the feasibility of the conservation surgery treatments (Abbas et al., 2011; Reyal et al., 2018).

1.4 Metastasis

Despite the advances in diagnosis and treatment of the primary tumors (PT), no significant improvements were made during last decades in the field of metastatic disease. More than 90% of cancer related deaths are due to metastases which are resistant to conventional therapies (Fidler, 2003; Redig and McAllister, 2013; Weigelt et al., 2005). Although metastases are detected in only 6% of newly diagnosed patients, around 30% of women with breast cancer ultimately develop metastases, with bone being the most frequent metastatic organ (O'Shaughnessy, 2005; Redig and McAllister, 2013). This number did not significantly change in the last decades pointing towards the fact that this process still remains the least understood aspect of cancer biology.

Existing knowledge shows that the metastatic cascade is a highly demanding multistep process where failure in any step will result in a failure of metastasis establishment. Therefore, only a small fraction of cancer cells acquire the ability to migrate and home to distant organs, making this a very inefficient process (Chambers et al., 2002; Valastyan and Weinberg, 2011; Weiss, 1990). The metastatic cascade starts with local invasion of cells originating from the primary tumor into the surrounding host tissue (1), when tumor cells migrate through the extracellular matrix (ECM) and stromal cells they reach lymphatic and/or blood vessels and crawl through the endothelial cells to intravasate into the circulation (2) where they face to survive in “unfriendly” conditions (shear stress, immunoevasion, flow) (3) until they reach a distant organ where they get stuck in the small blood vessels (4) and then extravasate to the distant organ (5), into the unknown hostile environment where they need to survive (6) and start proliferation in order to colonize the target organ and successfully establish a foothold for the metastasis (7) (Figure 4) (Bill and Christofori, 2015; Scully et al., 2012; Valastyan and Weinberg, 2011).

During metastatic invasion tumor cell plasticity is challenged. Therefore, cancer cells constantly undergo changes enabling them to survive and exert their function. The concept of epithelial-mesenchymal transition (EMT) preceding migration, followed by mesenchymal-epithelial transition (MET) at the distant site, a process conditional for proliferation and colonization is widely accepted in the scientific community (Bill and Christofori, 2015; Hartwell et al., 2006; Jung et al., 2008; Mani et al., 2007).

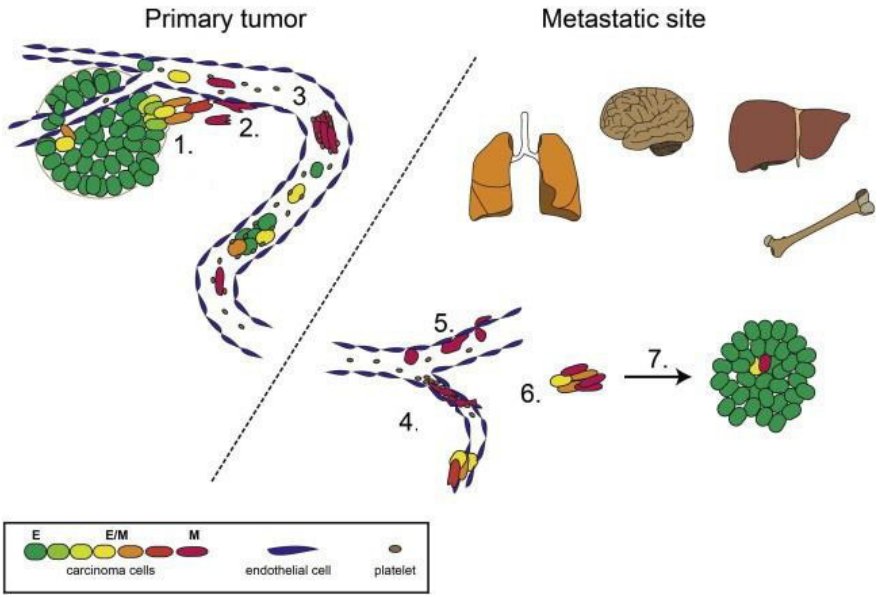

Figure 4: Metastatic cascade with involvement of EMT and MET. Tumor cells undergo EMT to acquire the potential to start local tissue invasion (1) and migration towards blood vessels. Upon intravasation into blood vessels (2) cells must survive (3) and arrive at target organs (4), where they are arrested in small capillary vessels mostly due to size and then they (5) extravasate. In the distant organs tumor cells must survive in a new type of environment. Therefore they need to adapt by reversing the phenotype in MET process (6), regains proliferating phenotype to establish micro- and macrometastases (7). Picture modified from (Bill and Christofori, 2015).

As previously mentioned, breast cancer metastasizes predominantly to bones, liver, lung and brain (Jin et al., 2018; Wang et al., 2017). This organotropism is not only seen in breast cancer (Lu and Kang, 2007), but also in other cancer entities such as colorectal, prostate, lung and prostate cancers (Jin et al., 2012; Milovanovic et al., 2017; Reichert et al., 2018; Thobe et al., 2011). Based on the knowledge acquired from the autopsies of 735 women with breast cancer, Stephen Paget proposed the "seed and soil" hypothesis claiming that tumor cells (the "seed") grew preferentially in the microenvironment of selected organs (the "soil"), and metastases can grow only when appropriate seed is planted in the corresponding soil (Paget, 1989). The basis for "seed and soil" mechanism is chemical attraction between cancer cells and factors expressed in metastatic organ. Several factors were identified to play a role, including osteopontin, osteonectin, chemokine ligand 21 (CCL21, 6Ckine) and stromal-derived factor-1 (SDF-1, CXCL12) expressed in bones (Ibrahim et al., 2000; Jacob et al., 1999; Luker and Luker, 2006; Muller et al., 2001). These chemokines are ligands for the receptors expressed on the breast cancer cells, such as C-C chemokine receptor type 4 (CXCR4, binds CXCL12) or C-C chemokine receptor type 7 (CXCR7, binds CCL21) (Luker and Luker, 2006; Mattern et al., 1996; Muller et al., 2001; Qian et al., 2018). An opposing theory was proposed by Ewing, who claimed that organ tropism is a consequence of the mechanical arrest of cancer cells in small capillaries (Chu and Allan, 2012). Nowadays it is commonly understood that these two theories are not mutually exclusive and both factors contribute to the organ specificity of metastases (Chu and Allan, 2012; Weiss, 1992).

1.5 Disseminated cancer cells

During migration through the circulatory system (lymph or blood) cancer cells are referred to as circulating cancer cells (CCC) while upon extravasation and lodging to distant organs they are termed disseminated cancer cells (DCC). DCCs in mesenchymal organs such as the bone marrow or lymph nodes are detected upon using cytokeratin (CK8, CK18, and CK19, expressed only in epithelial cells) staining as a marker for DCCs. 30% of breast cancer patients are found positive for DCCs in the bone marrow (Braun et al., 2005). DCC presence in the bone marrow aspirates of patients with cancer both, breast and prostate, is a risk factor for developing metastases (Janni et al., 2011; Mathiesen et al., 2012; Wiedswang et al., 2003). Furthermore, DCC persistence in the BM of patients diagnosed with breast cancer correlates to the decreased disease-free survival (DFS) and overall survival (OS) during the first 5 years following cancer diagnosis. (Janni et al., 2011). DCCs isolated using anti-CK staining can be used only for genomic studies, while these cells must be permeabilized prior to detection procedure and therefore the whole transcriptome is lost. Genomic analyses result in information which are insufficient in the battle against cancer as it is known that not only genetic changes, but also dysregulated gene expression contribute to the neoplastic transformation (Ferrone and Marincola, 1995; Timp and Feinberg, 2013). Therefore, epithelial cell adhesion/activating molecule (EpCAM, CD326), expressed on the surface of the cells, was introduced as a marker that enables isolation of living tumor cells. EpCAM is overexpressed in many different human carcinomas (Baeuerle and Gires, 2007; Kimura et al., 2007; Massoner et al., 2014; Osta et al., 2004; Spizzo et al., 2004; Stoecklein et al., 2006; Went et al., 2006) and it was the first human tumor-associated antigen identified with monoclonal antibodies (Herlyn et al., 1979). Cell isolation using anti-EpCAM staining enables simultaneous isolation of both genome and transcriptome of the same cell (Klein et al., 2002) and therefore a much broader spectrum of analyses.

For a long time it was accepted that cancer cell dissemination occurs in later stages of tumor development (Koscielny et al., 1984), but the evidence from previous years strongly challenges that theory, pointing to dissemination as a process that occurs early during tumor development (Klein, 2009). Studies performed on mouse models in melanoma (Eyles et al., 2010) and breast cancer (Hosseini et al., 2016b; Husemann et al., 2008) strongly support the hypothesis on early dissemination of cancer cells and parallel progression of primary tumors and metastases. The proposed model of parallel progression (Klein, 2009) suggests that cancer cells disseminate early, as supported by evidence from melanoma, where it was shown that lymphatic dissemination occurs shortly after dermal invasion of the primary lesion at a median thickness of ~0.5 mm, a phase when the primary tumor is undetectable by standard screening techniques (Werner-Klein et al., 2018). In the early phases of tumor development, cancer cells harbor fewer genetic aberrations compared to primary tumor cells at the time of diagnosis, which in the context of early dissemination is explained by two possible scenarios: (1) DCCs harbor

fewer aberrations than cells from PT, indicating that DCCs progress and evolve slower or (2) DCCs harbor the same number or more aberrations than cells from the PT, indicating that DCCs progress and evolve faster than PT cells and therefore metastases arise quickly. Analyses of the DCCs from BM aspirates of breast cancer patients show that DCCs are less aberrant than PT cells and even share very few aberrations with them (Schmidt-Kittler et al., 2003), additionally supporting the first scenario and the theory of parallel evolution of tumor cells at the primary site and the metastatic organs. Although dissemination is an undeniable process in tumor biology, the relevance of early DCCs in establishment of metastases was questioned. Using the rodent models Eyles (melanoma) and Hosseini (breast cancer) with colleagues showed that metastases in both, melanoma and breast cancer evolve from early DCCs (Eyles et al., 2010; Hosseini et al., 2016b).

1.6 Dormancy of disseminated cancer cells

Initial steps of the metastatic cascade, such as invasion and dissemination are very efficient processes (Chambers et al., 2002) but compared to that, metastasis formation rate is very inefficient. This indicates that the critical step for metastasis formation is colonization of the metastatic organ. Upon extravasation to distant organs DCCs can die, resume the growth immediately or enter a state of dormancy (Aguirre-Ghiso, 2007; Chambers et al., 2002; Ranganathan et al., 2006). The relevance of the state of dormancy of DCCs was intensively studied in the last decades.

Eyles and colleagues showed that single cells spread very early during oncogenesis of melanoma, 3 weeks after the clinical onset of the primary tumor, but detectable metastases became apparent much later in life, up to 1.5 years (Eyles et al., 2010), suggesting that these early DCCs remained dormant for a long period. In line with that BM-DCCs in Balb-NeuT mice do not proliferate but can be reactivated upon transplantation into lethally irradiated siblings, showing that they retain the potential to proliferate, but reside in a dormant state (Hosseini et al., 2016b; Husemann et al., 2008). This is not only the case in rodent animal models. Existence of dormant DCCs in humans was shown in the case of a patient that was treated for melanoma and died 16 years later due to brain death without any signs of secondary disease or detectable metastases. This patient was used as a kidney donor and 2 years after transplantation both recipients died from metastases of malignant melanoma, although they were never diagnosed with melanoma. Thus, even though the donor had no signs of clinical disease, melanoma cells survived and were transferred with the graft to the recipients. Since such patients are under immunosuppression therapy to avoid graft rejection, the condition of impaired immunosurveillance was favorable for the vigorous growth of metastases (MacKie et al., 2003). Such cases support the concept of dormancy in disseminated cells. Long latency periods observed between the treatment of primary tumors and metastatic recurrence in patients are also used as a proof for the existence of clinical tumor dormancy (Klein, 2011).

The fate of DCCs upon extravasation depends on both intrinsic and extrinsic signals (Bloom and Zaman, 2014). Prolonged period of dormancy is induced and maintained by different mechanisms, including tumor-microenvironmental factors (such as cytokines, immunosurveillance, angiogenesis), metastasis suppressor gene activity and anti-cancer therapy (Osisami and Keller, 2013). We can discriminate two main types of tumor dormancy: (1) dormancy of single cancer cell, when cells reside in a proliferation arrested state (G0/G1 arrest) that is reversible and they can re-enter the cell cycle (reactivate proliferation) and (2) tumor mass dormancy, a phenomenon when cells do not undergo cell cycle arrest, but the rate of cell proliferation correlates to the rate of apoptosis, resulting in maintainability of the size of metastases (Kareva, 2016). This second type, tumor mass dormancy, is often a result of systemic cooperation among tumor cells and the immune system (Koebel et al., 2007; Quesnel, 2008; Vesely et al., 2011). On the contrary, different mechanisms are suspected to regulate the dormant state of a single cancer cell. For example microenvironmental stress (Adam et al., 2009a; Aguirre-Ghiso et al., 2003), cytokines and other factors secreted by stromal cells (Kobayashi et al., 2011; Lim et al., 2011; Shiozawa et al., 2010). Further, the inability of DCCs to form cytoskeletal rearrangements and interact with environmental cells (Barkan et al., 2008), but also factors like anti-tumor therapy (Chaterjee and van Golen, 2011; Schewe and Aguirre-Ghiso, 2008) can result in single DCC dormancy. The existence of different types of tumor dormancy makes the concept of metastatic dormancy even more complex, since all of the above mentioned mechanisms can be employed in maintaining the dormancy of DCCs at distant sites, but there is also the contribution of the foreign environment.

1.7 Interleukin-6 signaling in physiological and pathological settings

Interleukin 6 (IL-6) is a proinflammatory cytokine that is known to be secreted by several different types of cells. In humans it is encoded by the *IL6* gene, located on chromosome 7. It belongs to a family of cytokines consisting of IL-6, IL-11, oncostatin M (OSM), leukemia inhibitory factor (LIF), ciliary neurotrophic factor (CNTF), cardiotrophin 1 (CT-1), cardiotrophin-like cytokine (CLC) and IL-27. Its main function is to mediate immune response, when secreted by T cells and macrophages, and to direct B cell differentiation. It is also known to be secreted by osteoblasts, and has a role in stimulating osteoclast maturation (Dienz et al., 2009; Eto et al., 2011; Udagawa et al., 1995; Yang et al., 2016). Nowadays it is known that IL-6 has many different functions and plays a role in numerous inflammation related diseases (Schaper and Rose-John, 2015; Tanaka and Kishimoto, 2014; Tanaka et al., 2014).

IL-6 acts by binding to the glycoprotein 130 (gp130) and can signal via two distinct pathways. The classical IL-6 signaling is mediated by direct binding of IL-6 to the heterodimeric receptor consisting of the IL-6 receptor α-chain, CD126 (gp80, IL-6Rα, IL-6Ra) and the ubiquitously expressed signal transducing receptor subunit glycoprotein 130 (gp130, IL-6Rβ) (Scheller et al., 2011) (Figure 5). Due

to the restricted expression of IL-6R to mainly hepatocytes and immune cells (Scheller et al., 2011), classical IL-6 signaling is limited to only few cell types. However, a soluble form of IL-6R (sIL-6R) can be produced by alternative splicing or limited proteolysis of the membrane-bound receptor. The complex of sIL-6R/IL-6 can bind to the ubiquitously expressed gp130 receptor subunit on recipient cells and thereby stimulate cells which do not express IL-6R (Rose-John and Heinrich, 1994). This type of stimulation, not mediated by a membrane receptor is referred to as trans-signaling. The binding of IL-6/IL-6R or IL-6/sIL-6R to the gp130 signaling subunit induces the homodimerization of gp130 which further triggers an intracellular signaling cascade activating several pathways including Ras/Raf, mitogen-activated protein kinase (MAPK), PI3K/Akt and Janus-activated kinase/signal transducers and activators of transcription (JAK/STAT) (Kishimoto, 2005; Murray, 2007; Streetz et al., 2003; Wegiel et al., 2008).

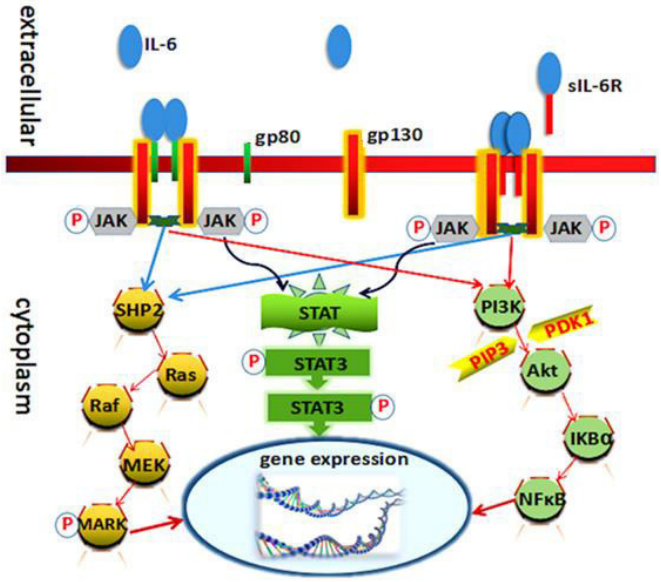

Figure 5: IL-6 signaling mechanism: IL-6 binds to the heterodimer receptor on the cell membrane, consisting of gp80 (carrying binding site for IL-6) and gp130 (IL-6Rβ), which then homodimerizes and activates JAK/STAT, MAPK/ERK and PI3K/Akt signaling cascades (classical signaling). In the trans-signaling pathway, sIL-6R, a soluble variant of IL-6Rα present in the intercellular space, binds IL-6. The complex IL-6/sIL-6R then binds to ubiquitously expressed gp130 and activates cells that do not express IL6R. Image taken from (Luo and Zheng, 2016).

In recent years the role of IL-6 was studied in different cancers. It was shown that IL-6 levels were increased in the sera of the patients with breast cancer, and this increase correlated with tumor stage and decreased patient survival (Bachelot et al., 2003; Kozlowski et al., 2003). Additionally, IL-6 plays a role in the biology of cancer stem cells in the mammary gland and breast tumors (Marotta et al., 2011; Sansone et al., 2007). IL-6 and the activation of an inflammatory feedback-loop have been shown to dynamically regulate the equilibrium between cancer cells with stem-like properties and non-stem cancer cells (Marotta et al., 2011) (Sansone et al., 2007). Studies on different cancer entities pointed to a role of IL-6 signaling in development of primary tumor, but also indicated they facilitate the formation

of metastasis, by supporting migration and invasion of cancer cells (Browning et al., 2018; He et al., 2018; Lee et al., 2019; Tang et al., 2018).

However, the effect of IL-6 signaling on non-transformed mammary tissue, as well as on putative metastasis founder cells (DCCs) has not been fully elucidated. To further investigate the role of this cytokine on mammary cells in physiological conditions, we used the non-transformed human breast cancer cell line, MCF10A and patient derived human mammary epithelial cells (HMECs). Additionally, we examined the IL-6 signaling in DCCs isolated from the bone marrow of the patients with mammary carcinomas.

2 Material and Methods

2.1 Methods

2.1.1 Patient material

Human non-cancerous mammary tissue was obtained from female patients undergoing reduction mammoplasty surgeries at Caritas-Krankenhaus St. Josef, Regensburg in collaboration with Dr. Norbert Heine after informed, written consent of patients was obtained (ethics vote number 07/043, ethics committee of the University Regensburg). After verification of the non-cancerous origin of the tissue by a pathologist at the Institute of Pathology, University hospital Regensburg, mammary glands were dissociated and primary human mammary epithelial cells (HMECs) isolated. The tissues showing the signs of breast cancer were excluded from the study and not used for this work. Due to hormone changes during menopause and proposed hormonal influence in mammary stem and progenitor cells, tissue were selected based on an arbitrary age limit (45 years).

Disseminated cancer cells were obtained from bone marrow aspirates of breast cancer patients with and without distant metastases. Human mesenchymal stem cells were obtained from bone marrow aspirates of breast cancer patients or healthy donors. Written informed consent of patients was obtained and the ethics committee of the University of Regensburg (ethics vote number 07/79) approved bone marrow sampling and analysis of isolated cells.

2.1.1.1 Digestion of the human mammary tissue and isolation of single epithelial cells

Mammary tissue was minced and dissociated in Ham's F12/Dulbecco's modified Eagle's medium [F12:DMEM; 1:1 (v:v)] supplemented with 10 mM HEPES, 2% bovine serum albumin (BSA; Fraction V), 5 µg/ml insulin, 0,5 µg/ml hydrocortisone, 10 ng/ml cholera toxin, 300 U/ml collagenase and 100 U/ml hyaluronidase in the sterile incubator at 37°C, 5% CO_2 and 7% O_2 for minimum of 18 h. On the next day, the digested cell suspension was centrifuged at 210 g for 2 minutes at room temperature. Supernatant from the first centrifugation step contained single mammary epithelial and stromal cells (fibroblasts), while in the pellet were the organoids (undigested tissue pieces of the tissue). Supernatant containing epithelial cells and fibroblasts was further centrifuged 4 minutes at 350xg to separate epithelial cell from fibroblasts. Supernatant containing fibroblasts was discarded and pellet (containing epithelial cells) was re-suspended in the basal medium, washed, and filtered through 100 µm and 40 µm cell strainers consecutively. Mammary epithelial cells were propagated in mammosphere medium in ultra-low attachment plates. For the propagation cells were seeded in density of 200.000 cells/ml,

and for the experiments where we assessed the numbers of the mammospheres cells were seeded in density of 50.000 cells/ml in 35 mm plates with 3 ml medium per plate.

For the disaggregation of the mammospheres they were collected after 7 days and centrifuged 1 minute at 100xg. Supernatant containing single cells transferred to another 50 ml falcon tube and centrifuged 5 minutes 500xg to collect quiescent single cells (QSC). Mammospheres were subjected to the mechanical/enzymatic digestion using 0,05% trypsin, 0,53 mM EDTA-4Na and 10 minutes of constant pipetting using Gilson 1 ml pipette. Trypsinization was inhibited by adding Trypsin neutralizing solution (TNS) and cells were washed and re-plated for growing second generation of mammospheres. In the first generation of mammospheres can be found some stromal cells, but they succumb anoikis and the second mammosphere generation is “pure” and contains only mammary epithelial cells. The obtained secondary mammosphere were used for the most of the downstream assays elaborated in this work.

2.1.2 Animals

2.1.2.1 Maintenance

NOD.Cg-Prkdcscid IL2rgtmWjl/Sz (also termed NSG) or Balb/c mice were purchased from the Jackson Laboratory USA and maintained under specific-pathogen free conditions, with acidified water and food ad libitum in the research animal facilities of the University of Regensburg, Germany. Transgenic mouse model (Balb-NeuT) was obtained from Dr. Guido Forni. Maintenance in the animal facility was performed according to the European Union guidelines. All animal experiments followed EU and national institutional regulations (Government of Upper Palatinate, 55.2-2532.1-27/14). At the age of 4 weeks Balb-NeuT mice were analyzed for the presence of transgene. Female hemizygotes (neuT+/neuT-) were further cultivated and regularly inspected (twice a week) for the presence of mammary tumors, which were thereafter measured in two perpendicular diameters. Transgene negative (neuT-/neuT-) homozygotes served as wild-type Balb/c controls.

2.1.2.2 Mice dissection

Mice were sacrificed by cervical dislocation. The organs of interest (mammary glands, tumors and lungs) were divided in two parts each and one part was snap frozen while the other was embedded in paraffin. Bone marrow was prepared as described in the following section.

2.1.2.3 Paraffin embedding of tissue samples

The dissected tissue samples were fixed in a 4% paraformaldehyde (PFA) solution for minimum 12 hours. Following fixation, the samples were washed 3 times in 1x PBS, dehydrated by series of washing steps in alcohol (70%, 85% and 100% ethanol, each step 1 hour) and washed twice for 30 min in 100% xylene. This step serves not only the removal of alcohol from the tissue, but also facilitates the

penetration of the paraffin during the subsequent embedding. After three incubation steps with paraffin (parablast embedding media), tissues were embedded. Paraffin embedded tissues are stored at room temperature. These samples have been used for IHC staining.

2.1.2.4 Isolation of the epithelial cells from mouse mammary gland

The mice were killed by cervical dislocation. Mammary glands were collected either from Balb/c or Balb-NeuT mice in a 50 ml tube with PBS. The tissue was minced with surgical blades to small pieces and digested in basal medium (DMEM/F12, 100 nM HEPES buffer, 10 mg/ml insulin, 0.5% BSA and 0.5x penicillin/streptomycin) with 0,1 mg/ml DNAse I 200 U/ml collagenase and 200 U/ml hyaluronidase. The tissue was digested for 1-1,5 hours at 37° C in the incubator and mixed after 20 minutes of incubation, then after 1 hour and every 10 minutes later until the organoids are disaggregated. The cell suspension originating from the digested tissue was filtered through 40 μm cell strainer and centrifuged 10 minutes at 300xg to isolate mammary epithelial cells.

2.1.2.5 Mammosphere transplantation

Before the transplantation of the GFP-labeled mammospheres (50 spheres per mouse, mammosphere generation described in paragraph 2.1.3.4) mice were anaesthetized using Midazolam 5mg/kg, Fentanyl 0,05mg/kg, Medetomidin 0,5mg/kg i.p. The skin around the mammary gland was shaved and small V-cut made around fourth left mammary gland and small pocket was made between the 4^{th} mammary gland and skin. Mammospheres were mixed with matrigel (final concentration of Matrigel 40%) and injected into the pocket between the mammary gland and skin of the 4-6 weeks old wt ($neuT^-$) and NSG mice. The skin was closed by a suture using polygelatin string and anesthesia was antagonized with Flumazenil 0,5mg/kg, Atipamezol 2,5mg/kg, Naloxon 1,2mg/kg s.c. The wound was disinfected with Braunol and Hansaplast spray. Mammosphere recipients were sacrificed 4 or 8 weeks after transplantation. Curative surgery or sacrifice of mice was done when the diameter of tumors was between 5-10 mm.

2.1.2.6 Bone marrow processing for staining and single cell isolation

Tibias and femurs were collected from NSG, Balb/c or Balb-NeuT mice and held in PBS. The soft tissue surrounding the bones was removed. Epiphyses were removed using scissors and the bone marrow was flushed out with 1x PBS into a 50 ml tube using a 26G needle. Afterwards, the cells were pooled and centrifuged at 200x g for 10 min. The supernatant was discarded and the pellet was resuspended in 9 ml of 1x PBS. Cell suspension was slowly and carefully overlaid onto 6 ml of 65% percoll in a 15 ml tube to form a layer and centrifuged for 20 min at 1000x g to remove erythrocytes and granulocytes. Interphase was carefully collected using a 5 ml pipette and transferred into a new 50 ml tube. The tube was filled up with 1x PBS and centrifuged for 10 min at 500x g for washing the cells. The cells were resuspended in 5 ml of 1x PBS and counted. For the preparation of slides for staining, 500.000 cells

were placed on each adhesion slide. For the isolation of $EpCAM^+$ cells, bone marrow was first subjected to CD45 depletion (section 2.1.2.8).

2.1.2.7 Bone marrow transplantation

Balb/c (9 weeks old) and NSG (6 weeks old) mice were irradiated previous to BM transplantation. Balb/c mice were irradiated twice, two days before transplantation and on a transplantation day 5-6 hours before BM transplantation, with 5 Gy. NSG mice were irradiated on transplantation day 5-6 hours before BM transplantation with 2 Gy. Bone marrow was isolated from 8-10 weeks old Balb-NeuT donors as described and naïve bone marrow cell suspension (without removing erythrocytes and granulocytes on 65% Percoll) was injected i.v. to previously irradiated mice ($7\text{-}10x10^6$ BM cells/mouse).

For the transplantation of the CD45-depleted BM, after isolation BM suspension was subjected to two rounds of CD45 depletion and the efficiency of the elimination of CD45+ cells was examined by FACS. To each of previously irradiated Balb/c mice (as described above) were injected $6{,}5x10^6$ CD45-depleted BM cells. On the following day one Balb/c mouse was sacrificed and 2-5 $x10^6$ BM cells were injected i.v.

2.1.2.8 CD45 depletion

Bone marrow of Balb/c and Balb-NeuT mice was isolated and CD45+ cells were depleted after the instructions of the vendor. Briefly, Cells were resuspended in MACS buffer (90 µl per 10^7 cells) and anti-mouse CD45 beads were added (10 µl per each 10^7 cells). After 15 minutes incubation at 4ºC cells were washed with 2 ml of 1x PBS and centrifuged 10 min at 300xg. Supernatant was removed and cells resuspended in MACS buffer (500 µl per 10^8 cells). Column was rinsed once with 2 ml buffer and afterwards cells were added to the column. $CD45^+$ cells are kept on the column and CD45- fraction collected in the tube. Column was washed twice, with 2 ml and 1 ml of MACS buffer respectively, CD45- cells (flow-through) were counted, centrifuged and resuspended in 1x PBS so that we get the needed density.

2.1.2.9 Progesterone treatment

For the progesterone treatment pellets of 5 mg with 21 days releasing time were implanted as proscribed by vendor. Briefly, small neck was made on the lateral side of the neck of the recipient mice (Balb/c and Balb-NeuT) and the pocket was formed 2 cm behind the cut using forceps. Pellets were placed into the pockets using forceps and the cut was sutured. No alcohol disinfectant was used as it can activate releasing of the pellet content before it is placed in the body of the recipient. After 4 or 8 weeks recipient mice were sacrificed.

2.1.2.10 Bone marrow staining for DTC detection

At least 10^6 cells per mouse were stained to detect positive cells and $0{,}5x10^6$ cells per mouse to control the Isotype positivity (Isotype control). Blocking solution (5% rabbit serum in 1x TBS) was added to the slides to rehydrate the cells and to block unspecific binding of antibodies to the cells. After 20 min the blocking solution was discarded and primary antibody against CK 8 and 18 was added and incubated for 60 min. The primary antibody was discarded and slides were washed 3 times for 3 min in 1x TBS. Then slides were incubated with the secondary antibody for 25 min, and washed 3 times for 3 min in 1x TBS followed by incubation with ABC complex for 25 min. Finally, the development system of the BCIP/NBT for alkaline phosphatase enzymatic substrate was added for 10 min. The slides were washed 3 times for 3 min and screened for CK8/18 positive cells. The positive cells were typically violet-to-black in color. TUBO, a tumor cell line derived from a primary mammary tumor of Balb-NeuT mice and expresses CK8/18, was used as a positive control.

2.1.2.11 Haematoxylin and eosin staining

Paraffin embedded tissue was cut into 5 µm sections onto poly-L-lysine-coated slide. Sections were dewaxed in Xylol for 10 min twice and rehydrated first in 100% ethanol for 3 min and then in 80% ethanol for 3 min. The sections were washed in PBS for 1 min thrice and incubated with hematoxylin for 45 sec. The slides were rinsed in tap water for a short duration and washed in tap water for 30 min in a glass cuvette. Eosin (0.1%) was added to the tissue sections and after 2 min they were washed with ddH_2O for 1 min. The stained sections were dehydrated in 70% ethanol for 2 min, 100% ethanol for 2 min and finally in xylol for 15 min. Mounting gel was added to the tissue sections and a cover slip was placed carefully on the gel avoiding bubbles and were left to dry overnight.

2.1.2.12 Immunohistochemistry

For Her2 immunohistochemistry of tissues, 5 µm sections of paraffin blocks were collected onto poly-L-lysine-coated slides. Samples were dewaxed by two 5-min washes in xylene and rehydrated with graded alcohol by 5-min washes and a final wash in water. A standard Tris-EDTA buffer and pressure cooking was the antigen retrieval procedure and then sections were blocked in 0.3% H_2O_2 in TBS and 10% normal goat serum. Sections were incubated for 1 hour with primary antibody and after washing secondary antibody was added based on manufacturers suggested dilution. After washing with PBS, sections were stained using the ABC detection system (Vector laboratory) according to the manufacturer's instruction. Visualization was performed with chromogen reagent (Dako) according to manufacture instructions.

2.1.3 Cell culture experiments

2.1.3.1 Storage and propagation of the cell lines

The identity of all used cell lines was controlled by ATCC recommended DNA fingerprinting and they were negative for mycoplasma contamination as confirmed by regular routine tests. Cell lines were preserved in liquid nitrogen in medium containing 50% FCS, 40% complete growth medium for propagation and 10% DMSO. Cell lines were propagated until 70-80% confluence and re-plated afterwards. Cell lines were de-attached using Trypsin/EDTA and re-plated in an appropriate cell density.

The non-tumorigenic mammary epithelial cell line MCF 10A (ATCC, 50) was cultured in Ham's Dulbecco's modified Eagle's/F12 (DMEM/F12) medium supplemented with 5% horse serum, 1% penicillin/streptomycin, 20 ng/ml EGF, 0.5µg/ml hydrocortisone, 10 µg/ml insulin and 0.1 µg/ml cholera toxin. MCF 10A-GFP cells were generated by transducing MCF 10A cells with pRRL.sin.cPPT.hCMV-GFP.WPRE. hTERT-HME1-derived cell line HME-EGFR (generously provided by Alberto Bardelli, Italy) was maintained in DMEM/F-12 medium supplemented with 10% fetal calf serum, 20 ng/ml EGF, 0.5 µg/ml hydrocortisone, 10 µg/ml insulin and 1% penicillin/streptomycin. Murine embryonic fibroblasts C3H10T1/2 (a generous gift from M. Wicha, University of Michigan, USA) cells were grown in DMEM medium supplemented with 5% fetal calf serum, 2mM glutamine, 1% penicillin/streptomycin. T4-2 and HUVEC cells were a kind gift from Dr. Cyrus Ghajar (Laboratory for the Study of Metastatic Microenvironments, Fred Hutchinson Cancer Research Center, Seattle, WA, USA). T4-2 cells were propagated in collagen-coated cell culture dishes in DMEM/F12 supplemented with 250 ng/ml Insulin, 10 µg/ml apo-Transferrin, 2,6 ng/ml sodium-selenite, 10^{-10} M β-estradiol, $1{,}4x10^{-6}$ M Hydrocortisone and 5 µg/ml Prolactin. HUVECs were propagated in complete EGM-2 medium (EGM-2 Kit, Lonza) and used maximum until passage 11. All cell lines were kept at 37°C and 5% CO2 in a fully humidified incubator.

2.1.3.2 Preparation of collagen coated plates

PureCol collagen is approximately 97% Type I collagen with the remainder being comprised of Type III collagen and it is used for the coating of the dishes for culture of the cell lines that need additional support from the matrix similar to their physiological environment. PureCol (stock concentration 3 mg/ml) was diluted in ice cold 1x PBS to working concentration of 67 µg/ml. This solution was added to the cell culture flask at least a day before cell seeding. Per one 75 cm^2 flask was added 10 ml of the collagen solution and it was incubated overnight at 4ºC. These dishes can be stored at 4ºC for 14 days. Before seeding cells the liquid was removed (carefully not to disturb the bottom layer of collagen) and gently washed with prewarmed growth medium.

2.1.3.3 Preparation of poly-HEMA (ultra-low attachment) plates

The mammary stem and progenitor cells are able to survive anchorage independent conditions while more differentiated progenies are undergoing anoikis. Cells are not able to anchorage to the dish bottom if the dishes are covered by poly-HEMA, an organic substance soluble in ethanol. For preparation of the coating solution, 2,4 g of poly-hydroxy-ethyl-methyl-acrylate (Poly-HEMA) was added to 20 ml of 95% ethanol and put on a heating magnetic plate warmed to 65° C and mixed using magnetic stirrer to dissolve for minimum ~8 hours. To the above dissolved poly-HEMA, 80 ml of 95% ethanol was added and mixed to get the final concentration of 12 mg/ml. The prepared solution could be stored indefinitely at 4° C. Poly-HEMA solution was applied to the culture dishes and left to dry overnight in a sterile hood with lids slightly opened. On the next day, a fine layer of poly-HEMA covers the culture dish. The poly-HEMA-coated plates can be stored indefinitely until use at 4° C. Prior to cell seeding poly-HEMA coated plates were sterilized by the UV light for 30-60 minutes and the traces of ethanol were removed by washing with PBS.

2.1.3.4 *In vitro* propagation of mammary cells under anchorage independent condition (sphere assay)

Mammary cell lines were propagated in 2D conditions until they reached the 70% confluence. Propagated cells were de-attached and washed in PBS at least two times. The washing steps were introduced to remove traces of serum used in the 2D cell line propagation culture strategy. Cell lines were propagated in ultra-low attachment plates in cell culture incubator at 37 °C, 5% CO_2 and 7% O_2 at a seeding density of 10 000 cells/ml in 35 mm plates with 3 ml medium per plate. All cell lines as well as the primary epithelial cells isolated from human and mouse mammary glands were propagated in the same mammosphere medium, comprising of a serum-free mammary epithelial growth medium (MEBM) supplemented with 0.5x penicillin/streptomycin, 1x B27, 10 ng/ml EGF and 10 ng/ml bFGF and 4 µg/ml heparin. To assess uniformity of seeding, cells were resuspended in master mix, containing 1 ml spare volume and distributed to the ultra-low attachment plates for the cultivation. Mammosphere forming ability was assessed 7 days post-plating. During this period, medium was not changed and disturbance of the cultures was avoided.

HIL-6 (a kind gift from Dr. Stefan Rose-John Christian-Albrechts-University, Kiel, Germany) was dissolved in DMSO and used at final concentration of 20 ng/ml. Gro-α, Rankl and Wnt4 were dissolved and used according to the manufacturer's instructions in final concentrations of 5 ng/ml, 50 ng/ml and 5 ng/ml respectively. Collagen I was dissolved according to the manufacturer's instructions and used in final concentration of 50 µg/ml. ALK5i, p38i and RTKi were dissolved and used according to the manufacturer's instructions in final concentrations of 10 µM, 2 µM and 2 µM respectively.

2.1.4 Microvascular niche

2.1.4.1 Production of the lentiviral (GFP) and retroviral particles (RFP)

For the production of lentiviral particles we used 293T cells and for the production of retroviral particles Phoenix Ampho (PA) cells. Both 293T and PA cells were propagated in DMEM medium supplemented with 10% FCS and 2 mM Glutamine. Antibiotics decrease virus production and their usage was avoided. PA cell line is a variant of 293T cell line that has been stably transfected to express viral packaging proteins, so they do not require addition of viral plasmids, but only the plasmid of interest. Transfection efficiency is strongly affected by cell culturing method, passage number, cell confluence, pH, temperature and many other factors. Therefore this procedure is very requiring and must be carefully conducted. Reaching confluence significantly decreases virus production capability and the cells must be passaged upon reaching 70% confluence.

For virus production 4 x 10^6 cells were seeded in a 10 cm petri dish in the evening before transfection. Transfection medium (DMEM with 10% FCS) containing 25 µM chloroquine was added to the cells 45 min before the start of transfection. Chloroquine blocks endosome/lysosome function which subsequently decreases degradation of plasmids and increases transfection rate. 30 to 60 minutes after chloroquine addition transfection mixture was added dropwise to chloroquine containing medium. Transfection mixture for 293T cells comprise of pMD2G (envelope plasmid), psPAX2 (packaging plasmid), lentiviral plasmid (target DNA, carrying a gene of interest) and 0,25 M $CaCl_2$ in HeBS buffer (pH of buffer must be 7,05 at room temperature). In the case of viral production by PA cells viral (packaging and envelope) plasmids are not added to transfection mixture. Plasmid DNA generates calcium-phosphate–DNA co-precipitates with potassium from $CaCl_2$ and phosphate from buffer. Calcium phosphate facilitates the binding of the condensed DNA in the co-precipitate to the cell surface, and the DNA enters the cell by endocytosis. The transfection mixture was added drop wise to the cells and they were incubated 6-8 hours. After incubation in transfection medium it was replaced with post-transfection medium (growth medium with HEPES buffer). Medium with produced viral particles was collected 48h and 72h post transfection when cell confluence was 70% and 90% respectively. Upon collection viral containing media were centrifuged, filtered through 0,22 µm sterile filter and stored at -80ºC. Since virus related work belongs to biosafety level 2 (S2 work) higher precautions must be met than in regular cell culture work. From the moment of adding transfection mixture to the cells recommendation prescribed for the S2 work must be followed.

2.1.4.2 Virus titer determination

In order to determine the number of viral particles in the medium of virus producing cells we used easily transducable cell line C3H10T1/2, murine mesenchymal cells. Cells are cultured in DMEM supplemented with 10% FCS and 1% P/S. 12 to 24 hours prior to transduction 10.000 cells were seeded

per well in 12 well plate and incubated overnight in incubator with 37°C and 5% CO_2. On the next day average number of cells per well was counted by counting the number of cells in 2-3 wells. Transduction medium is growth medium with 4 µg/ml polybrene, which increases retrovirus gene transfer efficiency by enhancing receptor-independent virus adsorption on target cell membranes. Serial dilution of virus containing medium was added to transduction medium and to cells according to the scheme in the table 1. Cells were incubated with virus-polybrene-containing medium 12-16 hours after which medium was exchanged with regular growth medium. 48 hours after cells were harvested and fixed using 1% PFA. After 10 minutes incubation in 1% PFA, all the viruses are dead and cells were analyzed on FACS.

For (multiplicity of infection) MOI calculation the well with 10-20% fluorescent cells (positive in FACS analysis) was taken. The MOI is calculated from the following equation:

$$\text{Positive} \times N \times DF = IU/ml$$

Positive - percentage of positive cells
N – number of cells at the time of transduction
DF – dilution factor
IU – number of infectious units

Table 1: Dilution scheme for native viral SNTs, the indicated volume refers to one well of a 12 well plate

Dilution factor	Virus supernatant [µl]	Polybrene containing medium [µl]
Non-transduced	0	1000
Undiluted	1000	0
5	200	800
10	100	900
50	20	980
100	10	990
500	2	998

2.1.4.3 Generation of the microvascular niche

Microvascular niche is a co-culture of hMSCs and endothelial cells that form a fine continual microvasculature net. hMSCs were isolated and propagated as described. Human Umbilical Vein Endothelial Cells (HUVEC) transduced with adenoviral *E4ORF1* gene, as well as H2B-GFP-T4-2 breast cancer cell line were a generous gift from Dr. Cyrus Ghajar, Laboratory for the Study of Metastatic Microenvironments, Fred Hutchinson Cancer Research Center, Seattle, USA. Introduction of *E4ORF1* gene into human HUVECs increased the long-term survival of these cells in serum/cytokine-free conditions, while preserving their *in vivo* angiogenic potential for tubulogenesis and sprouting (Seandel et al., 2008).

Before seeding MVNs HUVECs were transduced with pBMN/mCherry plasmid in order to generate stably expressing mCherry endothelial cells (Ghajar et al., 2008) and cultured to achieve post-confluence (Figure 6). For MSC or MVN generation MSCs were seeded alone at a density of $5x10^4$ cells/well in 96-well culture plates or with mCherry-E4-ECs at a 5:1 ratio to generate stromal or bone marrow-like microvascular niches, respectively. Cells were suspended in EGM-2 medium at a concentration $5x10^4$ cells/100 µl (stroma only) or $6x10^4$ cells/100 µl (stroma + ECs). After depositing 100 µl of cellular suspension per well of a 96-well plate, plates were left undisturbed on a flat surface for 20 min to allow even cell seeding prior to incubation. Cells were always inspected under the microscope for even distribution in the well prior to transferring into incubator. Growth medium was changed regularly every two days. After ten days the cultures were inspected and when they formed nice continuous vascular net (Figure 6), breast cell line cells were added. GFP labeled MCF10A or H2B-GFP-T4-2 cells were trypsinized and carefully counted. The density of cells was adjusted to have determined number of cells in 100 µl EGM-2 medium and 100 µl of cell suspension was seeded in each well with stromal (control) or microvascular niche. Cells were allowed to settle for 15 min at room temperature, then a 100µl of Cultrex Basement Membrane Extract (BME) in DMEM/F12 was slowly added to each well (final concentration = 20%). BME was left to condense for 10 min at room temperature before polymerizing fully at 37ºC. Cultures were maintained with media changes every three days and further analyzed at day 10.

For cell growth measurement MSC and MVN cultures were imaged and quantified. The same ROI (surface area marked and surrounded) was applied to all the wells and gave the level of GFP fluorescence. Statistical analysis was performed using GraphPad Prism software.

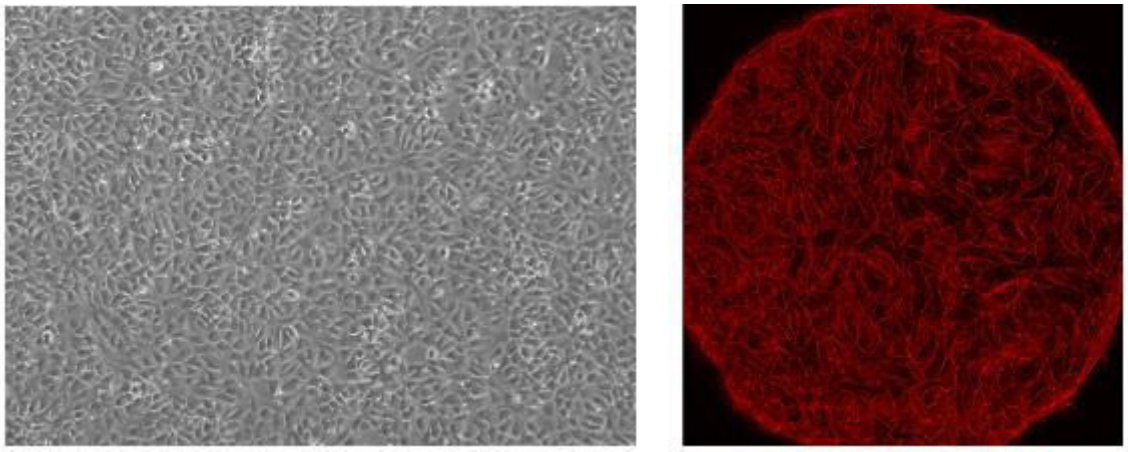

Figure 6: Left panel: post-confluent HUVECs, before seeding MVN; Right panel: Microvascular net at day 7 after seeding

2.1.4.4 Isolation of the single breast cancer cells from MVN and MSC niches

To isolate breast cancer cells we first collected the gelatinous layer of BME using p200 tip and Gilson pipette. Then, each well was washed three times with ice-cold 1x PBS to remove residual BME. After

that only thin layer of the artificial tissue was left in the well. We added 200 µl of ice-cold 1x PBS to the well, scratched gently the "tissue", collected using p200 tip and transferred to 1,5 ml microcentrifuge tube. Next we mixed the cell suspension using a syringe with 19 gauge needle to mechanically separate the cells. All the steps were performed on ice, because residual BME quickly polymerizes and makes gelatinous suspension. This suspension was then transferred to picking slides and GFP-positive cells were isolated.

2.1.5 Osteoblastic niche

2.1.5.1 Isolation and cultivation of hMSCs from cancer patients

Isolated human bone marrow was centrifuged on 65% Percoll gradient and interphase was washed once with 1X PBS. $2x10^6$ cells were plated per 75 cm^2 flask in 15 ml of media (low glucose DMEM supplemented with heat inactivated FBS, 2 mM L-Glutamine and 1% Penicillin/Streptomycin). Medium was changed weekly and when clusters formed, cells were trypsinized to achieve homogeneous distribution. After 3-4 weeks of culturing $1\text{-}1{,}3x10^6$ cells were harvested from each flask. This is Passage 0 (P0) of the cells. Numerous freeze-thaw cycles as well as long culturing time were avoided with these cells.

2.1.5.2 Osteoblasts differentiation from MSCs and co-culture with MCF10A cells

200.000 human mesenchymal stromal cells (hMSCs) from 80% confluent flask cells were seeded pro well of 6 well plate and cultivated in hMSCs medium for three days until achieved 95% confluence. After achieving confluence cells were moved to incubator with 3% O_2 and 5% CO_2 and medium was changed with medium for osteogenic differentiation (high glucose DMEM without Sodium-pyruvate supplemented with 10% FBS, 0,1 µM Dexamethasone, 25 µg/ml L-ascorbic acid and 3 mM Monosodium phosphate (NaH_2PO_4)). Medium was changed every 2-3 days for 21 days. After 21 days osteogenic differentiation was confirmed by Alizarin Red staining. After 21 days of differentiation of OBs, MCF10A cells were stained with CFDA-SE and seeded on top of osteoblasts and cultivated in growth medium in incubator with 3% O_2, 5% CO_2. For FACS analysis cells were washed with 1X PBS, trypsinized 5 minutes with 0,05% trypsin and scraped using cell scraper. Intensive pipetting with Gilson p1000 pipette was applied in order to break clusters and get single suspension. After washing with 1X PBS cells were filtered through 40 µm cell strainer, stained and analyzed by FACS.

2.1.5.3 Co-cultures of MCF10A with MSCs, OBs, HUVECs

MSCs and HUVECs were plated at a density of $4x10^5$ cells/well of a 6 well plate (Corning, Germany) in their growth medium. The next day, medium was exchanged to MCF10A growth medium and $1x10^5$ MCF10A-GFP cells were added to each well. In case of co-cultures with OBs, $4x10^5$ MSCs per 9.6 cm^2 surface of a 6 well plate were plated and differentiated into OBs for 21 days. On day 22 medium was

exchanged to MCF10A growth medium and $1x10^5$ MCF10A-GFP cells were added to each well. For cultures with transwells, MSCs were plated at $1.75x10^5$ cells per $4.2cm^2$ of a 6-well transwell insert.

2.1.5.4 Selective activation/inhibition of individual IL-6 signaling

MCF10A cells were cultured as mammospheres in the presence of 10 ng/ml IL6, 10 ng/ml IL6 + 0.1 ng/ml rh sgp130-Fc or 20 ng/ml Hyper-IL6 for 12 and 24 hours. Triplicates were seeded for all conditions and time points. After 12 and 24 hours, cells were collected by centrifugation for 5 min at 500xg and RNA was isolated using RNeasy Mini Kit according to the manufacturer's protocol. Microarray analysis was performed using the Whole Human Genome Microarray Kit, 4x44K (G4112F) and Agilent chips. For transcriptome analysis of BM-DCCs of metastasized and non-metastasized patients, cDNA was generated from manually isolated single cells using whole-transcriptome amplification.

Labelling of cDNA was performed by PCR with Cy5-labelled primers. Reaction mix contained 5 µl of buffer I, 3% (v/v) deionized formamide, 0,35 mM each dNTP, 2,5 µM 5'-U*CAGAAU*TCAUGCCC*CCCC*CCCC*C-3' primer (*denotes nucleotides conjugated with Cy5 fluorophore; Metabion), 3,75 U of PolMix and 1 µl of WTA-product or 100 ng cDNA from bulk RNA preparations of MCF10A cells in a final volume of 49 µl. PCR parameters were: one cycle with 1 min at 95 °C, 11 cycles with 15 s at 94 °C, 1 min at 60 °C, and 3 min 30 s at 65 °C, 3 cycles where the elongation time was increased 10 s per cycle, and finally one cycle with an elongation time of 7 min. Labelled products were purified using a PCR purification kit according to the instructions of the vendor. Purified Cy5-labelled DNA was denatured by incubation for 5 min at 95 °C followed by incubation on ice. Hybridization solution was prepared by mixing 42 µl of denatured Cy5-labelled DNA, 55 µl of 2x HiRPM hybridization buffer, 11 µl of 10 × GE Blocking agent, 4 µl of 25% (v/v) Tween-20, and 4 µl of 25% (v/v) Igepal. Four 100 µl samples of hybridization mix were overlaid on 4 hybridization fields of Agilent Whole Human Genome (4x44K) Oligo Microarray with SurePrint (G4122F) microarray slides and incubated for 17 h at 65 °C under constant rotation. After hybridization, slides were washed in Agilent Wash buffer 1 for 1 min on a shaker in the dark and incubation continued in Agilent Wash buffer 2 pre-warmed to 37 °C. Slides were dried by washing for 30 s in acetonitrile and scanned on a GenePix 4400 A scanner. Numerical readouts of fluorescence intensities (GPR files) were generated using GenePixPro 7.

2.1.6 Staining procedures

2.1.6.1 CFDA-SE staining

CFSE (5-(and 6)-Carboxyfluorescein diacetate succinimidyl ester, CFDA SE) is cell division tracking dye and is a golden standard in proliferation tracking in label retention assays. Cells were washed once

with 1X PBS, resuspended in 4 µM CFDA-SE diluted in FACS buffer (1% FCS in 1X PBS) and immediately vortexed and incubated 10 minutes in water bath on 37°C (in dark). After incubation cells are washed with 50 ml medium containing 10% FCS and afterwards with 50 ml PBS.

2.1.6.2 PKH26 staining

PKH26 is a general cell membrane labeling dye that is visible under Cy3 filter. Cells isolated from human mammary tissue were washed once in 1x PBS and centrifuged 5 min at 500xg to remove any traces of serum. The supernatant was discarded and the cell pellet was resuspended in 1 ml Diluent C. to make 1:25 dilution from recommended by vendor we mixed 2 µl of PKH26 with 48 µl of ethanol and from that suspension we took 4 µl and added to 996 µl of Diluent C solution. The dye solution was added to the cell suspension, mixed quickly because the binding of the dye to the cell is immediate and incubated for 5 min. The staining reaction was stopped by adding 2 ml of medium containing 10% FCS for 1 min and centrifuged 5 min at 500xg. After discarding the supernatant, the pellet was resuspended 1x PBS and centrifuged again for 5 min at 500xg. The cells were washed in total 3 times with 1x PBS to remove unbound dye.

2.1.6.3 Staining of cell surface markers for FACS analysis

To reduce non-specific binding single cell suspensions were incubated for 5 min at 4°C with PBS/10% AB-serum, subsequently stained with fluorescence-labeled or biotinylated antibodies for 15 min at 4°C and washed once with PBS/2% FCS/0.01% NaN3. In case of biotinylated primary antibodies, PE-labeled streptavidin was used as secondary staining reagent. Cells were stained using the following antibodies:, anti-human CD44-V450 (G44-26), biotinylated anti-human IL6R (UV4), isotype control mouse IgG2a-APC (MOPC-21), isotype control mouse IgG2b-V450 (MOPC-21), isotype control IgG1-biotin (MOPC-21) (all purchased from BioLegend, Germany) and anti-human EpCAM (HEA-125). Viability dye eFlour 780 was used for live/dead cell discrimination. Cells were analyzed on a LSR II machine equipped with FACS DIVA 5.03 software and data was analyzed with FloJo 8.8.6 or 10.1.

2.1.7 T cell experiment

2.1.7.1 T cell isolation and stimulation

50ml of blood was drawn from a healthy individual in heparin pre-coated syringe and washed once with double volume of Hanks Salt solution. Yellow supernatant containing fat and platelets is removed and washed blood was slowly subjected to gradient centrifugation on 65% Percoll (1:1 volume). After 20min centrifugation at 1000xg the interphase with target cells was collected and washed. For cell labeling CD8+ T cell Biotin-Antibody Cocktail was incubated with the cells for 5 minutes at 4°C. After washing and adding CD8+ T cell MicroBead Cocktail cells were incubated for 10 minutes at 4°C and washed. Magnetic separation was performed using MACS columns. Cell suspension was applied to the

MACS column (prepared by rinsing with MACS buffer) and washed twice with 1 ml of MACS buffer. Antibodies are labeling all the other cells except of CD8+ T cells, so the aimed CD8+ T cells are enriched in flow-through. Cells were counted and 100.000 cells were taken to check the purity of isolated cell suspension (by FACS analysis). Cells were cultured in RPMI medium supplemented with 10% FCS, 1% Penicillin/Streptomycin (P/S) and 50 µM β-mercaptoethanol. For PMA/ionomycin stimulation, cells were incubated with PMA (20 ng/ml) and ionomycin (1 µM) 6-8 hours. After stimulation cells were collected and washed trice with 50 ml prewarmed complete growth medium. Cells were cultivated for 48h before cell cycle analysis.

2.1.7.2 DNA staining for cell cycle analysis (DAPI and Hoechst 33342) and cell sorting

Cells were checked under microscope. In stimulated cultures can be seen many small cell clusters of proliferating cells. Cells were collected, centrifuged 5 minutes at 500xg and resuspended in prewarmed medium with 10 µg/ml Hoechst 33342 (for pilot experiment 5 µg/ml DAPI was used). After incubation at 37°C for 40 min in the dark viability dye (7-AAD) was added to final concentration of 0,5 µg/ml and cells were incubated additional 10 minutes at 37°C in the dark. After incubation cells were analyzed and sorted on BD LSR II.

2.1.8 Whole transcriptome amplification and PCR

2.1.8.1 Whole transcriptome amplification (WTA) of single cells

Target cells were stained for EpCAM or other marker of interest. For live/dead cell discrimination cells were stained with DAPI and single viable cells showing the phenotype of interest were isolated with a micromanipulator. Whole transcriptome amplification of single cells was performed as previously described (Hartmann and Klein, 2006). The quality of WTA products was assessed by expression analysis of three housekeeping genes: β-actin, GAPDH and EF-1α. Only samples which were positive for at least two of three analyzed markers were used for downstream analyses.

2.1.8.2 Gene specific end-point PCR

Endpoint PCR was conducted to verify the presence of selected genes of interest in WTA products. Template (1 µl) was mixed with 1 µl of 10x Fast Start buffer, 0,2 µl dNTP Mix (10 mM each), 0.5 µl of forward and reverse primer (8 µM each), 0.2 µl BSA, 0.1 µl Fast Start Taq Polymerase and HPLC Grade H_2O to a final volume of 10 µl (6,5 µl). PCR was run using the following program: initial denaturation of 4 min at 95°C was followed by 40 cycles of 30 s at 94°C, 30 s at predetermined annealing temperature, 90 s at 72°C and a final elongation step for 7 min at 72°C. Positive and negative control was included in every PCR run. Annealing temperature used for three housekeeping genes was 58ºC.

2.1.8.3 IL6, IL6RA, gp130, MKI67 and MCM2 mRNA expression analysis

IL6, membrane IL6 receptor and spliced IL6 receptor expression was assessed by PCR using the MJ Research Peltier Thermal Cycler Tetrad with the following primers: IL6 (forward primer: 5'-GAG AAA GGA GAC ATG TAA CAA GAG T-3', reverse primer: 5'-GCG CAG AAT GAG ATG AGT TGT-3', annealing 62°C, amplicon size 388 bp), membrane versus spliced IL6RA (forward primer: 5'-CTG CAA ATG CGA CAA GCC TC-3', reverse primer: 5'-GTG CCA CCC AGC CAG CTA TC-3', annealing 62°C). The spliced and membrane-bound IL6 receptor were distinguished according to their PCR product size: mIL6RA 380 bp, spliced IL6RA 286 bp. gp130 expression was assessed by end-point and quantitative PCR that was performed on a LightCycler 480 (Roche, Germany) using following primers: for end-point PCR forward primer: 5'-GGA CCA AAG ATG CCT CAA CT-3', reverse primer: 5'-GGC AAT GTC TTC CAC ACG A-3', annealing 58°C, size of the amplicon 280 bp, and for qPCR forward primer: 5'-ATA TTG CCC AGT GGT CAC CT-3', reverse primer: 5'-AGG CTT TTT GTC ATT TGC TTC T-3', annealing 57°C, size of the amplicon 125 bp.

MKI67 (Ki-67) and MCM2 expression was assessed by end-point and quantitative PCR with the following primers: MKI67 forward 5'-GCGGAGTGTCAAGAGGTGT-3' and reverse 5'-CAGACCCAGCAAATCCAAAGT-3' (amplicon length 247 bp); MCM2 forward 5'-GAAGCAGTTAGTGGCAGAGC-3' and reverse 5'-CATAGGGCCTCAGAACTGCT-3' (amplicon length 217 bp). Annealing temperature for both genes was 58°C.

2.1.8.4 Agarose gel electrophoresis

Amplified products of the specific PCR were separated with gel electrophoresis, on 1.5% agarose in TBE buffer with ethidium-bromide (0,5 μg/ml). Samples were mixed with a loading dye and loaded in the gel. PCR amplicons were separated at 160 V for 45 min. IL-6 and IL-6R amplicons were separated on 2% agarose gel for at 160 V for 60 min.

2.1.8.5 Re-amplification of primary WTA single-cell products

Re-amplification of primary WTA products was performed in a reaction volume of 50 μl comprising 5 μl Expand Long Template Buffer 1, 6 μl of CP2-15C or CP2-9C primer (2.88 μM), 1.75 μl dNTPs (10 mM each), 7.5 μl 20% Formamide, 1.5 μl DNA Pol Mix (5 U/μl, Expand Long Template PCR System), 27.25 μl PCR HPLC Gradient Grade H_2O and 1 μl template (primary WTA product). Re-amplification was run on PTC DNA Engine 2 Tetrad Thermocycler using the following program: 1 min at 95°C, 5 cycles comprising 15 s at 94°C, 1 min at 60°C and 3 min 30 s at 65°C, 3 cycles of 15 s at 94°C, 1 min at 60°C and 3 min 30 s at 65°C (elongation step was extended by 10 s per cycle) and a final elongation step of 7 min at 65°C. Negative control was included in every run. Quality of re-amplified product was examined using the same endpoint PCR assay as the one used for primary WTA products (see above).

2.1.8.6 Purification of WTA products

Purification of WTA samples was conducted to remove buffer and remaining WTA reagents (dNTPs, proteins and primers) that may negatively influence downstream processes (i.e. cDNA yield quantification and qPCR). 15 µl of primary or re-amplified WTA product was purified using QIAquick PCR Purification Kit according to the manufacturer's instruction with several changes: (i) No pH-indicator was added to the PB buffer. (ii) Purified cDNA was eluted from the purification column using HPLC Gradient Grade H_2O instead of EB buffer provided by the manufacturer of the kit. (iii) PCR HPLC Gradient Grade H_2O (typically 20 µl) used for elusion was pipetted on the silica membrane of the column, followed by 5 min incubation at room temperature prior to the final centrifugation (elution) step. To allow a more optimal distribution of elution liquid in the silica membrane on the purification column, spin assembly was centrifuged at 500 rpm for 30 s followed by the final centrifugation at 13.000 rpm for 60 s. Concentration of each purified sample was measured using NanoDrop 2000c.

2.1.8.7 Quantitative Real-Time PCR

Quantitative PCR (qPCR) was performed for selected genes of interest (gp130, MKI67 and MCM2) using a LightCycler 480 instrument (Roche). Each qPCR comprised 5 µl of the template cDNA, 10 µl iQTM SYBR® Green Supermix (Bio-Rad), 1 µl of each forward and reverse primer (8 µM each) and 3 µl PCR HPLC Gradient Grade H_2O. QPCR was run using the following program: 1 cycle for 5 min at 95°C (temp. ramp of 4.4°C/s), 38 cycles for 20 s at 95°C (ramp 4.4°C/s), 15 s at 58°C (ramp 2.2°C/s) and 15 s at 72°C (ramp 4.4°C/s; fluorescence signal was measured at the end of each elongation step). Subsequently, melting curves were generated using the following procedure: 1 cycle for 5 s at 95°C (ramp 4.4°C/s), 1 cycle for 1 min at 50°C (ramp 2.2°C/s), 1 cycle of DNA melting, wherein temperature was continuously increased to 95°C with a ramp of 0.11°C/s with continuous fluorescence measurement 5 times/s) followed by a final cooling to 40°C for 30 s (2.2°C/s). Melting plots were examined to validate the specificity of PCR amplification. Crossing point (Cp) values were determined with the LightCycler 480 Software using the second derivative maximum method applying the high sensitivity algorithm. All single-cell WTA products were analyzed in technical triplicates. Cp-values were averaged across the technical replicates before further data processing. Samples with average Cp-values >33 were considered as negative. No template control was included in any qPCR run.

2.1.8.8 Absolute qPCR quantification analysis

Quantification of cDNA yields in the individual samples was spectrophotometrically conducted using the NanoDrop 2000. To allow an accurate measurement of cDNA, yields of WTA products were purified (see section 2.1.8.6). DNA input for each qPCR was normalized to 5 ng and run as described above. The obtained Cp-values generated by the LightCycler 480 Software (Roche) were converted into log10 copy numbers. For this, a standard curve measurement was conducted with serially diluted cDNA

standards comprising amplicons of the target transcript. Concentrations of the standards ranged from 10^{-8} to 10^{-4} ng/µl covering copy numbers from $3x10^2$ to $3x10^6$ molecules/µl.

2.1.9 Gene expression analysis using micro array

2.1.9.1 Mammary cell subpopulation mRNA microarray data.

Human mRNA expression data from Lim et al. based on Illumina HumanWG-6 v3.0 BeadChip microarrays were downloaded from the Gene Expression Omnibus (GEO) (series GSE16997).

2.1.9.2 LRC/QSC/nLRC mRNA microarray data.

Agilent 44kx4 v1 microarrays (Design ID 014850) for 8 LRC, 10 QSC and 5 nLRC samples were hybridized. All chips passed quality assessment and were preprocessed as described for MCF 10A cells above. Annotation was retrieved from the Agilentarray platform (June 2015). Using the 6000 genes with the highest variation across all samples, unsupervised consensus clustering (R-package ConsensusClusterPlus, method k-means 55 was applied assuming three clusters. From the clustering results it was concluded that the LRC and QSC groups respectively consist of two sub-groups, resulting in five groups in total (LRC1, LRC2, QSC1, QSC2, nLRC). Differentially expressed genes were then determined according to a linear model (limma R-package) including all pairwise contrasts between the five groups and an FDR threshold of 0,05. Pathway enrichment analysis was performed employing the R-package enrichR (version 1.0).

2.1.10 Statistical analysis

Statistical analysis was done using GraphPad Prism 6.0 software (GraphPad Software, Inc., USA). Differences in medians between groups were analyzed by Student's t-test, one-way ANOVA and multiple t-test with correction for multiple comparisons (Holm-Sidak's) or fisher's exact test where appropriate. When data did not follow normal distribution corresponding non-parametric tests were used. All tests were performed two-sided. A p-value of less than <0.05 was considered to be statistically significant.

2.2 Material

2.2.1 Reagents

Product	Manufacturer	Cat. Number
2-Log DNA-Ladder 1kb	NEB	N32005
7-AAD	BioLegend	420403

AB-Serum	Bio-Rad	805315
Acetic acid	Merck, Darmstadt	100063
Agarose	Sigma Aldrich GmbH	A3038
Ampicillin	AppliChem GmbH	A0839
B27	Invitrogen	17504-44
BCIP/NBT	BioRad	1706432
B-estradiol	Sigma Aldrich GmbH	E4389
bFGF	Sigma Aldrich GmbH	F0291
Bovine serum albumin (BSA), 20 mg/ml	Roche	10711454001
BSA	Roche	1071145001
$CaCl_2$	Sigma Aldrich GmbH	C5080
CFDA-SE	eBioscience	65-0850-84
Chloroquine	Sigma Aldrich GmbH	C6628
Cholera toxin	Sigma Aldrich GmbH	C9903
Collagen I	Sigma Aldrich GmbH	C3867
Collagenase	Sigma Aldrich GmbH	C0130
Cultrex Basement Membrane Extract (BME)	Trevigen	3432-001-01
DAB	DAKO	K3468
DAPI	Roche Dignostics	32670
DEPC-H2O	Invitrogen	750023
DMEM high glucose	Pan-Biotech	P04-03500
DMEM low glucose	Life Technologies GmbH	11885-084
DMEM/F12	Pan-Biotech	P04-41500
DMSO	Sigma Aldrich GmbH	41640
EGF	Sigma Aldrich GmbH	E9644
EGM-2 Kit	Lonza	CC-3162
Eosin	Sigma Aldrich GmbH	54802
b-Estradiol	Sigma Aldrich GmbH	E2758
Ethanol absolute	J.T. Baker	8006
Ethidium bromide (1 %)	Sigma Aldrich GmbH	E8751
Eukitt (Mounting gel)	Sigma Aldrich GmbH	03989-100ML
Expand Long Template Enzyme Mix	Roche Dignostics	11 759 060 001
FastStart Taq-Polymerase	Roche Dignostics	11435094001
FCS	PAN Biotech	P30-3702
Fetal bovine serum (FBS)	Pan Biotech, Aidenbach	P30-1506
Formaldehyde	Merck, Darmstadt	104003
Formamide	Merck, Darmstadt	344 205
Formamide, deionized	Sigma Aldrich GmbH	F9037
Glutamine	PAA Laboratories GmbH	M11-004
Goat serum	DAKO	X0907
GRO-α	RnDsystems	275GR
Hematoxylin	Sigma Aldrich GmbH	MHS16
Heparin	Sigma Aldrich GmbH	H3149
HEPES buffer	Sigma Aldrich GmbH	H7523
Hexadimethrine bromide (Polybrene)	Sigma Aldrich GmbH	H9268
HIL-6	A gift from Dr. Rose-John	
Hoechst 33342	Sigma Aldrich GmbH	B2261
Horse Serum	Sigma Aldrich GmbH	H1270
Hyaluronidase Type IV-S	Sigma Aldrich GmbH	H4272
Hydrocortisone	Sigma Aldrich GmbH	H0888-1gr
Igepal	Sigma Aldrich GmbH	I3021-50ML
Insulin	Sigma Aldrich GmbH	I9278

Isopropanol	Fluka	59300-2.5ML
Levamasol	Sigma Aldrich GmbH	L9756
L-Glutamin (200 mM)	Pan-Biotech	P04-80100
Matrigel	BD Biosciences	356231
MEBM	Lonza	CC-3151
Methyl cellulose	Sigma Aldrich GmbH	M0512-100G
Mouse serum	DAKO	X0910
Paraformaldehyde	VW	104005
Penicillin/Streptomycin (10 U/µL)	Pan-Biotech	P1-010
Percoll	Amersham Biosciences	17089102
PKH26	Sigma Aldrich GmbH	MINI26-1KT
Polyhydroxyethylmethylacrylate	Sigma Aldrich GmbH	P3932
Progestrone pellet	Innovative research of America	P-131
PureCol	Cell systems	5005
RankL	Abcam plc	ab151200
RPMI 1640	Pan-Biotech	P05-17500
Sodium-selenite	Sigma Aldrich GmbH	S5261
apo-Transferrin	Sigma Aldrich GmbH	T2252
Trypsin/EDTA	Anprotec	AC-EZ-0020
Trypsin neutralizing solution (TNS)	Lonza Verviers SPRL	CC-5002
SB203580 (p38i)	Calbiochem	S1076
SB431542 (ALK5i)	Calbiochem	S1067
S1042 (RTKi)	Calbiochem	S1042
Wnt4	R&D Systems	475-WN-005
Xylol	Roth	9713.3

2.2.2 Consumables

Product	Manufacturer	Cat. Number
6 well plates	Corning	CLS3516
6-well transwell insert	VWR	353090
100 mm Transwell with 0,4 µm Pore Polycarbonate Membrane Insert	Corning	3419
Adhesion slides	Roth	H8701
Cell culture flasks	Sarsted	831.810.302
Cell culture plates	Schubert and Weiss, OMNILAB	FALC351007
Cell strainer 100 mm	Corning	431752
Cell strainer 40 mm	Corning	431750
Filter (0.22 µm)	Roth	P666.1
Glass slides	Langenbrinc	03-0001
MACS separation LD columns	Miltenyi Biotec	130-042-901
MACS separation LS columns	Miltenyi Biotec	130-042-401
Reaction tubes 0,2 ml	Abgen	AB-0337
Reaction tubes 1,5 ml	CLN Gmb	CLN-BÖT1.5
Syringe needles (26G)	Braun	C7181

2.2.3 Kits

Kit	Manufacturer	Cat. Number
ABC (Avidin-Biotin Complex)	Linaris	AK-5000
ABC-HRP-System	Vector Laboratories	PK-4000
CD8+ T cell isolation kit	Miltenyi Biotec	130-096-495
DAB-System	DAKO	K3468
DNA extraction Mini Kit	Qiagen	51304
DNA Gel Extraction Kit	Qiagen	28706
ECL Detection kit for western blotting	GE Healthcare	RPN2109
Expand Long Template PCR System	Roche Diagnostics GmbH	3321053103
FastStart PCR	Roche Diagnostics GmbH	11435094001
Mouse CD45 depletion	Miltenyi Biotec	130-097-153
MTT	Roche	11465007001
Pierce BCA protein assay	Thermo scientific	23227
PKH26 general cell membrane labeling	Sigma-Aldrich	PKH26GL
Plasmid purification	Qiagen	12381
QIAquick PCR Purification Kit	Qiagen	28106
Revers trascript	Qiagen	205311
RNeasy mini-kit	Qiagen	74104
SYBR® Green Supermix	Bio-Rad Laboratories GmbH	170-8885
Whole Human Genome Microarray Kit	Agilent	G4845A

2.2.4 Devices

Device	Company
Balance	Kern, Balingen
BD LSR II	BD Bioscience, USA
BenchMark Ultra	Ventana, USA
Capillary holder for micromanipulation	Eppendorf, Hamburg
Cauterizer	Fine Science Tools, Hedelberg
Cell culture incubator	Heraeus, Hanau
Cell culture incubator	Heraeus
Cell culture laminar flow	Heraeus, Hanau
Centrifuge	Heraeus, Hanau
Centrifuge	Eppendorf, Hamburg
Centrifuge, tabletop	Grant Bio, USA
Centrifuge, tabletop	Eppendorf, Hamburg
Cytospine Centrifuge	Hettich, USA
Dissection tools for murine surgery	Heiland
DM RXA Fluorescence microscope	Leica, USA
Electrophoresis gel chamber	Biostep, Jahnsdorf
Flourescence microscope	Leica
Heat block thermo mixer 5436	Eppendorf
Imagequant LAS 4000	GE Healthcare
Inverted microscope	Leica
Magnetic stirrer	VELP Scientifica
Micromanipulator Microinjector 5242	Eppendorf
Mini-PROTEAN Tetra Cell	Bio-Rad
MJ Research Peltier Thermal Cycler Tetrad	Bio-Rad
MJResearch Peltier Thermal Cycler PTC-200	Bio-Rad
Multipipette Stream	Eppendorf, Hamburg
Neubauer chamber - Cell counter	Schubert und Weis, Munich
Optical microscope	Optech, Canada
pH-meter	Eutech Instruments, The Netherlands
Photometer, GeneQuant II	Pharmacia Biotech, USA
Pipette controller	Brand, Wertheim
Pipettes (2 µl, 20 µl, 200 µl, 1000 µl)	Eppendorf, Hamburg
Power supply for gel chamber electrophoresis	MRC, Israel
StuartTM Scientific roller mixer	Stuart Scientific, UK
Thermo mixer	Eppendorf, Hamburg
UV illuminator	Intas, Gottingen
Vortex mixers	VELP Scientifica, Italy
Water bath	Memmert, Schwabach

3 Results

3.1 Overview of the research rationale

Studying the state of cellular dormancy in DCCs from breast cancer patients required addressing the following aspects, (i) modeling *in vitro* the conditions in which dormant cells survive, (ii) gene expression profiling of dormant DCCs and (iii) analyses of the pathways relevant for tumor cell dormancy. Most important was to find the appropriate *in vivo* and *in vitro* model(s). Therefore, previously published models were tested and adapted, and novel methodological strategies and approaches had to be developed and previously published models were tested and adapted. After having identified the ´best suited` model inducing dormancy in single cells, molecular analyses were performed resulting in distinct "stem cell" and "dormancy" gene signatures. Further pathway analysis followed by functional analysis revealed the involvement of an inflammatory signaling pathway in controlling cell hierarchy and stem cell function. The key steps of my investigation and workflow are outlined in the Figure 7.

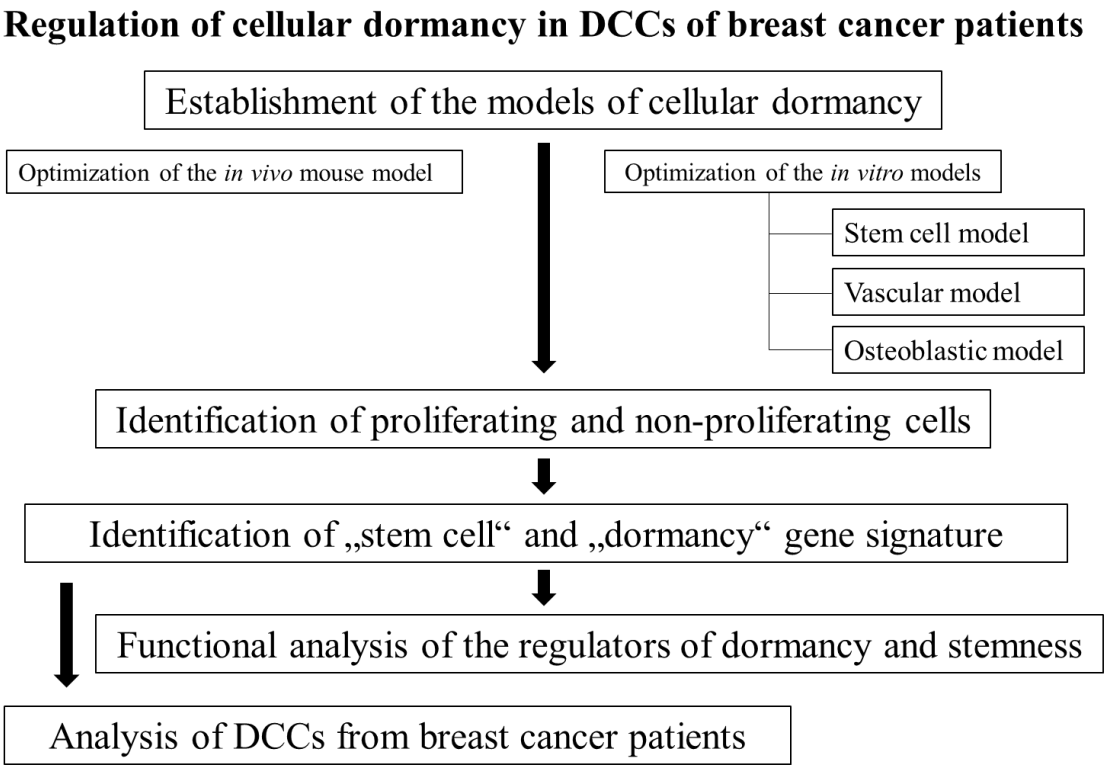

Figure 7: Workflow outlining steps of investigation of dormancy in DCCs from breast cancer patients.

3.2 Balb-NeuT as an *in vivo* model of tumor cell dormancy

3.2.1 Short background information of previous work with the Balb-NeuT model as the starting point of the experiments

In some breast cancer patients DCCs are detected in the BM at the time of the primary tumor removal, and can be detected in post-operative BM biopsies, but these patients never develop metastases. Similar is seen in Balb-NeuT mouse model, which was extensively studied in our group in previous years. DCCs can be detected in the BM of the very young transgenic mice and they stay there and do not proliferate over the whole lifespan, but they stay dormant. Opposite to BM-DCCs, in lung, which is another metastatic organ, DCCs were actively proliferating and gave rise to metastases. That prompted us to isolate and study dormant DCCs from Balb-NeuT mice and learn about the dormancy phenomenon. Relevant literature and previous results needed for understanding *in vivo* experiments in my work are summarized in next few pages.

Balb-NeuT mice express rat *Her2* (*NeuT*) oncogene in a Balb/c background under the control of the mouse mammary tumor virus (MMTV) promoter (Cornelissen et al., 2014; Pannellini et al., 2004). In this model (1) independent tumors develop in each of the 10 mammary glands; (2) breast tumor development is followed by dissemination of cancer cells to lung and bone marrow; (3) lung metastases are found in later stages of tumor development. The MMTV promoter is activated by progesterone, therefore expression of the transgene starts around the age of 4 weeks and disseminated cancer cells (DCC) can be detected in the bone marrow of mice shortly after activation of the *Her2*-transgene (Husemann et al., 2008). At this time point the mammary ducts are not yet completely formed, but increased proliferation can be detected in them. From the sixth week on expanding buds completely form mammary ducts and give rise to atypical ductal hyperplasia (ADH). As of week 13, carcinoma *in situ* can be detected by manual palpation. These lesions become invasive around week 19, while overt metastases can be detected in lungs as of week 26 (Figure 8).

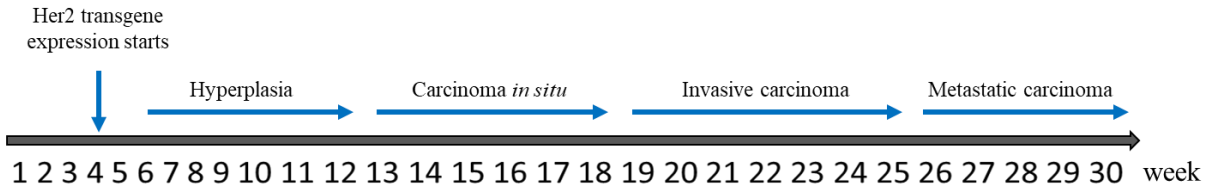

Figure 8: Development of mammary tumors in Balb-NeuT mice over life time. From the 4th week of life production of progesterone and consequently activation of the MMTV promotor and *Her2* transgene expression starts. Protein product of NeuT transgene is constitutively active inducing hyperproliferation and development of mammary tumors as described on the time line (Husemann et al., 2008)

DCCs in bone do not give rise to metastases but stay solitary over the whole life time of mice. Therefore, the lung is considered the permissive environment supporting the outgrowth of DCCs and bone marrow is the non-permissive niche that imposes the quiescent state.

DCCs are detected as cytokeratin (CK)- or Her2-expressing cells among the peripheral blood leucocytes (PBLs) isolated from the bone marrow samples of analyzed mouse models. Dissemination was shown to occur early during breast cancer development, in Balb-NeuT model already at the age of 4 weeks (Figure 9) (Hosseini et al., 2016a). No change in the number of CK+ and Her2+ cells in the bone marrow of Balb-NeuT mice was observed from the early stage of cancer development (week 4) up to the stage of invasive carcinoma (week 27-30) (Figure 9) indicating the existence of the mechanism that prevents outgrowth of these cells and keeps them in the state of dormancy.

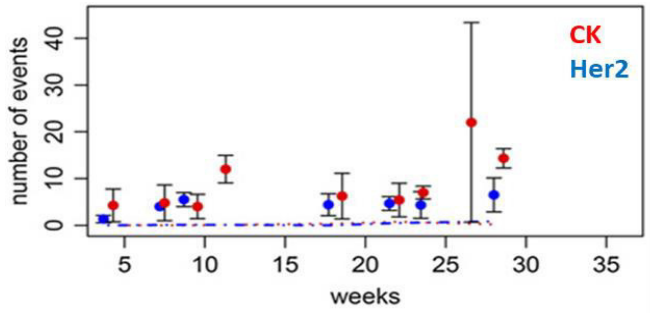

Figure 9: Number of CK+ (red dots) and HER-2+ (blue dots) cells detected per 500.000 cells isolated from the bone marrow of Balb-NeuT mice. Dashed blue-red line marks the result of the analysis of non-transgenic control mice (Husemann et al., 2008)

Mammary origin of the DCCs in the bone marrow was proved using the transplantation model. Single mammary glands were transplanted from young transgenic donors (3- to 12-week old) to 3-week old wild-type siblings (Balb/c mice) and 7-26 weeks later their bone marrow was examined for the presence of CK+ and Her2+ DCCs. Total number of DCCs detected in the bone marrow of recipients of the transgenic mammary gland animals was significantly lower than in transgenic mice (Figure 10A), which is most likely a consequence of seeding from only one transplanted mammary gland, opposite to ten mammary tumors in Balb-NeuT mice. Analogous to the transgenic model, the number of DCCs detected in the bone marrow of transplantation model did not change during progression of primary tumor (Figure 10B) confirming the existence of mechanism controlling the progression of DCCs in the bone marrow.

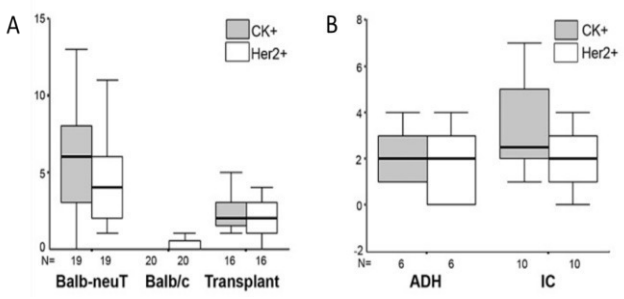

Figure 10: Number of CK+ and HER-2+ cells detected per 500.000 cells isolated from the bone marrow of (A) Balb-NeuT, Balb/c (controls) and recipients of transgenic mammary gland. (B) Box plots representing the number of DCCs detected in the bone marrow of recipients of the transgenic mammary gland at the different phases of tumor development (Atypical ductal hyperplasia, ADH and invasive carcinoma, IC) (Husemann et al., 2008).

In both, CK+ and Her2+ cells isolated from bone marrow of different mouse models, multiple chromosomal aberrations were detected by CGH analysis, confirming their malignant origin. Phylogenetic analysis in the Balb-NeuT model showed that 79,5% of lung metastases originate from

the cancer cells that leave the primary site in the early phases of tumor development (early DCCs) (Hosseini et al., 2016a). The mechanism of an early dissemination of cancer cells was addressed in the work of Hosseini and colleagues (Hosseini et al., 2016a) who found that the same signals activate different responses in the non-advanced cells from early cancerous lesions and in advanced primary tumor cells. Progesterone induced signaling mediated by Wnt and RANKL, induces migrating and stem-like phenotype (determined as a capability of sphere formation) in cells from early cancerous lesions (Figure 11), but in advanced tumor cells it induces proliferation. This switch is found to be regulated by increased Her2 expression and tumor-cell density. Analysis of human DCCs isolated from the bone marrow of breast cancer patients, whose malignant origin was confirmed by CHG analysis, showed that none of 26 analyzed cells displayed progesterone receptor, confirming the lack of the signaling that induces its outgrowth (Hosseini et al., 2016a). This confirmed the findings from Balb-NeuT model can also be applied to humans.

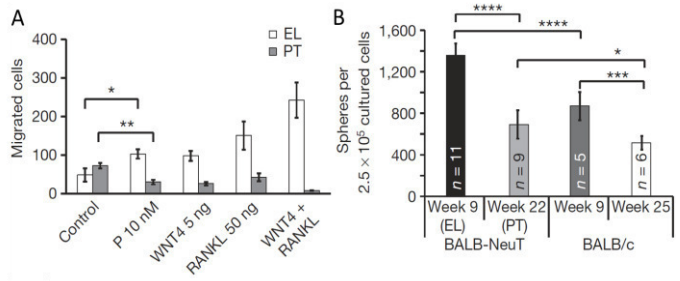

Figure 11: Progesterone induces migration and sphere formation of early lesion cells. (A) Early lesion and primary tumor cells respond to progesterone or its mediators (WNT4, RANKL) with increased (early lesions, EL) or decreased (primary tumors, PT) migration. (B) Mammosphere formation depends on the age of the mice (Hosseini et al., 2016a).

In the search for the mechanisms to "wake up" dormant DCCs, Hüsemann and colleagues transplanted the bone marrow of young Balb-NeuT mice (9 weeks) to lethally irradiated age mated Balb/c recipients what resulted in an outgrowth of the dormant DCCs that exist within transplanted bone marrow cells and led to the development of the bone marrow carcinosis (10-31% of CK+ cells in bone marrow) within 19-22 weeks upon transplantation ((Husemann et al., 2008), Figure 12).

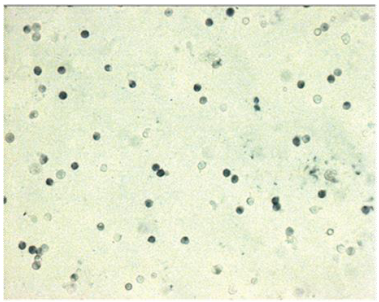

Donor			Recipient		
identifier	CK+ cells / 0.5 X 10^6 BM cells	absolute number of transplanted tumor cells	identifier	Weeks after transplantation	Percentage of CK+ cells in BM
D-1	11	154	M1-1	22	**19,71**
		154	M1-2	20	*
		154	M1-3	20	*
		154	M1-4	20	*
D-2	12	240	M2-1	22	**22,21**
		240	M2-2	22	**30,20**
		240	M2-3	22	**15,51**
		240	M2-4	20	*
D-3	4	80	M3-1	19	**31,40**
		80	M3-2	19	**28,01**
		80	M3-3	19	**10,39**
C-1 (wild-type)	0	0	C1-1	19	**0**
		0	C1-2	28	**0**
		0	C1-3	43	**0**

* not available because mice were found dead before analysis

Figure 12: Balb-NeuT bone marrow transplantation to Balb/c recipients induces outgrowth of DCCs inducing bone marrow carcinosis. Data from Hüsemann et al. Bone marrow was taken from three donor mice (D-1 to D-3). At the time of transplantation cells suspension frombone marrow was applied on glass slides, which were later stained using anti-CK antibody. The number of CK+ cells was used for calculation of the absolute number of transplanted DCCs. All recipients of the bone marrow from transgene mice (M1-1 to M3-3) were sacrificed 19-22 weeks after transplantation when first signs of disease were detected. The percentage of CK+ cells was determined also by CK-staining of bone marrow cell suspension applied to glass slides.

Having in mind all these findings we decided to use the transplantation model in which we isolated mammary tissue from young Balb-NeuT female mice, cultured cells as mammospheres (i.e. in anchorage independent conditions) and transplanted them to age matched wild type (wt) siblings. The goal of our work is to model human disease. Therefore, we aimed to isolate and analyze human and mouse DCCs from the analogous stages of disease. As the isolated DCCs in our collective originate from the bone marrow of patients, we wanted to get cancer cells from the same distant organ of our mouse model. For this purpose we used only DCCs isolated from bone marrow of transplanted mouse models.

3.2.2 Search for good candidate marker for isolation of BM-DCCs

In described analyses, DCCs were detected by CK staining, which is unsuitable method for isolation of living cells, which we aimed. To detect disseminated cancer cells in our model, we used GFP as a marker to label mammary cancer cells before transplantation to wt recipients. Transduction of the intact spheres resulted in lower efficiency than transduction of disaggregated spheres with 7% and 21% of GFP^+ cells, respectively (Figure 13) in cells derived from second generation mammospheres.

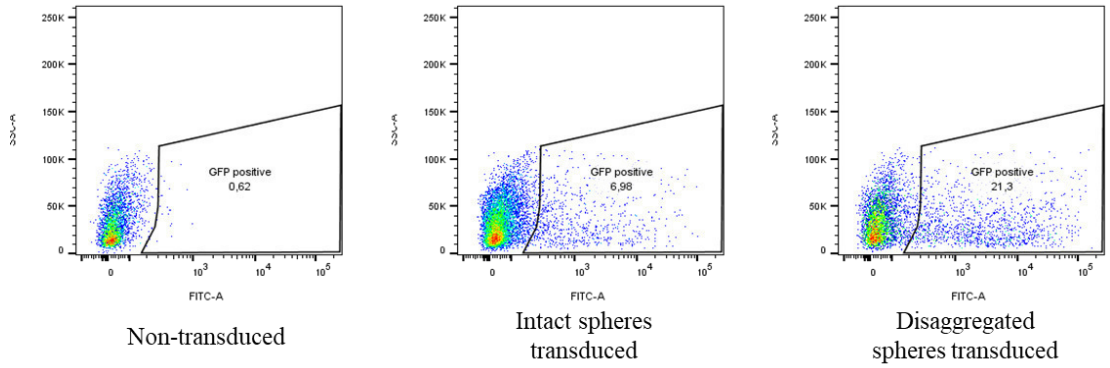

Figure 13: In a pilot experiment Balb/c-NeuT-derived mammospheres were transduced with pRRL-CMV-GFP virus in two different ways: (i) Intact primary mammospheres were transduced or (ii) primary mammospheres were disaggregated to single cells and then transduced. Efficiency of transduction was determined by FACS as percentage of GFP^+ cells in disaggregated second generation mammospheres.

Next, we transplanted GFP-labeled ADH-derived mammospheres to wt recipients (Figure 14) at the age of 4-6 weeks. After 8 weeks no tumor formation was detected in any recipient and no GFP^+ cells were found in the bone marrow of recipients. These data are consistent with observations that GFP is highly immunogenic in Balb/c mice, meaning that GFP marked cells do not survive and cannot be accurately traced over time when transplanted to Balb/c recipients (Ansari et al., 2016; Gambotto et al., 2000).

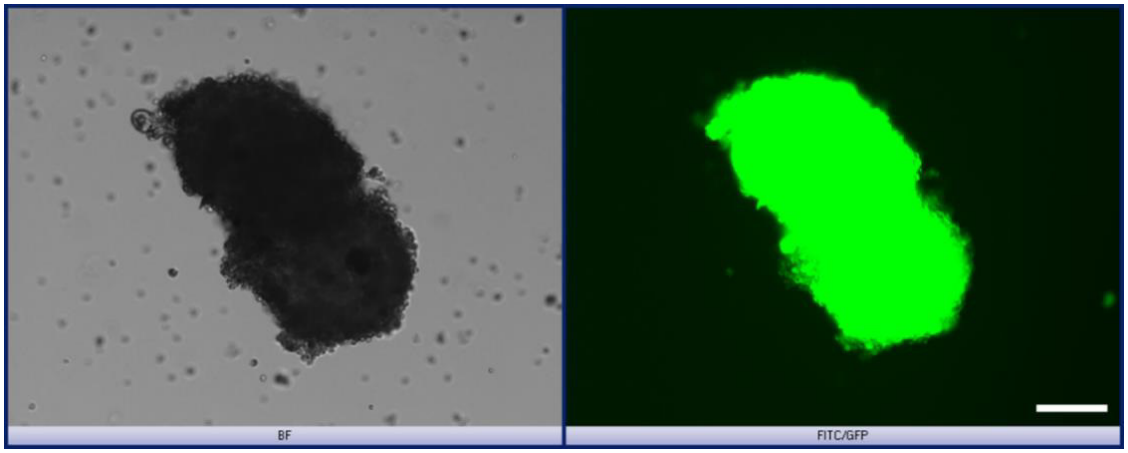

Figure 14: GFP-labeled mammosphere: Mammary cells were isolated from a young Balb-NeuT donor (8 weeks) and propagated in anchorage independent conditions. After 12 days spheres were disaggregated, transduced with pRRL-CMV-GFP virus and propagated for additional 16 days. Scale bar 100µm.

To avoid immune rejection, we transplanted GFP-labeled ADH-derived mammospheres into NSG mice and waited for 8 weeks. Primary tumors were detected in the fat pad of the recipients with an increase in tumor formation rate upon implantation of a progesterone pellet. In the group that received progesterone all mice (n=3) developed tumors opposite to the control group (n=3), where very small tumor was detected in only one out of three recipients (Table 2). We also noticed that in the group treated with progesterone, detected primary tumors were also bigger.

Table 2: Summarized data of mice transplanted with GFP-labeled mammospheres

	Treatment	Number of mice	Age at time of transplantation (weeks)	Period between transplantation and sacrifice (weeks)	Number of mice in which primary tumor was detected
Balb/c recipients	Control	n = 5	4-6	4 and 8	0/3
	Progesterone	n = 6	5-6	4 and 8	0/3
NSG recipients	Control	n = 3	6	8	1/3 (very small)
	Progesterone	n = 3	6	8	3/3

Analysis of the $CD45^-$ subset of bone marrow cells of Balb/c and NSG recipients displayed no GFP^+ tumor cells. From this we concluded that dissemination of mammosphere derived cells to BM did not occur over the course of four weeks. Hence, we decided to look for a new approach and chose look for another marker for detection and isolation of DCCs from bone marrow samples.

3.2.3 Improvement of detection and isolation of DCCs from the bone marrow

Since GFP labeling of the cancer cells in transplantation models did not enable isolation of living DCCs, we focused again on our Balb-NeuT model. Epithelial cell adhesion molecule (EpCAM) is regularly used as a marker for selection and isolation of living DCCs from bone marrow of cancer patients. EpCAM-positive ($EpCAM^+$) cells are found not only in bone marrow samples of cancer patients, but also in the bone marrow of people without any evidence for tumor presence (Guzvic et al., 2014). Still many studies showed that increased EpCAM expression is associated with poor prognosis in different cancers, amongst others breast cancer (Cimino et al., 2010) which makes it the best of all known markers for detection of tumor cells of epithelial origin in predominantly mesenchymal organs, such as bone marrow and lymph nodes. Similarly, although the number of $EpCAM^+$ cells is higher in the bone marrow of Balb-NeuT mice, they were also detected in wt Balb/c mice. The average fluorescent signal of all $EpCAM^+$ cells seems stronger in Balb-NeuT mice, but it cannot be used for true discrimination of DCCs and $EpCAM^+$ haematopoietic cells. Individual $EpCAM^+$ cells from BM of Balb/c and Balb-NeuT mice cannot be distinguished due to high variance of fluorescence intensity in both models (Figure 15).

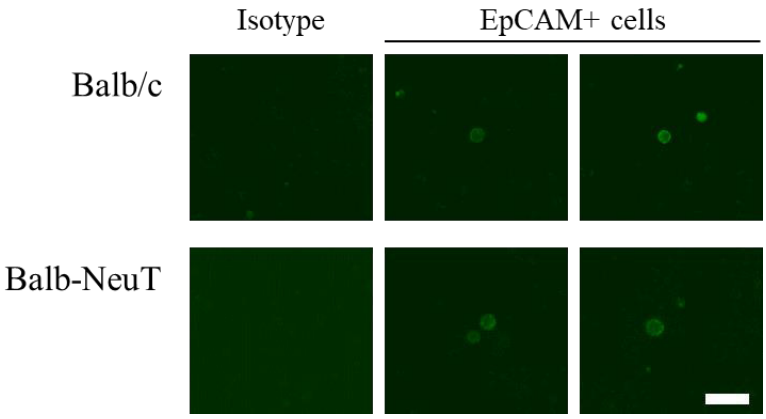

Figure 15: Detection of $EpCAM^+$ cells in bone marrow samples isolated from Balb/c and Balb-NeuT mice. Mononuclear bone marrow cells were isolated by centrifugation on 60% Percoll and stained using anti EpCAM antibody. No significant difference in terms of morphology and staining intensity was seen between cells isolated from wt and transgenic mice. Scale bar 20µm.

3.2.4 CD45 expression enables discrimination between DCCs and EpCAM-positive hematopoietic cells

In human samples, EpCAM is mainly expressed by epithelial cells, but some cells from the erythroid lineage also express it during early phases of their development (Choesmel et al., 2004). To investigate this in mice samples and to discriminate between epithelial $EpCAM^+$ cells and hematopoietic $EpCAM^+$ cells, we isolated bone marrow from Balb/c and Balb-NeuT mice of different age, separated $CD45^+$

from CD45$^-$ cells by CD45-depletion, stained both, CD45$^+$ and CD45$^-$ fractions using FITC conjugated anti-EpCAM antibody and picked EpCAM+ cells from both subsets of cells. No EpCAM$^+$ cells could be detected in the CD45$^-$ population of bone marrow cells of two Balb-NeuT and two Balb/c mice younger than 10 weeks. In the bone marrow of Balb-NeuT mice of 14 weeks and Balb/c mice of 13 weeks we detected and isolated both CD45$^+$/EpCAM$^+$ and CD45$^-$/EpCAM$^+$ cells. EpCAM$^+$ cells from the CD45$^+$ fraction had lower fluorescence intensity than EpCAM$^+$ cells from the CD45$^-$ fraction (Figure 16).

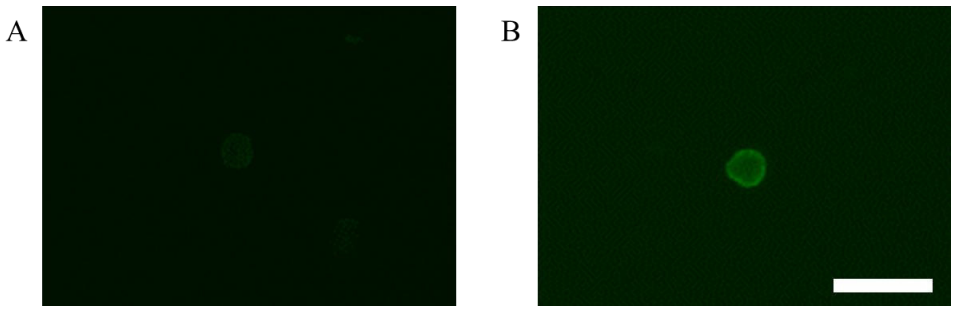

Figure 16: Isolation of EpCAM+ cells from CD45+ population (A) and CD45$^-$ population (B) isolated from bone marrow of Balb/c mice. Scale bar 20 µm.

To further profile "true" DCCs and discriminate them from hematopoietic EpCAM$^+$ cells we isolated: (i) 14 CD45$^+$/EpCAM$^+$ and 11 CD45$^-$/EpCAM$^+$ bone marrow cells from one Balb/c mouse and (ii) 20 CD45$^+$/EpCAM$^+$ and 29 CD45$^-$/EpCAM$^+$ bone marrow cells from two Balb-NeuT mice. Mice were 13-16 weeks old at the time of sacrifice. The cells with maximal quality of WTA products (7 CD45$^+$/EpCAM$^+$ and 9 CD45$^-$/EpCAM$^+$ cells from Balb/c mouse and 15 CD45$^+$/EpCAM$^+$ and 22 CD45$^-$/EpCAM$^+$ cells from Balb-NeuT mice) were analyzed using qPCR for CD45 expression to discriminate true hematopoietic from non-hematopoietic cells among picked ones. In cells isolated from Balb/c mice, CD45 mRNA was detected in 57% of CD45$^+$/EpCAM$^+$ cells but in none of CD45$^-$/EpCAM$^+$ cells (Table 3). In CD45$^+$/EpCAM$^+$ population 33% expressed CD45 mRNA, whereas in CD45$^-$/EpCAM$^+$ population only 4,5% did (Table 3).

Table 3: CD45 expression analysis in cells isolated from BM samples from Balb/c and Balb-NeuT mice. BM aspirates were divided using MACS depletion kit and from both, CD45$^+$ and CD45$^-$ fraction EpCAM$^+$ cells were picked and subjected to analysis of CD45 mRNA expression by qPCR

	Balb/c		Balb-NeuT	
	CD45$^+$/EpCAM$^+$	CD45$^-$/EpCAM$^+$	CD45$^+$/EpCAM$^+$	CD45$^-$/EpCAM$^+$
Analyzed BM cells	7	9	15	22
CD45$^+$ qPCR	4/7 (57%)	0/9 (0%)	5/15 (33%)	1/22 (4,5%)

Expression analysis of CD45 mRNA in CD45$^+$ and CD45$^-$ populations of bone marrow cells showed that MACS depletion accurately separates CD45-expressing cells from cells that do not express those

hematopoietic cell markers both in Balb/c (p=0,0192) and Balb-NeuT (p=0,0306) mice (Fischer's Exact test).

3.2.5 Effect of progesterone on dissemination of cancer cells in the Balb-NeuT mice

Having in mind that dissemination occurs very early to bone marrow of Balb-NeuT mice and progesterone upregulates Her2 expression and consequently increases migration rate in early lesion cells as shown in Figure 11Figure 11 (Hosseini et al., 2016a), we tried to increase the number of DCCs for isolation. Therefore, young Balb-NeuT mice (5-8 weeks) were treated with progesterone. However, after 4-8 weeks there was no significant difference in the number of EpCAM-positive cells in the $CD45^-$ fraction of bone marrow samples of control and treated mice (Figure 17).

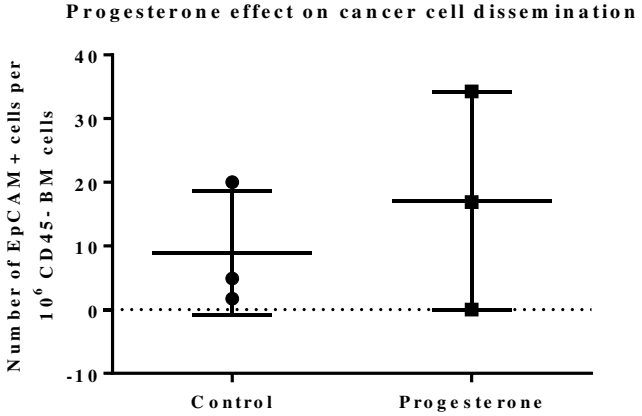

Figure 17: Number of detected $EpCAM^+$ cells in the bone marrow samples of Balb-NeuT mice upon progesterone treatment. n=3, Student´s t-test, p=0,512. All error bars correspond to standard deviation (Mean ±SD).

3.2.6 Bone marrow transplantation induces DCC outgrowth

In routine patient analysis, disseminated cancer cells are isolated from bone marrow of breast cancer patients undergoing removal of the tumor and detected based on expression of cytokeratins (for genome isolation and analysis) and EpCAM (for transcriptome and genome isolation and analysis). The number of cells detected in the bone marrow of Balb-NeuT mice over lifetime (from week 4 until week 25-30) remains stable (Hosseini et al., 2016a), confirming that they reside in a state of dormancy. Since the number of cells in the bone marrow is very low, we aimed to increase the number of DCCs in bone marrow and/or to increase cell isolation efficacy. Transplantation of the bone marrow of young Balb-NeuT mice (9 weeks) to lethally irradiated age matched Balb/c recipients results in an outgrowth of the dormant DCCs that exist within transplanted bone marrow cells and leads to bone marrow carcinosis (10-31% of CK^+ cells in bone marrow) within 19-22 weeks upon transplantation (Husemann et al.,

2008). We aimed to increase the number of dormant DCCs in our collective and decided to utilize this approach for DCC enrichment.

We lethally irradiated young Balb/c and NSG recipients and transplanted them with bone marrow of 9-week-old Balb-NeuT donors (Figure 18).

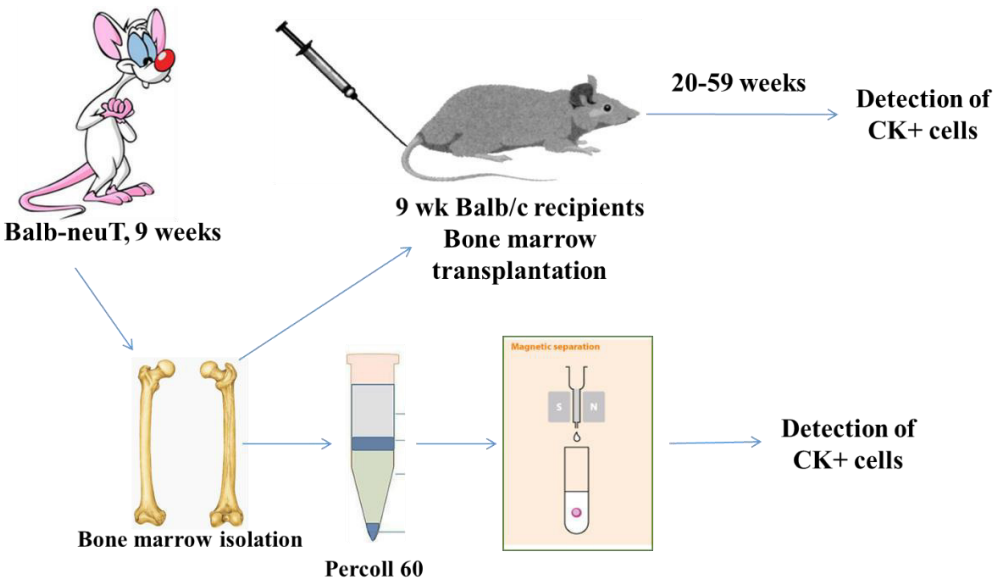

Figure 18: Scheme of bone marrow carcinosis experiment: Bone marrow of 9 week old Balb-NeuT mice was isolated and transplanted to lethally irradiated age matched Balb/c mice. Starting from week 20 after transplantation recipient mice were sacrificed and the frequency of CK^+ cells in bone marrow was determined.

No recipient showed any sign of bone marrow disease 20 weeks after transplantation. The number of CK^+ cells in the bone marrow of sacrificed recipients was in range of the number of CK+ cells in donors (few cells per 10^6 bone marrow cells) which was much lower (Table 4) than in the initial experiments (0-120 vs. 80-240 CK^+ cells per recipient) questioning either immunohistochemical staining or dissemination.

Table 4: Calculated number of CK+ DCCs transplanted to Balb/c and NSG recipients

Balb/c recipients non-depleted BM		**NSG recipients non-depleted BM**		**Balb/c recipients depleted BM**	
Balb-NeuT donor	Number of DCCs in transplanted 10^7 cells	Balb-NeuT donor	Number of DCCs in transplanted 10^7 cells	Balb-NeuT donor	Number of DCCs in transplanted 10^7 cells
4852	20	6269	0	CD45- pool of BM cells	98
4853	0	6253	0		
4854	0	4851	20		

None of the recipient mice developed any symptoms of bone marrow disease. They were all sacrificed by week 58 (NSG) or 59 (Balb/c) after transplantation, but none of them showed an increase in the number of CK^+ cells in the bone marrow. The fact that mice did not develop BM carcinosis supports our hypothesis that an impaired dissemination is a possible reason for decreased number of transplanted DCCs.

Since the number of transplanted CK^+ DCCs was around 10 times lower than in previous work published by Hüsemann, Geigl et al., we depleted $CD45^+$ cells from pooled bone marrow of 9 donors (11 weeks old) and transplanted them into Balb/c recipients (Figure 19) to increase the number of transplanted DCCs. Hematopoietic cells are competing with cancer cells for homing to bone marrow niches, as shown in prostate cancer (Shiozawa et al., 2011). Therefore, we decided to give an advantage to cancer cells by dividing bone marrow cells into two populations, $CD45^+$ and $CD45^-$ and injecting $CD45^-$ cells a day before the rest of bone marrow cells, the $CD45^+$ fraction. Although we seemingly reached a higher number of transplanted DCCs (98 DCCs vs. 80-240 CK^+ cells per recipient, Table 4), recipient mice did not develop bone marrow disease by the time of sacrifice of the last recipient, 36 weeks after transplantation. All these findings confirmed the hypothesis that dissemination of cancer cells is impaired.

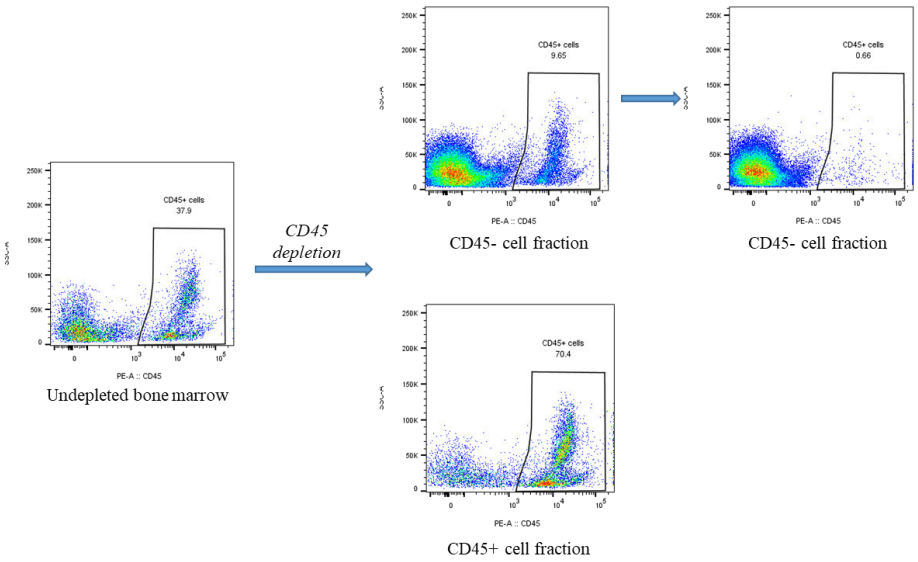

Figure 19: Enrichment of bone marrow with DCCs: Pool of bone marrow samples from 9 mice was subjected to CD45 depletion using two MACS columns. After the first column, purity of $CD45^-$ fraction was not high enough (90%). However, after the second column the fraction consisted of 99% of $CD45^-$ cells. This "pure" $CD45^-$ population was injected to Balb/c recipients.

3.2.7 Analysis of DCCs in the lungs of BM recipient mice

Dissemination was shown to occur not only from primary tumor to blood and distant organs, but also in opposite direction when CTC can colonize their tumors of origin (Kim et al., 2009). To investigate whether cancer cells transplanted with bone marrow of Balb-NeuT donors via tail vain can colonize other organs, we analyzed the lungs of the recipient mice, while lung is, next to bone the organ that is most frequently colonized by mammary cancer cells. Using Her2 as a marker for DCCs, we were not able to detect any $Her2^+$ cells in any of the analyzed samples (Figure 20), indicating either impaired survival or colonizing ability of the transplanted DCCs or their absence in transplanted bone marrow.

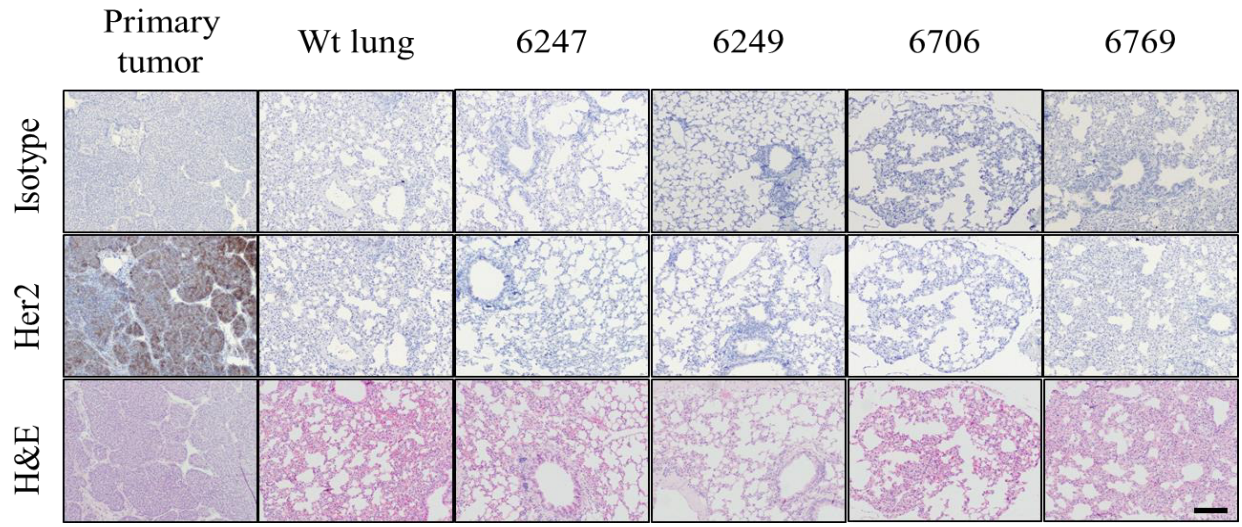

Figure 20: Her2 staining of the lungs of recipients of BM from transgenic mice. Mice were sacrificed 20-36 weeks after transplantation. Primary tumor is a positive control and wt lung is negative control. Mice 6247 and 6249 are Balb/c recipients of naïve BM of Balb-NeuT donors, 6706 is a Balb/c recipient of enriched BM cell suspension and 6769 is NSG recipient of naïve BM of Balb-NeuT mice. From each mouse ten sections of 5µm were cut. Three sections (sections 1, 5 and 10) from each mouse were analyzed. Scale bar 100µm.

3.2.8 *In vitro* expansion of the mouse DCCs isolated from bone marrow

Knowing that patients without detectable DCCs can develop metastases (Braun et al., 2005; Mansi et al., 1999), we concluded that some of the metastasis founder cells lack markers which are routinely used for their detection and isolation. To minimize the chance of missing these cells, we depleted $CD45^+$ cells from the bone marrow samples of young Balb-NeuT mice and cultured the remaining negative fraction cells in ultra-low attachment plates, promoting the growth of cells with stem cell properties. Neither the naïve population (non-depleted BM cells) from Balb/c and Balb-NeuT mice, nor the depleted cell population cultured in anchorage independent conditions gave rise to mammospheres. We initially applied the medium broadly used for mammosphere culture (MEBM supplemented with insulin, heparin, B27, EGF and bFGF) (Dontu et al., 2003), which did not result in growth of mammospheres. We mined the literature and looked for the factors to promote mammary stem cell growth and supplemented the medium with different cytokines whose potent mitogenic effect was already shown, such as growth-related oncogene-α (GRO-α) (Bhat et al., 2017; Smith et al., 1995), HIL-6 (Aden et al., 2016; Grivennikov et al., 2009) and a combination of Wnt4 and receptor activator of nuclear factor kappa-B ligand (RANKL) (Hosseini et al., 2016a). GRO-α belongs to the CXCL1 family of chemokines and is known to have a potent mitogenic effect on the neighboring cells especially on premalignant epithelial cells (Coppe et al., 2010). IL-6 is a pro-inflammatory cytokine known to play a role in cell proliferation. It signals through two membrane bound receptors, specific IL-6R, and ubiquitously expressed non-specific gp130 that is bound to the activated IL-6R and transduces the signal to the cell. Hyper IL-6 (HIL-6) is a fusion protein, consisting of IL-6 and soluble IL-6R. While it already contains the specific part of the receptor it can also bind to the unspecific transducer, gp130 and

stimulate cells that do not express IL-6R (Fischer et al., 1997). Wnt4 (cytokine from WNT family, regulates female reproductive system development in human) and RANKL (a member of the tumor necrosis factor cytokine family binds to RANK on cells of the myeloid lineage and functions as a key factor for osteoclast differentiation and activation, but also regulates cell survival, proliferation, and has a role in immune system) are found to be main mediators of progesterone mitogenic and migratory effect in mammary cells (Hosseini et al., 2016a). Unfortunately supplementing the sphere cultures with any of these cytokines did not induce growth of the mammospheres. After 7, 10 and 15 days of culture no spheres were detected (Table 5).

Table 5: Number of mammospheres and single cells in cultures from CD45-depleted bone marrow cells. Experiment with each mouse model performed once, in triplicates. Number of cells shows the range of detected survived single cells per plate.

	Spheres (days 7, 10 and 15)				Single cells (day 10)	
	Sphere medium	GRO-a	HIL-6	GRO-a + Wnt4 + RANKL	GRO-a	GRO-a + Wnt4 + RANKL
Balb/c	0	0	0	0	NA	NA
Balb-NeuT	0	0	0	0	NA	NA
Metastatic mouse	0	0	0	0	7-10	10-12

To increase the chances of finding cancer cells in bone marrow we isolated the bone marrow from mice with overt metastases in the lung. The $CD45^-$ fraction of the bone marrow was cultured in media with and without GRO-α and a combination of Wnt4 and RANKL (WR). We did not detect any spheres in these cultures, but at day 10 we could observe some surviving single cells whose number was increased in WR supplemented cultures (Table 5). On day 15 no more single cells could be detected. We concluded that stimulatory effect of Wnt4 and RANKL does not promote growth of murine BM cells in 3D conditions but might increase survival of $CD45^-$ cells isolated from the bone marrow of metastatic mice.

3.2.9 Effect of Collagen I on sphere forming ability of mammary cells

The most abundant extracellular protein in bones is collagen I that was shown to greatly enhance the capacity of ErbB2 cells (primary tumor cells isolated from the mammary tumor of MMTV-Neu(YD) mice, with a wild-type form of rat Neu under the control of the CMV promoter) (Guo et al., 2006) to form primary and secondary tumor spheres (Gao et al., 2016). We aimed to investigate its effect to mammary cells upon entering the BM. Therefore, we supplemented the mammosphere medium with collagen I and examined tumor sphere formation in our mouse model with *Her2* driving oncogene. Single cells from mammary gland of Balb/c mouse and Balb-NeuT mice of different age were isolated and propagated in sphere medium with and without addition of collagen I. There was no significant difference in the number of mammospheres seeded in medium with collagen I compared to control for

any of the tested mice, meaning that neither cells from normal mammary gland, nor early lesion cells nor cells isolated from mammary tumors could be activated by collagen I (Figure 21).

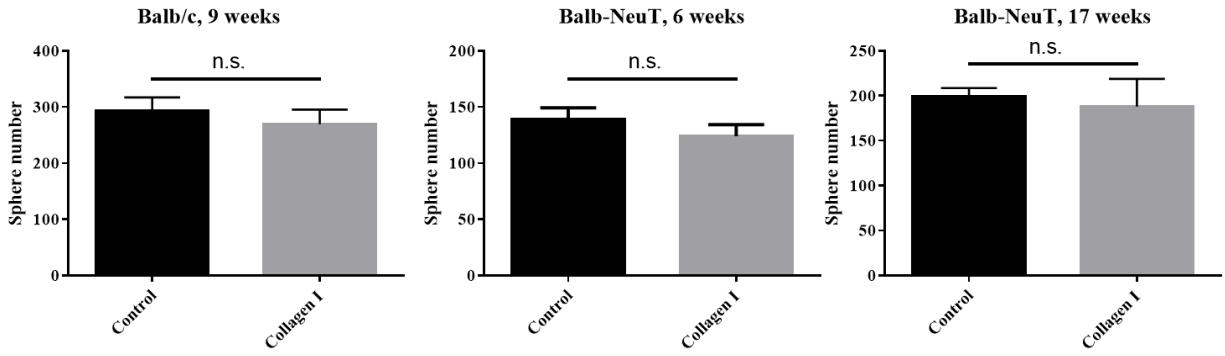

Figure 21: Collagen I treatment does not affect sphere formation of mammary cells from normal mammary tissue, early hyperplastic lesion and mammary tumors. Student's t-test. non-significant. All error bars correspond to standard deviation (Mean ±SD).

All different approaches we applied in our intensive *in vivo* work resulted in findings, which all brought us to one conclusion: Dissemination of cancer cells to BM is impaired, resulting in no DCCs in BM of Balb-NeuT mice.

Encountering the problems in the finding and isolation of single dormant cancer cells from *in vivo* models, we next focused on establishing *in vitro* models of dormancy.

3.3 Establishment of the *in vitro* models of tumor cell dormancy

Not being able to isolate DCCs from the BM of Balb-NeuT and transplantation model, we focused on *in vitro* models. Since DCCs in our collective originate from BM samples of breast cancer patients, we aimed to model these conditions and examine the effect of BM environment on mammary cells. Bone marrow environment comprises different subniches (osteoblastic, endothelial, and mesenchymal) consisting predominantly of hematopoietic cells, osteoblastic cells (OBs), mesenchymal stromal cells (MSCs) and endothelial cells that form blood vessels. All these cells release a myriad of different factors affecting the surrounding cells. We aimed to examine the influence of these different cells and niches on DCCs behavior.

3.3.1 Implementation of the "stem cell model" for isolating dormant and proliferative epithelial cells from human mammary gland

In the mammary gland one can discriminate stem and differentiated cells in the pool of mammary cells. These cells go through different phases during development. All differentiated cells originate from the stem cells, which in physiological conditions reside in a quiescent state (Cheung and Rando, 2013; LaBarge et al., 2007). Extracellular signals (mostly hormone signals during menstrual cycle or pregnancy) activate them and induce proliferation. Stem cell consequently divides once, gives progenitor cell and renews itself. This new stem cell re-enters the quiescent state. We aimed to analyze the quiescence associated to stemness and apply the analyzed results to patient derived DCCs.

3.3.2 Overview of samples derived from mammary reduction surgeries

Traditionally cell lines are used to study development of both normal mammary gland and breast cancer. With improvement of the techniques for isolation and propagation of the cells *in vitro* primary cells became prevalent models for studying the biology of mammary gland, using isolated cells from patients who underwent reduction mammoplasty. The drawback of this method is still the low viability of the isolated cells. To maximize the efficiency of cell isolation and improve viability we used a protocol performing slow digestion and differential centrifugation that was recently shown to result in the best yield and viability of cells isolated from human mammary gland (Zubeldia-Plazaola et al., 2015).

For detection and isolation of single dormant cells we adapted the protocol in use for human mammary stem cell isolation. In brief, mammary tissues obtained from healthy donors that underwent reduction mammoplasty were first examined by a pathologist. Tissues suspected to have some neoplastic changes were not further processed, while the ones in which the absence of such changes was confirmed, were mechanically and enzymatically digested, centrifuged with differential centrifugation steps resulting in

separation of epithelial cells from fibroblasts and labeled with PKH26, a cell proliferation tracking dye. Cells which proliferate only limited number of times retain the PKH26 labeling (label retaining cells, LRCs) and can therefore be discriminated and separated from the cells that proliferate more and do not retain the labeling (proliferating non-label retaining cells, nLRCs). Epithelial cells were then propagated for 7 days in anchorage independent conditions. These conditions favor the growth of early progenitor/stem cells and enable removal of anchorage-dependent fibroblasts which escape anoikis only in the presence of serum (Koechli et al., 1994; McGill et al., 1997). After 7 days of culture, mammospheres and single cells were separated, and cell proliferation was estimated by the intensity of PKH26 fluorescence. Single non-proliferating cells (quiescent single cells, QSCs) were picked and the mammospheres were dissociated and cultured for additional 7 days. Second generation mammospheres were disaggregated and LRCs and nLRCs were manually picked for further molecular analyses. This strategy is depicted in Figure 22.

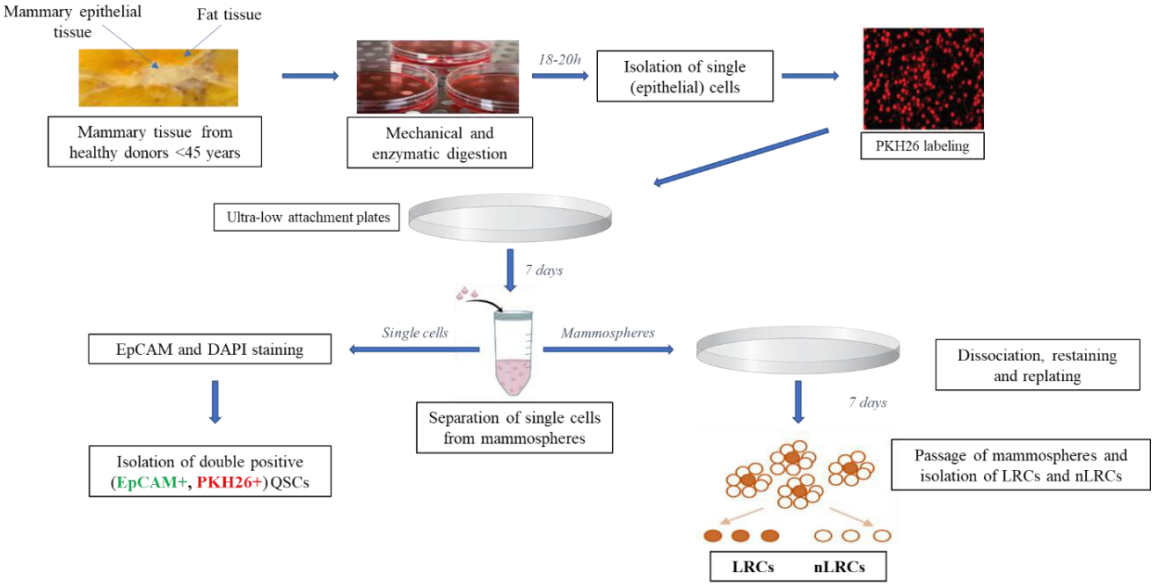

Figure 22: Schematic overview of isolation and propagation of human mammary epithelial cells (HMEC)

Cell isolation efficiency was not the only complication that was encountered during our work. The majority of the obtained samples could not be used for several reasons: (1) patient samples were delivered to us in semi sterile conditions which resulted in contamination *in vitro*, (2) some of the samples did not give rise to mammospheres, but they were forming clusters and (3) adult stem cells, which we aim to isolate, are very rare among the HMECs and their function decreases with age (Behrens et al., 2014; Pollina and Brunet, 2011; Wu et al., 2016). Therefore, exclusion criterion was the age of a donor above 45 years at the time of surgery.

From a total number of 32 obtained samples 13 gave rise to spheres; in 9 of them only clusters could be detected in the second generation of spheres or in both; 4 samples came in inadequate conditions (in formalin or in unsterile bags); in 3 of them contamination was seen in days after HMECs isolation and from 3 of them only a non-sufficient number of cells could be isolated for downstream assays (Figure

23). In the cases where only clusters were detected after 7 days of cultivation we could not judge whether they were a result of cell division or clustering and therefore these samples were excluded from our study. Overall, 13 out of 32 samples deriving from patients younger than age 45 (37,5%) gave rise to mammospheres and were used for further assays and analyses.

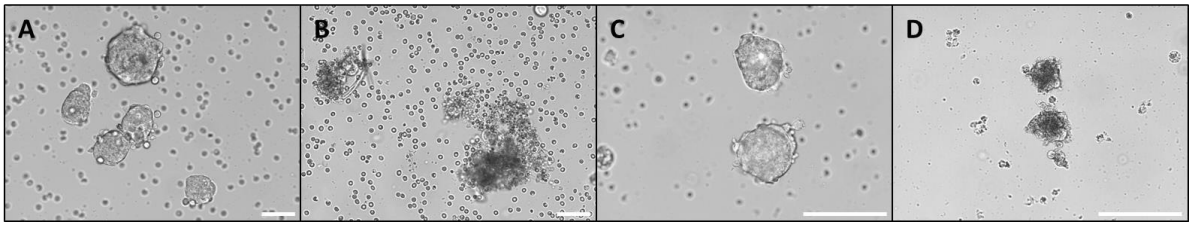

Figure 23: Examples of the sphere growth in the samples from different donors. Mammary tissue sample gave rise to the regular mammospheres in first generation (A) and to clusters in second generation (B). Mammary tissue sample giving rise to the regular mammospheres in both, first (C) and second (D) generation. Scale bar 50 µm.

3.3.3 Optimization of the cell labeling procedure

Stem cells reside in a quiescent state until stimulated with some extracellular signal, which induces their proliferation. For tracking the proliferation in specific cells fluorescent dyes are intensively used. They unspecifically label cytoplasmic proteins or cell membrane and are equally distributed to daughter cells upon division. For precise tracking of proliferation appropriate cell tracking dye had to be chosen and its optimal concentration needed to be determined.

The "gold standard" among cell tracking dyes in proliferation analysis is CFSE (carboxyfluorescein diacetate succinimidyl ester) which easily crosses the plasma membrane, enters the cell and gives an amine-reactive product that binds to intracellular proteins and produces detectable fluorescence. In parallel with CFSE we tested PKH26, a more general membrane labeling dye. PKH26 is a lipophilic dye that stably incorporates into the lipid regions of the cell membrane and emits strong fluorescence. We labeled half of the isolated cells from one sample with each of these dyes and seeded them in ultra-low attachment plates. On the first day after cell labeling the cultures were observed and we detected a more homogeneous staining within the cell population labeled with CFSE. Cells were propagated as described in Figure 22 and QSCs, LRCs and nLRCs were isolated at day 7 and day 14. Whole transcriptome was isolated and amplified from each isolated cell, followed by the quality control (QC) (Figure 24). Cells expressing 2 or 3 out of 3 tested transcripts of housekeeping genes were classified as “good quality cells” whereas those with 0 or 1 expressed genes were classified as “bad quality cells”.

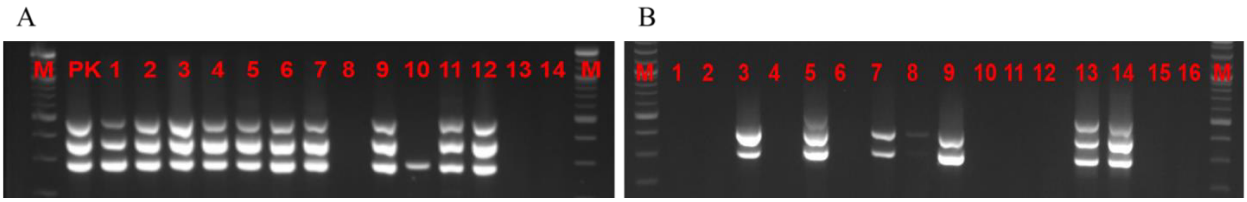

Figure 24: Visualization of GAPDH (up), ACTB and EF-1α (down) gene expression in cells initially labeled with (A) PKH26: 1-12: isolated single cells, 13-14: Negative controls; M – DNA-ladder and (B) CFSE: 1-12: isolated single cells, 13-14: Single cell pools, 15-16: Negative controls; M – DNA-ladder.

Although CFSE displayed a more homogeneous staining, the quality of WTA products of isolated cells was significantly better in PKH26 labeled cells (Figure 25). Therefore, PKH26 labeling was chosen for further experiments.

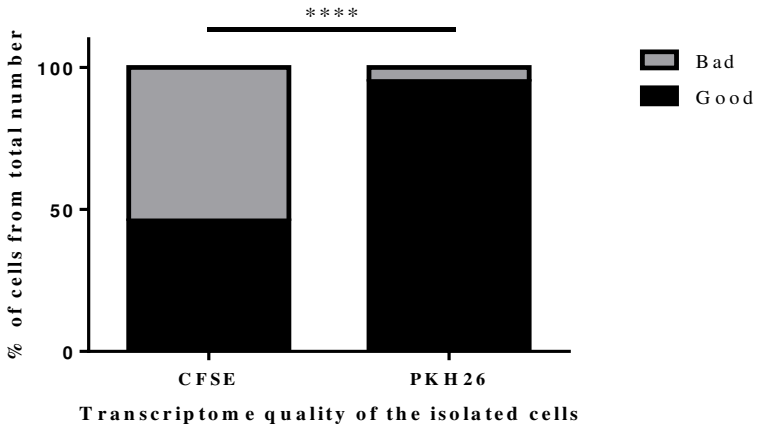

Figure 25: Quality of the WTA products of isolated cell depends on the cell labeling tracker: CFSE labeled cells isolated 7 and 14 days after cultivation in anchorage independent conditions showed significantly lower quality of the WTA products (cells expressing 2-3 housekeeping genes have good quality, while those expressing only 0-1 genes have bad quality) than cells labeled with PKH26. Fisher's exact test, two-tailed, **** $p < 0{,}0001$.

Next, optimizing the concentration of the cell tracking dye was assessed, as the concentration of the PKH26 for cell labeling recommended by the vendor (2 μM) was too high and after two weeks all the cells in the culture were still showing a very strong fluorescent signal. Towards this end, it was necessary to find the optimal concentration that would result in proliferating cells completely diluting the dye after 14 days of *in vitro* culture, while quiescent cells would retain the dye. To define the optimal concentration, several dilutions were tested: 1:2 (1 μM), 1:5 (400 nM), 1:10 (200 nM), 1:25 (80 nM) and 1:50 (40 nM) dilutions from the concentration recommended by the vendor.

Cultures were monitored on the day of labeling as well as on the first day after labeling to confirm the uniformity of staining. On day 7 and 14, spheres were observed before disaggregation as well as single cells from disaggregated spheres to determine whether the distribution of the staining was gradually distributed in the observed mammospheres and whether the single cells in the culture plates still retained the dye.

In the staining protocol recommended by the manufacturer, the final concentration of PKH26 is 2 μM for staining 10^7 cells in a final volume of 2 ml. Cells labeled with dilutions 1:2 and 1:5 were homogeneously stained and showed a very strong fluorescent signal, both on the first day after staining and on the later time points. After sphere disaggregation on day 14 we could not detect any non-label retaining cells. On the other side, dilution 1:50 resulted in non-homogeneous staining on day 1. Many stained cells did not have any fluorescent signal. Dilutions 1:10 and 1:25 resulted in homogeneous staining. Further, we observed that staining results can also depend on the sample itself, as some of them took up more dye than others and cells were stained more intensively. Overall, a PKH26 concentration of 80 nM (dilution 1:25, Figure 26) was chosen for all the following assays.

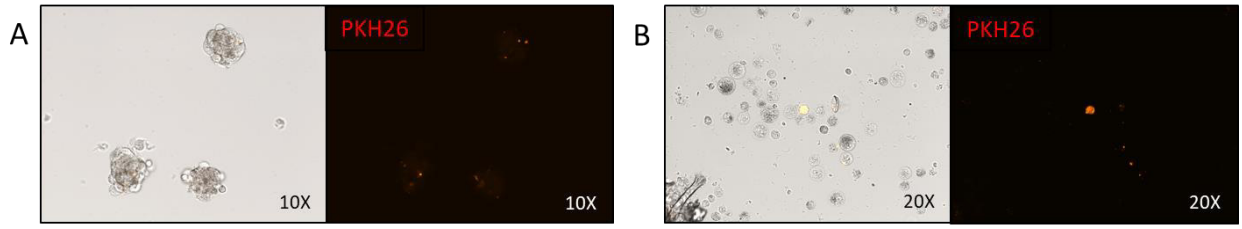

Figure 26: A representative sample stained with PKH26, 80nM. Second generation of mammospheres before disaggregation (A) and LRCs and nLRCs after sphere disaggregation (B). Magnification as indicated on each picture.

3.3.4 Density of cell seeding does not affect the frequency of sphere formation of HMECs

We aimed to perform two different types of experiments with HMECs: (1) propagation in anchorage independent conditions in order to isolate and characterize stem cells, and (2) estimation of the stem cell function, measured by sphere counting. Adult stem cells are very rare, with maximum of 2% in adult mammary tissue (Spike et al., 2012). To increase the chances of finding and isolating those cells a very high number of HMECs is required. Therefore, HMECs needed to be cultured at higher density. However, adequate distribution and avoidance of sphere fusion is mandatory to investigate the number of formed mammospheres. Finding optimal conditions for high cell number without sphere fusion and equal sphere distribution requires the consideration of two factors: (1) high density of cells may result in fusion of mammospheres while (2) low cell density can reduce paracrine cell influences. To investigate the effect of cell density on sphere formation, HMECs were seeded in poly-HEMA coated petri dishes (see Material and Method) in 3 different seeding densities: 10.000 cells/ml, 50.000 cells/ml and 500.000 cells/ml. After 7 days spheres were counted. The final number of counted spheres (Figure 27A) was normalized to 30.000 cells, corresponding to the number of cells in the plate with a seeding density of 10.000 cells/ml (Figure 27B).

A

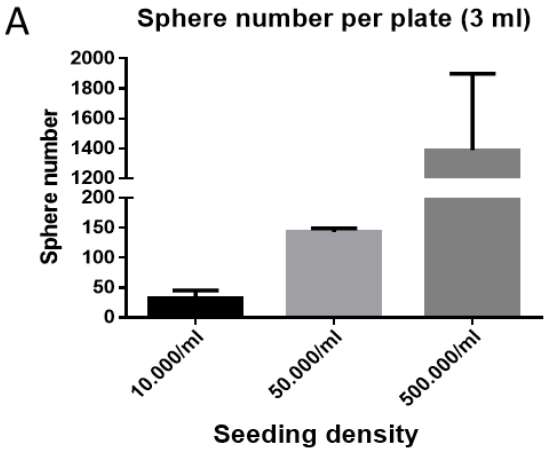

B

Seeding density	Experimental Data	Mathematical prediction
10.000 cells/ml	33,00	33,00
50.000 cells/ml	142,25	165
500.000 cells/ml	1391,75	1650

Figure 27: HMECs were seeded in different densities and cultured for 7 days in anchorage independent conditions. The number of mammospheres was counted on day 7 (A) and normalized to 30.000 seeded cells (B) which is the number of cells in the plate with a seeding density of 10.000 cells/ml. No significant differences were detected in the multiple comparison. Experiment was performed with one tissue specimen in technical quadruplicates, one-way ANOVA. All error bars correspond to standard deviation (Mean ±SD).

If sphere formation is not affected by the seeding density, then the numbers of obtained mammospheres in higher densities (50.000 cells/ml and 500.000 cells/ml) should correlate to the number of mammospheres obtained under 10.000 cells/ml condition multiplied by the seeding factor. The number of obtained mammospheres in 10.000 cells/ml condition was set as a reference for the mathematical prediction. For the mathematical prediction of the number of mammospheres in conditions with higher seeding densities, the number of counted mammospheres in 10.000 cells/ml conditions was amplified 5 or 50 times for conditions with 50.000 cells/ml or 500.000 cells/ml, respectively (Figure 27B). Obtained experimental data were comparable with the mathematical prediction, confirming consistent sphere forming capacity of HMECs, irrespective of the tested density of seeded cells.

The capacity of cells to form spheres did not differ between the cultures with different seeding densities, but the density and the observed fusion rate of the mammospheres was higher in plates where 500.000 cells/ml were seeded (Figure 28). Since seeding density did not affect sphere forming ability of HMECs, but affected the fusion rate of mammospheres further experiments were performed in the following way: (1) propagation of HMECs in anchorage independent conditions for isolation of QSCs, LRCs and nLRCs was performed with a seeding density of up to 300.000 cells/ml, while (2) experiments in which the sphere number was assessed as a final readout, were performed with a seeding density of 50.000 cells/ml.

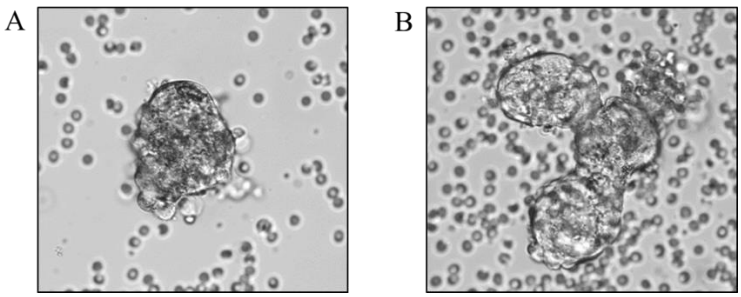

Figure 28: The capacity of sphere formation and the size of formed mammospheres do not differ between the cultures with seeded 10.000 cells/ml (A) or 500.000 cells/ml (B), but the fusion rate is very high in cultures with high density of seeded cells.

3.3.5 Separation of single cells from mammospheres

After 7 days of culture in anchorage independent conditions, HMECs either form mammospheres or stay as a solitary, non-dividing cells. Separation of the spheres from single cells can be done in two different ways: (1) using a 40 µm cell strainer or (2) by differential centrifugation. To examine which of these methods is resulting in a higher yield, we engaged hTERT-HME1 cell line. Cells of this cell line form mammospheres which in regard to the size, morphology and frequency of sphere formation (Figure 29) correspond to the spheres deriving from primary mammary cells.

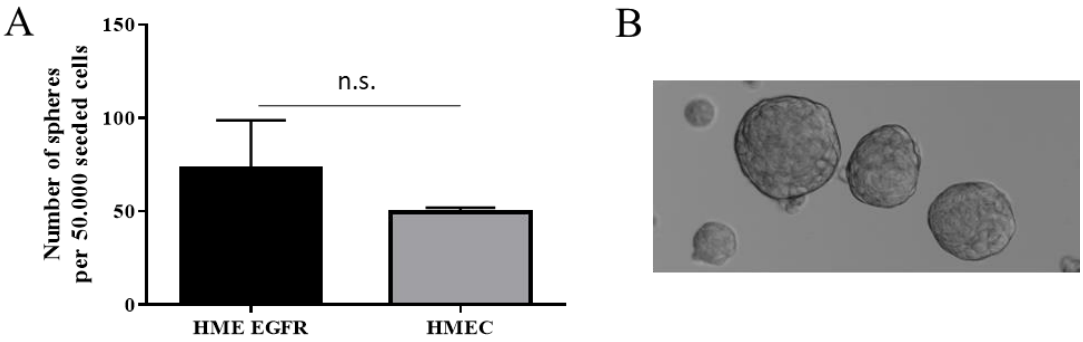

Figure 29: HME EGFR cells express similar behavior like HMECs in anchorage independent conditions in regard to (A) frequency of sphere formation, p=0,204 and (B) morphology. Magnification 20X.

We tested both methods on the hTERT-HME1 cell line that carries mutation in the receptor for epidermal growth factor (HME EGFR cell line). Therefore, cells were seeded in twelve 6 cm plates at a density of 10.000 cells/ml and cultured for 7 days in ultra-low attachment conditions. One half of the samples (pool of 6 plates) was subjected to separation using a cell strainer and the other half to differential centrifugation. After separation, mammospheres were dissociated and isolated cells were counted. This experimental outline is depicted in Figure 30.

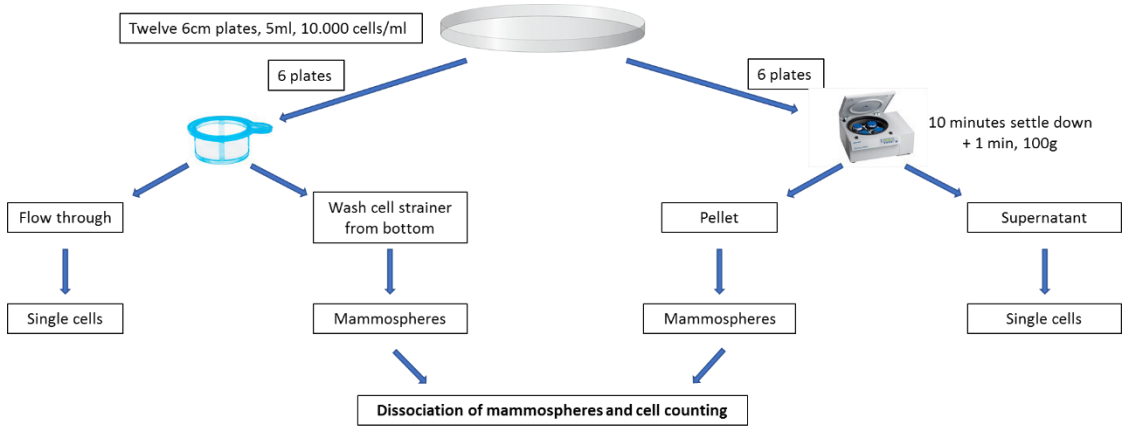

Figure 30: Schematic overview of testing the separation methods of mammospheres from SCs in HME EGFR cultures

Separation using the cell strainer and subsequent dissociation of mammospheres resulted in 5.000 cells, while differential centrifugation and subsequent dissociation produced 105.000 cells. In addition, in separation method based on centrifugation, mammosphere fraction was contaminated with approximately 25% of single cells (Figure 31), while the single cell fraction comprised of mostly single cells. Despite of contamination of sphere fraction, due to much higher yield we chose differential centrifugation as the method for separation of single cells from mammospheres in the following experiments.

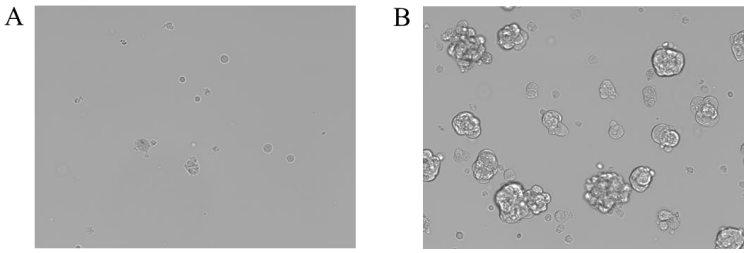

Figure 31: Separation of the mammospheres from single cells by centrifugation. Supernatant fraction (A) consists only single cells while mammosphere fraction (B) is contaminated with 25% from the total number of single cells next to the mammospheres. Magnification 10X.

3.3.6 Dormant cells reside among non-divided single cells after 7 days

The term “cellular quiescence” is very broadly used and indicates cell cycle inhibition that can be reversible (dormancy) or irreversible (senescence). To investigate the quiescent state in which HMECs reside, we cultured them in anchorage independent conditions for 7 days and then separated QSCs from mammospheres by centrifugation. Supernatant fraction, which contained only QSCs of different size was replated in new poly-HEMA coated plates and cultured for additional 7 days. After that period, we investigated sphere formation, which is a result of proliferation in anchorage independent conditions. We detected mammospheres in cultures originating from QSCs, indicating that these cells could be reactivated and re-entered the cell cycle (Figure 32A).

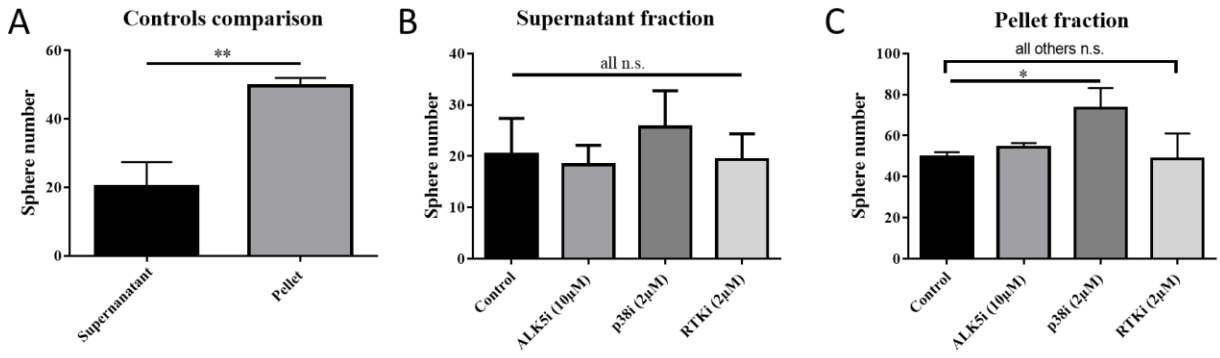

Figure 32: The number of mammospheres originating from QSCs and dissociated mammospheres. One-way ANOVA, stars indicating significance between groups in multiple comparisons. Statistically significant differences are marked with asterisks, * p<0,05, all error bars correspond to standard deviation (Mean ±SD).

Next, we tested whether different inhibitors, whose mitogenic or pluripotency effects were previously shown, affect sphere formation in our culture conditions. After 7 days of cultivation mammosphere- and supernatant (QSC) fractions were separated. As in the first experiment supernatant fraction was immediately replated, while mammospheres from pellet fraction were first dissociated to single cells and then replated onto new poly-HEMA coated plates. Both single cells and mammosphere-derived cells were seeded at a density of 50.000 cells/ml and treated with the following inhibitors: (1) SB431542, a potent and a specific inhibitor of transforming growth factor-beta (TGF-β) superfamily type I activin receptor-like kinase (ALK) receptor, known to maintain pluripotency of stem cells (ALK5i) (Du et al., 2014; Nakashima and Omasa, 2016; Yook et al., 2011), (2) SB203580, an inhibitor of p38 MAPK pathway that is upregulated in dormant cells (p38i) (Aguirre-Ghiso et al., 2003; Aguirre-Ghiso et al., 2001) and (3) S1042, a multi-targeted receptor kinase inhibitor (VEGFR, PDGFR, c-Kit) (RTKi). After additional 7 days of cultivation, we counted the mammospheres in the cultures.

The treatment with inhibitors did not increase the number of mammospheres in the cultures originating from QSCs (Figure 32B), however p38 MAPK inhibitor treatment increased sphere formation in the cultures originating from dissociated mammospheres (Figure 32C). Treatment with other inhibitors did not alter sphere formation or number (Figure 32 B, C). We concluded that inhibition of the p38 MAPK pathway increased sphere forming ability of progenitor cells, since these cells are mostly contained in mammospheres. This indicates existence of dormant cells or cells ready to enter a dormant state among stem and progenitor cells originating from the mammospheres. Further, we showed that active dormancy program in these cells can be interrupted by inhibition of the p38 MAPK pathway.

3.3.7 CD44 and CD24 expression in LRCs and nLRCs

The aim of our study was to isolate both dormant and stem cells. Therefore, we used the label retention assay described in previous section that enables detection and isolation of stem and progenitor cells. Only stem cells can survive and give progeny in anchorage independent conditions and due to their asymmetric division, resulting spheres consist of few LRCs (stem-like cells) and many progenitor cells

(Figure 33). Labeling cells with proliferation tracking dye before seeding in anchorage independent conditions therefore results in mammospheres with different levels of retained dye. We were interested in the phenotype of the cells enriched in mammospheres culture. To answer that, we analyzed expression of stem cell markers in our cultures.

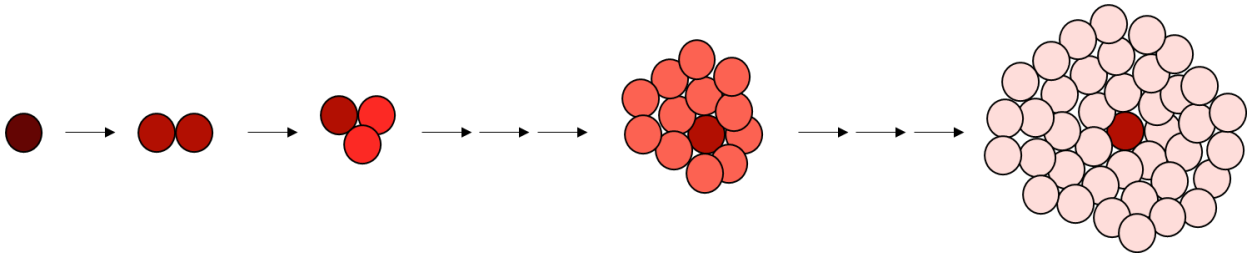

Figure 33: Label retention assay: Cells are labeled before propagation. Stem cells are dividing rarely, and their division is asymmetric resulting in renewed stem cell and progenitor cell. Consequently, stem cells are most intensively stained, label retaining cells (LRCs) and their progeny retains less dye the more they proliferate. Cells which divided the most are weakly labeled and referred to as non-label retaining cells (nLRCs).

For this purpose we again used HME EGFR cell line that we labeled using PKH26. Since these cells are proliferating, and therefore diluting the membrane dye, faster than primary mammary cells, we used higher concentration of the cell linker dye (200 nM). Cells were seeded in a density of 10.000 cells/ml and propagated in anchorage independent conditions for 7 days. Spheres were dissociated on day 7 and stained with anti-CD44-Pacific Blue and anti-CD24-APC antibodies. FACS analysis showed an enrichment of $CD44^{hi}$ $CD24^{lo/-}$ stem cells in the $PKH26^{+}$ population of 24,7% compared to the $PH26^{-}$ population with only 7,58% (Figure 34). These findings confirm the enrichment of stem cells in mammosphere cultures.

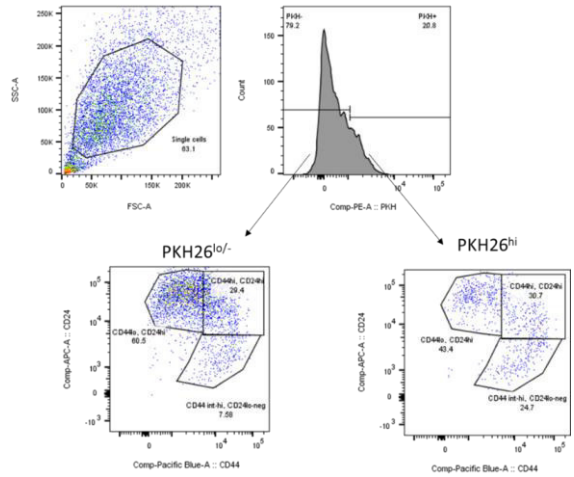

Figure 34: FACS analysis of CD44 and CD24 expression in single cells from dissociated PKH26 labeled spheres. $PKH26^{hi/+}$ cells are enriched with cells expressing stem cell markers (bottom right graph) compared to $PKH26^{lo/-}$ cells (bottom left graph).

3.3.8 Isolation of LRCs and nLRCs from mammosphere culture

The final goal of the establishment of the stem cell model was the isolation of cells of distinct differentiation stages and proliferation status. To isolate single LRCs and nLRCs, second generation

mammospheres were dissociated using trypsin and manual dissociation using a pipette. This type of digestion resulted in a lot of small clusters that could not be completely disaggregated which complicated isolation of target single cells. Increased disaggregation time to 10 minutes with constant pipetting did not decrease viability of isolated cells but decreased the number of clusters. This disaggregation procedure was used in all following experiments except for the FACS analysis of IL-6R.

3.3.9 Transcriptional analysis of SCs isolated from mammary gland

As we successfully established procedure for the isolation of single mammary cells from mammosphere cultures, we applied this method to mammary gland samples obtained from reduction mammoplasty surgeries. From five of the obtained mammary tissues with best sphere growth we successfully isolated single non-divided cells (QSCs) that did not give rise to mammospheres, as well as label retaining (LRCs) and non-label retaining (nLRCs) from disaggregated mammospheres of second generation. As already mentioned, these cells represent populations with distinct differentiation stages and proliferation status. It was shown that these populations in mammary gland display different transcriptional profiles (Colacino et al., 2018; Lawson et al., 2015) which led us to the idea to isolate and analyze transcription profiles of the isolated single mammary cells. Out of five specimens whole transcriptome amplification (WTA) products from 78/97 SCs, 46/55 LRCs and 58/82 nLRCs were used for further analysis.

3.4 The effect of the vascular niche on growth of breast cancer cells

Breast cancer patients develop metastases predominantly in the skeletal system, which is highly vascularized. The vasculature plays an important role in the regulation of bone development, but also in hematopoiesis by providing niches for hematopoietic stem cells. These niches can also serve as the lodges for DCCs (Shiozawa et al., 2011). During the process of dissemination, cancer cells enter the bone marrow upon leaving the circulation. Ghajar et al. showed that whether DCCs will start to proliferate depends on their relative position and proximity to the blood vessels in and BM lung. Cells that lay close to neovascular tips proliferate while cells lying on the trunks of the blood vessels enter a dormant state. In the organotypic model of the bone marrow microvascular niche they further showed that the mature vasculature sustains the dormant state of breast cancer cells. (Ghajar et al., 2013). Opposite to these cultures, tumor cells seeded in mesenchymal stromal niches exhibit a highly proliferative phenotype. We aimed to isolate single cells from both of these models for further characterization.

3.4.1 Microvascular niche does not affect the growth of breast cancer cells

Having concluded that neither stromal nor vascular niches support proliferation of non-tumorigenic cells, we investigated the effect of MSC (mesenchymal stromal cell) and MVN (microvascular niche) cultures on the growth of tumor cells. Towards this, we used GFP labeled human breast cancer cells HMT-3522 T4-2 (T4-2) cells and cultured them on MSC and MVN niches for 10 days. On day 1 after seeding tumor cells, only single GFP-positive cells were detected in the niches, the same as was seen with the non-tumorigenic cells. Nine days later, tumor cell clusters as well as solitary cells were observed in both types of co-cultures. Cell number and proliferation were determined as GFP-emitted fluorescent signal. Measurement of the fluorescent signal showed equal growth of T4-2-GFP cells in both types of niches (Figure 35, Table 6).

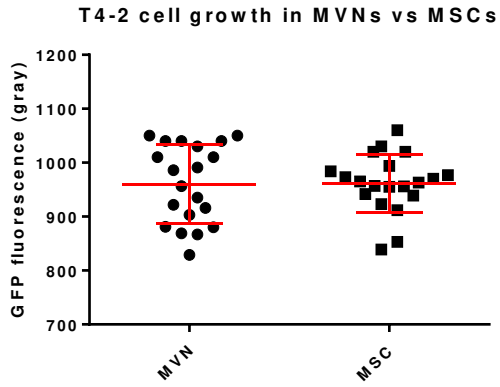

Figure 35: GFP labeled T4-2 cells were seeded on 10 days old MSC and MVN niches. After 10 days of cultivation in both niches, tumor cell growth was determined. No difference was measured in growth of tumor cells in MVN and MSC niches, Mann-Whitney test, p=0,9478.

Table 6: GFP fluorescence signal measured in MSC and MVN cultures. Fluorescent signal intensity indicates proliferation rate of T4-2 – GFP cells. Experiment was performed twice, with 10 replicates per group in each experiment.

	MVN	MSC
GFP-Fluorescence (gray)	1050,00	964,84
	1010,00	970,35
	1050,00	938,95
	1040,00	957,00
	956,34	972,74
	1030,00	1060,00
	915,76	1020,00
	921,62	984,07
	934,76	911,90
	866,92	838,85
	1040,00	853,46
	991,13	963,20
	1040,00	955,00
	1010,00	1020,00
	986,04	955,89
	880,02	1030,00
	903,35	993,75
	869,36	976,79
	881,43	942,33
	829,54	922,87
Mean	**960,3**	**961,6**
St dev	**72,8**	**53,74**

Although there was no statistically significant difference between the growth rates of tumor cells in these two niches, we observed that some MSC niches were enriched with clusters of tumor cells and some microvascular niches had only few small clusters and many solitary cells. We collected MSC

niches with high proliferating tumor cells (many cell clusters) and MV niches with predominantly solitary cells, disaggregated them and isolated single viable cells (Figure 36).

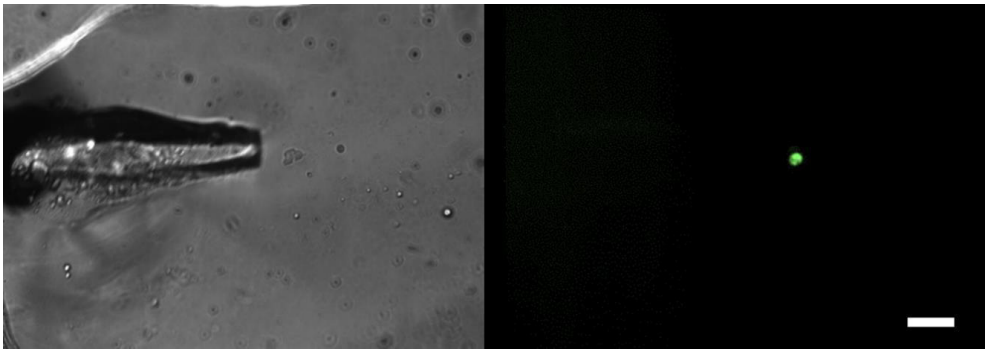

Figure 36: Manual isolation of single cells from MSC and MV co-cultures. MSC cultures enriched with clusters and MV niches enriched with single cells were collected and disaggregated. Single GFP-positive cells were picked using a micromanipulator. Scale bar 50 µm.

3.4.2 Non-transformed mammary cells neither grow in the stromal nor in the microvascular niche

To examine the influence of endothelial cells on the growth of normal mammary cells we used the non-tumorigenic mammary cell line MCF10A. GFP-labeled MCF10A cells were seeded on top of MSC and MVN cultures and observed. To create the niche with the most potential to induce dormancy in MCF10A cells, MVN cultures were grown for 10 days. After this period all the vessels are connected and there are no neovascular tips, promoting proliferation (Ghajar et al., 2013). On day 1 only single cells were detected, the same as on days 7 and 10. MCF10A-GFP cells neither grew nor died in MSC and MVN co-cultures (Figure 37). We concluded that both, stromal and vascular niches support survival, but not proliferation of non-tumorigenic MCF10A cells.

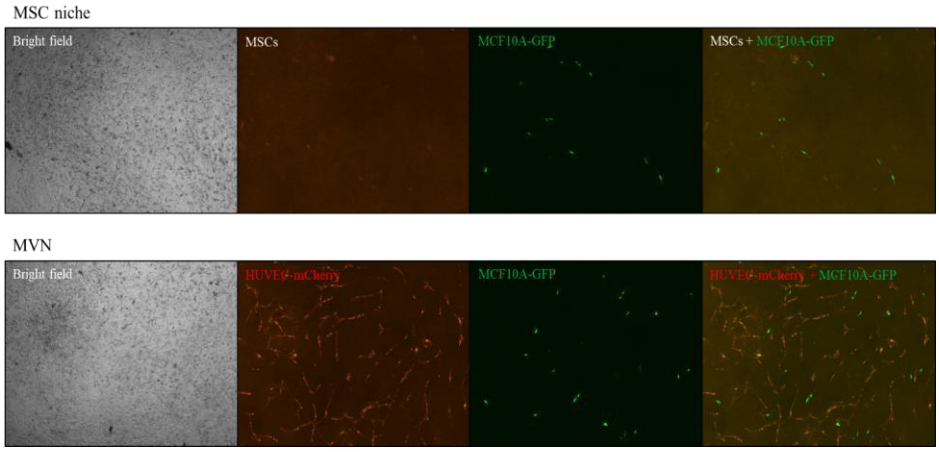

Figure 37: MCF10A cells seeded in stromal (MSC) or microvascular (MVN) niche 7 days after seeding mammary cells. Endothelial cells (HUVECs) are labeled using pBMN/mCherry plasmid (red) (Ghajar et al., 2013) and MCF10A cells with GFP (green) using Histone H2B-GFP plasmid (Ghajar et al., 2013; Tanner et al., 2012)

3.4.3 Mammary cells isolated from MVN and MSC cultures provide low quality WTA products

Isolated mammary cells from microvascular and stromal cultures were subjected to whole transcriptome (WTA) and genome (WGA) isolation. Obtained WTA products were further analyzed for expression of housekeeping genes. Quality control of isolated cDNA amplified products showed very low quality of cells isolated from these co-cultures. Only 4/39 (10%) of cells isolated from stromal niches and 8/33 (24%) of cells isolated from microvascular niches expressed all three tested housekeeping genes. Therefore, we decided to include cells expressing two of three analyzed housekeeping genes in our further analysis. Of 39 cells isolated from stromal niche, 15 (38%) and 18/33 (55%) cells isolated from microvascular niche met this quality criterion and were included in further analysis (Table 7). Cells expressing minimum 2 of 3 analyzed housekeeping genes were taken for further analysis.

Table 7: Quality of the WTA products of the cells isolated from stromal and microvascular niches. Expression of three housekeeping genes was examined using multiplex endpoint PCR.

Number of expressed housekeeping genes	**0/3**	**1/3**	**2/3**	**3/3**
Cells isolated from MSC niches	**19/39 (49%)**	**5/39 (13%)**	**11/39 (28%)**	**4/39 (10%)**
Cells isolated from MV niches	**8/33 (24%)**	**7/33 (22%)**	**10/33 (30%)**	**8/33 (24%)**

Although we succeeded to establish microvascular niches and cultivate the breast cancer cells in them, we could not detect any difference in the growth of mammary cells by observation. Still, we collected the breast cancer single cells from some of the MVN co-cultures where proliferation rate of the mammary cells was very low and MSC co-cultures where proliferation rate of the mammary cells was higher than in others. These findings indicated us that endothelial niche might not be involved in regulation of the dormancy in BM-DCCs and we continued our investigation into the direction of other type of niche in BM, osteoblastic niche. Cells isolated from both co-cultures were in later steps subjected to the analysis of the expression of Ki67 and MCM2, proliferation markers.

3.5 The effect of the osteoblastic niche on breast mammary cell growth

Bone marrow is a semi-solid tissue primarily located in the spongy structures of the big bones. The most important function of the bone marrow is the production of hematopoietic cells. Located inside the bones, the bone marrow is confined by osteoblastic cells forming osteoblastic niches. Hence, osteoblasts (OB) are a very abundant cell type in bones, whose major function is bone formation, as well as the production of the organic matrix of the bones. They are specialized cells produced by terminal differentiation of mesenchymal cells.

We aimed to investigate the role of osteoblasts in altering growth of mammary cells. It was previously shown that culturing human prostate cancer cells (PC3) with osteoblasts-like ST2 cells decreases the proliferative (Ki-67 positive) population of cells within 48h (Kim et al., 2013a). Knowing that DCCs compete with hematopoietic cells for stem cell niches (Shiozawa et al., 2011) and that osteoblasts are involved in stem cell niche formation, we aimed to examine the influence of osteoblasts on dormancy induction in mammary cells.

To test the effect of OBs on mammary cells growth, we cultivated MCF10A cells on top of the confluent OB layer. To discriminate the effect of culture conditions on mammary cell growth from the specific effect of OBs on the growth of mammary cells, we first cultivated MCF10A cells -fluorescently labeled with Carboxyfluorescein Diacetate Succinimidyl Ester (CFSE) in a flask confluent with unlabeled MCF10A cells (the same cell type, homotypic culture) for 72 hours. Proliferation of the MCF10A-CFSE cells was slower in co-cultures with confluent MCF10A cells than in the control population cultivated in the wells without pre-seeded cells Despite slower proliferation we did not detect any dormant cells, indicating that all cells passed through division at least once within 72 hours (Figure 38 A, B). This indicated that homotypic co-cultures (MCF10A labeled cells grown on top of confluent MCF10A culture) confer slower proliferation on the population level, but not dormancy in single cells.

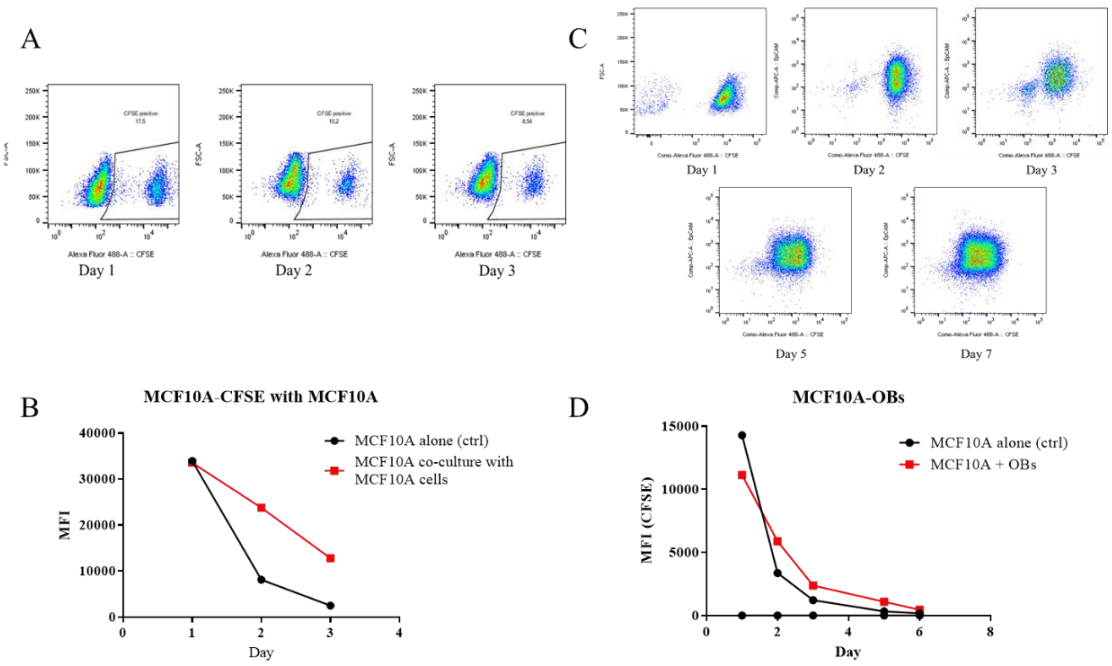

Figure 38: Proliferation of MCF10A-CFSE as a function of fluorescence level of CFSE. By cultivation in co-cultures of MCF10A cells with MCF10A cells (A, B) and osteoblasts (C, D) cell proliferation was decreased, but constant compared to controls, but it was not completely inhibited. Experiment performed once in technical duplicates. MFI - Mean fluorescence intensity. A, C: FACS plots show constant proliferation of MCF10A cells upon cultivation with osteoblasts. Single dormant (label retaining) cells were not detected. Osteoblasts were separated from MCF10A cells by HLA-A2 staining as described in text.

While we found out that MCF10A cells constantly proliferate, both alone and in confluent co-cultures with unlabeled MCF10A cells, we next asked whether OBs could stimulate the entry of mammary cells into a dormant state. To investigate this and isolate non-proliferating cells, we established co-cultures of MCF10A-CFSE cells and osteoblasts. As a reminder, non-proliferating cells are the cells which retain the initial level of CFSE fluorescence within several days of cultivation. MCF10A-CFSE cells were seeded on top of differentiated osteoblasts in a 1:10 ratio. Every consecutive day one co-culture was harvested and the CFSE level of mammary cells was measured. As described in Material and Methods, MSCs (and osteoblasts) derive from a patient with a HLA-A2 haplotype and MCF10A cells are HLA-A2 negative. Thus, osteoblasts were separated from MCF10A cells by HLA-A2 staining and the CFSE level was examined in MCF10A cells.

Although CFSE fluorescence in all the measurements from day 2 was higher in cells from co-cultures with OBs than in controls, indicating their slower proliferation (Figure 38D), we could not detect any non-cycling cell with the fluorescent signal equal to the initial fluorescence (Figure 38C). We concluded that although co-culture with osteoblasts slows down proliferation, it does not induce cell cycle arrest in MCF10A cells. Therefore, this model is not appropriate for studying dormancy of single mammary cells.

3.6 Analysis of the proliferation in single mammary cells

Having established *in vitro* models which mimic the influence of different BM components to mammary cells we aimed to analyze isolated cells from these models. Therefore, we wanted to set up a PCR assay that enables us to discriminate proliferating from non-proliferating cells. This enables further analysis and profiling of dormant and proliferating cells in our model(s) and analysis of BM-DCCs from breast cancer patients.

3.6.1 Establishment of proliferation marker analysis for single cells classification

We base the analysis of single cells on the isolation of their transcriptome. Therefore, we decided to establish a proliferation assay that is based on transcriptome analysis in which expression of specific gene transcripts enables us to determine the proliferative status of analyzed cells.

First, we established an endpoint PCR for chosen specific transcripts. As markers of proliferation *MKI67* (antigen identified by monoclonal antibody Ki-67), *MCM2* (minichromosome complex maintenance component 2), and *PCNA* (proliferating cell nuclear antigen) genes were selected and primers were designed. Restriction digestion of the PCR amplicons carried out after gene-specific PCR showed that designed primers amplified the desired sequence fragments and thus specifically detected the transcripts of *MKI67, MCM2,* and *PCNA* genes. The establishment of the primers for proliferation markers was carried out by Nina Patwary, as a part of her PhD project.

Next, we validated the established markers in single cells of known proliferation status. We chose to test these markers in a population of naïve and activated CD8+ T-cells. Unstimulated CD8+ T-cells isolated from the blood of healthy individuals are non-proliferating cells, residing in the G0 phase of the cell cycle. Their activation results in the entry of the cell cycle and consequent proliferation. FACS analysis of cells stained with fluorescent DNA binding dyes, such as DAPI or Hoechst 33342, is one of the most direct ways of cell cycle analysis (cells are staged based on DNA content). Cell cycle analysis of unstimulated and stimulated CD8+ T-cells demonstrated that naïve cells reside in the G0 phase and stimulated cells are staged in all other cell cycle phases (Figure 39).

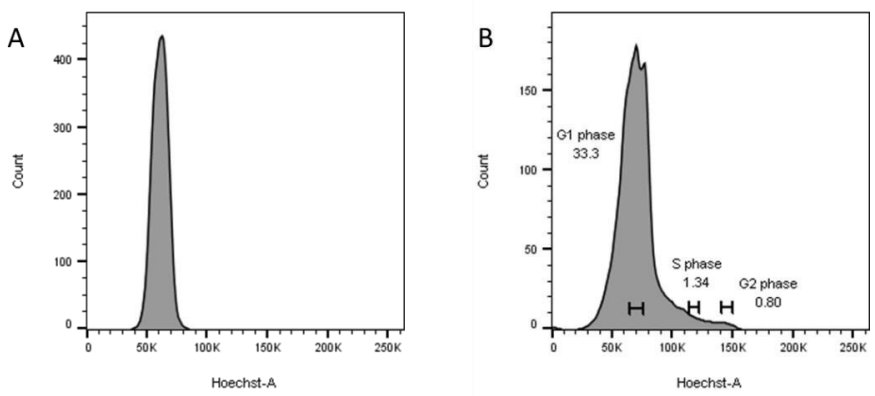

Figure 39: DNA histogram of cell cycle analysis in unstimulated (A) and stimulated (B) (activated) CD8+ T cells. In this case the x-axis represents the fluorescent signal of Hoechst 33342 and values on the y-axis represent the cell number. The bars within each phase indicate the narrow cell populations that have been sorted.

In the pilot experiment naïve CD8+ T-cells (purity 88,5%) were stimulated with phorbol 12-myristate 13-acetate (PMA) and ionomycin and analyzed 12h, 24h, 36h, 48h, 60h, and 72h after stimulation to determine the best time point for activation analysis (Figure 40). After 48h stimulation distribution of cells in different cell cycle phases was stabilized; thus, the 48h time point was chosen as the best one for the cell sorting experiment.

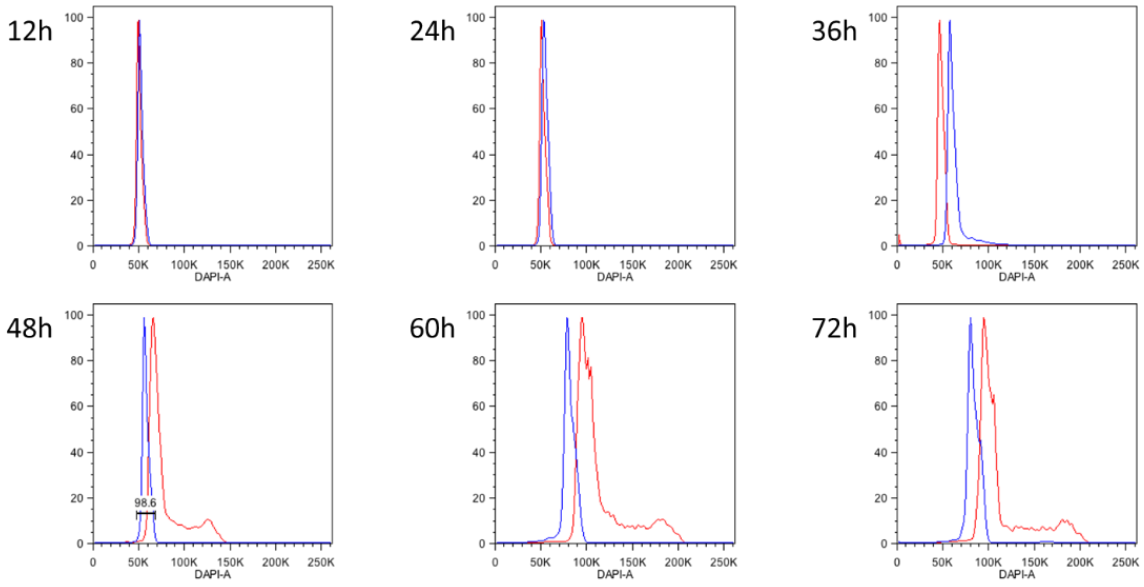

Figure 40: Determining the best time point for cell cycle analysis. The fluorescence intensity of DAPI, which corresponds to the DNA content, is plotted on the x-axis. The y-axis represents the cell number, with the height of the curve corresponding to the number of cells. Unstimulated and PMA/ionomycin stimulated CD8+ T-cells were stained using DAPI at different time points. Blue bars represent unstimulated CD8+ T-cells whereas red bars represent stimulated cells.

Since DAPI is a passively transported dye, that only labels dead cells, for our live cell sorting experiment we chose the dye that actively enters to the cells, Hoechst 33342. Since Hoechst 33342 is actively pumped in and out the cell, the profile of cell distribution was not completely fitting the profile seen with DAPI, where the dye was steadily bound to the DNA. Therefore, we picked cells from narrow populations comprising of the cells with average DNA content in the target population (Figure 39B) avoiding contamination with cells from other cell cycle phases. In total we isolated 21 single cells from

G1 phase and 20 single cells from other cell cycle phases. Since CD8+ T-cells are quiescent in the blood of a healthy donor, G0 phase cells were isolated from non-stimulated CD8+ T-cell population prior to stimulation. Transcriptomes of 16/20 (80%), 18/21 (86%), 17/20 (85%) and 16/20 (80%) isolated cells from G0, G1, S and G2 phases, respectively, satisfied quality criterion (expressing 3/3 analyzed housekeeping genes) and were subjected to further analysis, resulting in 16 naïve (G0) and 51 activated T-cells for proliferation marker validation (Table 8).

Having confirmed that naïve CD8+ T-cells do not proliferate and upon stimulation enter the cell cycle (Figure 39 and Figure 40), cells sorted from all phases of the cell cycle were further analyzed for the presence of transcripts of previously selected proliferation markers.

Table 8: The number of isolated single cells from different phases of the cell cycle and the outcome of quality control analysis.

Cell cycle phase	**G0**	**G1**	**S**	**G2**
Isolated cells	**20**	**21**	**20**	**20**
Fulfilled QC requirements	**16 (80%)**	**18 (86%)**	**17 (85%)**	**16 (80%)**

3.6.2 Validation of the established proliferation markers

Transcriptome analysis showed that 100% of the activated T-cells from all cell cycle phases (51/51) expressed *MKI67* and *PCNA* genes (Figure 41). The *MCM2* transcript was detected in 62,75% (32/51) of the activated T cells. On the opposite, the expression of *MKI67* and *MCM2* was not detected in any of the naive T cells (Figure 41), but *PCNA* transcript was detected in one naive T-cell (1/16, 6,25%). Statistical analysis of the expression of proliferation markers in activated and naive T cells showed the significant differences in expression of these genes (*MKI67*: $p < 0{,}0001$, *MCM2*: $p < 0{,}0001$, *PCNA*: $p < 0{,}0001$, Fischer's Exact test, two-tailed). Tests showed sensitivity of 100% for the *MKI67* and *PCNA* genes and 62,75% for *MCM2* and specificity of 100% for *MKI67* and *MCM2*, and 93,75% for *PCNA*. Since specificity of the PCNA was not 100% we excluded this marker from the analysis.

A

	Cell 2	Cell 4	Cell 5	Cell 6	Cell 7	Cell 8	Cell 9	Cell 10	Cell 11	Cell 12	Cell 14	Cell 15	Cell 16	Cell 17	Cell 19	Cell 20	% of cells expressing analyzed gene	
Ki-67	0	0	0	0	0	0	0	0	0	0	0	0	0	0	0	0	0% (0/16)	
PCNA	0	0	0	0	0	0	1	0	0	0	0	0	0	0	0	0	6% (1/16)	G0 0h
MCM2	0	0	0	0	0	0	0	0	0	0	0	0	0	0	0	0	0% (0/16)	

B

	Cell 1	Cell 3	Cell 4	Cell 6	Cell 7	Cell 9	Cell 10	Cell 11	Cell 12	Cell 13	Cell 14	Cell 15	Cell 16	Cell 17	Cell 18	Cell 19	Cell 20	Cell 21	% of cells expressing analyzed gene	
Ki-67	1	1	1	1	1	1	1	1	1	1	1	1	1	1	1	1	1	1	100% (18/18)	
PCNA	1	1	1	1	1	1	1	1	1	1	1	1	1	1	1	1	1	1	100% (18/18)	G1 48h
MCM2	0	1	1	0	0	0	1	0	0	0	1	1	1	0	1	1	1	1	56% (10/18)	

C

	Cell 1	Cell 2	Cell 4	Cell 5	Cell 6	Cell 7	Cell 8	Cell 9	Cell 11	Cell 12	Cell 13	Cell 14	Cell 15	Cell 17	Cell 18	Cell 19	Cell 20	% of cells expressing analyzed gene	
Ki-67	1	1	1	1	1	1	1	1	1	1	1	1	1	1	1	1	1	100% (17/17)	
PCNA	1	1	1	1	1	1	1	1	1	1	1	1	1	1	1	1	1	100% (17/17)	S 48h
MCM2	1	1	1	0	1	1	1	0	1	0	1	0	1	1	0	1	1	71% (12/17)	

D

	Cell 1	Cell 2	Cell 3	Cell 5	Cell 6	Cell 8	Cell 9	Cell 10	Cell 11	Cell 13	Cell 14	Cell 15	Cell 16	Cell 17	Cell 19	Cell 20	% of cells expressing analyzed gene	
Ki-67	1	1	1	1	1	1	1	1	1	1	1	1	1	1	1	1	100% (16/16)	
PCNA	1	1	1	1	1	1	1	1	1	1	1	1	1	1	1	1	100% (16/16)	G2 48h
MCM2	1	0	1	1	0	0	1	1	0	0	1	1	1	1	1	0	62% (10/16)	

Figure 41: Results of endpoint PCR analysis of proliferation markers in sorted T cells: A) unstimulated T-cells, activated T-cells in G1 (B), S (C) and G2-phase (D) of cell cycle. Labeling system: 1 – Target transcript detected in the cell, 0 - target transcript was not detected in the cell.

Expression of proliferation markers significantly differ in activated and naïve CD8+ T-cells (Figure 42) confirming that the chosen proliferation markers discriminate proliferating from non-proliferating single cells and can be used for determination of the proliferation status of single cells isolated from previously described models of dormancy.

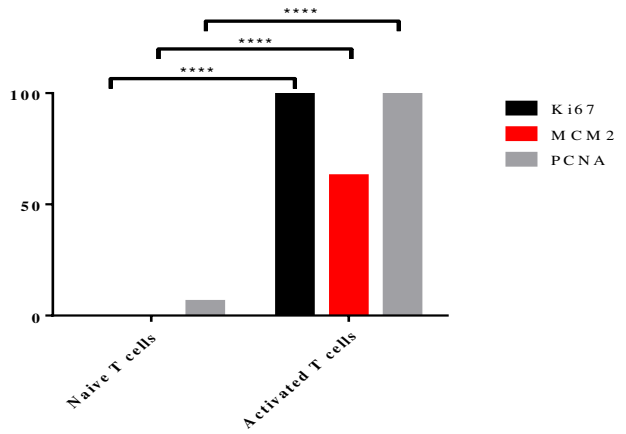

Figure 42: Gene expression of *MKI67*, *MCM2* and *PCNA* in naive and activated T cells. On the x-axis are proliferation markers in naïve and activated T-cells. On the y-axis is the percentage of naive or activated T cells expressing *MKI67*, *MCM2,* and *PCNA* respectively. Fisher's Exact test, **** p<0,0001.

After defining proliferative and non-proliferative cells we aimed to profile the state of dormancy in the cells we isolated from established *in vitro* models.

3.7 Determination of the proliferation status of cells isolated from dormancy models

Successful validation of MKI67, MCM2 and PCNA as proliferation markers enabled us to study the proliferation status of single cells isolated from previously established stem cell and endothelial niche models (chapters 3.3 and 3.4). From these models we were able to isolate candidate proliferative and non-proliferative cells, which we could not from osteoblastic niche. Therefore, we further turned to these models and further analyzed mammary cells derived from them.

3.7.1 Proliferation analysis of single cells isolated from stromal and vascular niches

From the stromal and microvascular niches we isolated respectively 39 and 33 T4-2 cells. From all of them, only 38% (15/39) cells from the MSCs and 55% (18/33) from MVN had good quality and were further analyzed. Ki67 expression was detected in 2/18 (11%) cells isolated from microvascular niches and 2/15 (13%) cells isolated from stromal niches indicating that these are proliferating cells. These cells did not express MCM2. The rest 89%of the cells isolated from stromal niche and 87% of the cells isolated from the microvascular niche expressed neither Ki67 nor MCM2 transcripts, most likely representing cells residing in G0 phase. Statistical analysis showed that there is no significant difference in distribution of proliferating and non-proliferating cells in these two niches (Figure 43). This finding confirmed our initial observation that none of these niches specifically induced proliferation or quiescence in mammary cancer cells. Therefore, we continued further profiling using the stem cell model.

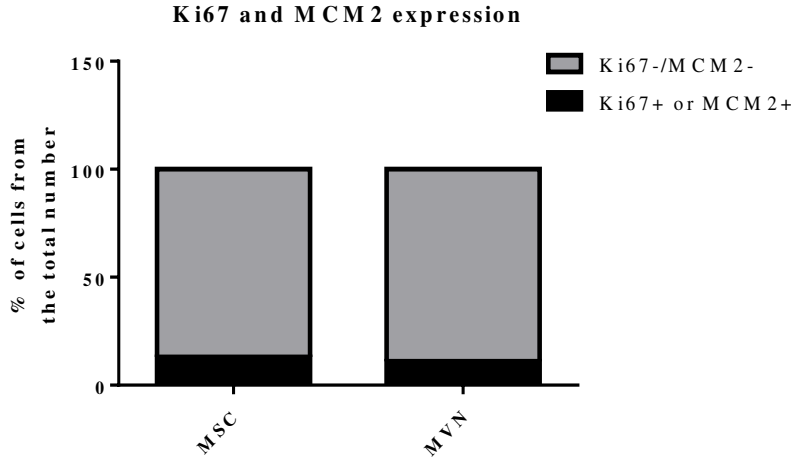

Figure 43: Percentage of proliferating and non-proliferating cells in stromal (MSC) and vascular (MVN) niches. Y axis represents the percentage of cells from all the analyzed cells from corresponding niches. There is no difference in frequency of proliferating and non-proliferating cells in MSC and MVN (Fischer's exact test, two-tailed, non-significant).

3.7.2 Proliferation analysis of QSCs, LRCs, and nLRCs isolated from the stem cell model

The ultimate goal of our analysis is to discriminate proliferating from non-proliferating cells within our DCCs isolated from breast cancer patients, in order to recognize patients with higher risk of developing metastases. Since early DCCs that seed metastases (Hosseini et al., 2016a) harbor few genetic changes (Husemann et al., 2008) the best model resembling these cells are cells isolated from mammary gland. Therefore, for proliferation analysis in the stem cell model we chose cells of the three best specimens using following criteria: (i) Growth of the regular spheres in both generations, (ii) expression of EpCAM in QSCs population and (iii) clear distinction between PKH26+ and PKH26- cells in population of cells from secondary mammospheres. From the three specimens 45 QSCs, 19 LRCs and 31 nLRCs met required quality criteria and were used in following analysis (Table 9).

Table 9: Overview of patient derived HMECs used for proliferation analysis.

	QSC	LRC	nLRC
Patient 1	14	8	9
Patient 2	14	3	5
Patient 3	17	8	17
Total	45	19	31

Proliferation analysis showed that 93% (42/45) of QSCs and 95% (18/19) of LRCs express neither Ki67 nor MCM2, resulting in 7% of SCs and 5% of LRCs expressing any of proliferating markers. Among nLRCs the percentage of proliferative cells was higher with 23% (7/31) cells expressing at least one of the analyzed proliferation markers (Figure 1Figure 44). Pairwise comparison showed there is no

significant difference between percentages of proliferating and non-proliferating cells between QSCs and LRCs. The percentage of Ki67- and/or MCM2-positive cells is significantly different in the nLRC group compared to QSCs and LRCs, (p=0,0025 and p=0,0004 respectively) (Figure 44). This justifies the label retention assay as a relevant method for initial separation of proliferating and non-proliferating cells, but also emphasizes the necessity of additional analysis for the final answer whether a cell is in the proliferative state.

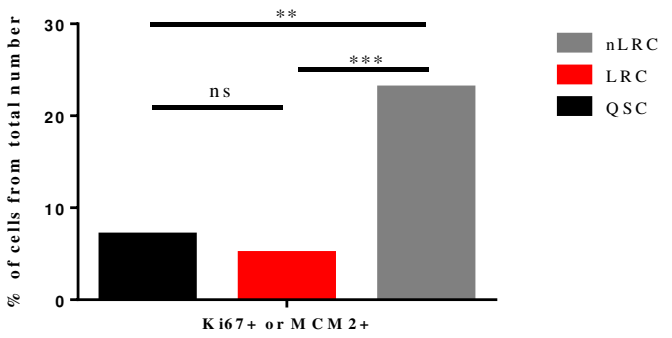

Figure 44: Analysis of the proliferative status of patient derived HMECs. Percentage of Ki67+ and /or MCM2+ is significantly different in nLRC group compared to QSCs and LRCs, but not between LRC and QSC groups (Fisher's exact test, two-tailed, **p<0,01, ***p<0,001, ns non-significant).

3.8 Profiling the state of cellular dormancy

To select the best candidate cells for the proliferation analysis in mammary cells, we employed two tests. First, the label retention assay, where cells were classified in three groups (non-cycling QSCs, non-cycling LRCs and cycling nLRCs) was used. Second, we utilized the proliferation analysis based on the expression of the proliferation markers (as described in chapter 3.6). All label retaining (non-cycling) cells which in addition did not express analyzed proliferation markers, as well as non-label retaining (actively proliferating) cells which expressed Ki67 or MCM2 were chosen as good candidates for gene expression analysis. Having in mind that PCNA was not specific only for activated, proliferating T-cells, we decided to use this gene only as exclusion marker, meaning the cells that expressed only PCNA were not considered non-proliferating and were eliminated for further analysis. On the other side these cells (that expressed only PCNA) were also not considered proliferating, since PCNA was expressed by one naïve (non-cycling, G0) T-cell. Therefore, for gene expression analysis only non-label retaining cells that expressed Ki67 or/and MCM2 were considered proliferative cells and label retaining cells that did not express any of the three proliferation markers were considered non-proliferative cells. The selection process of candidate cells for gene expression analysis is depicted in the Figure 45.

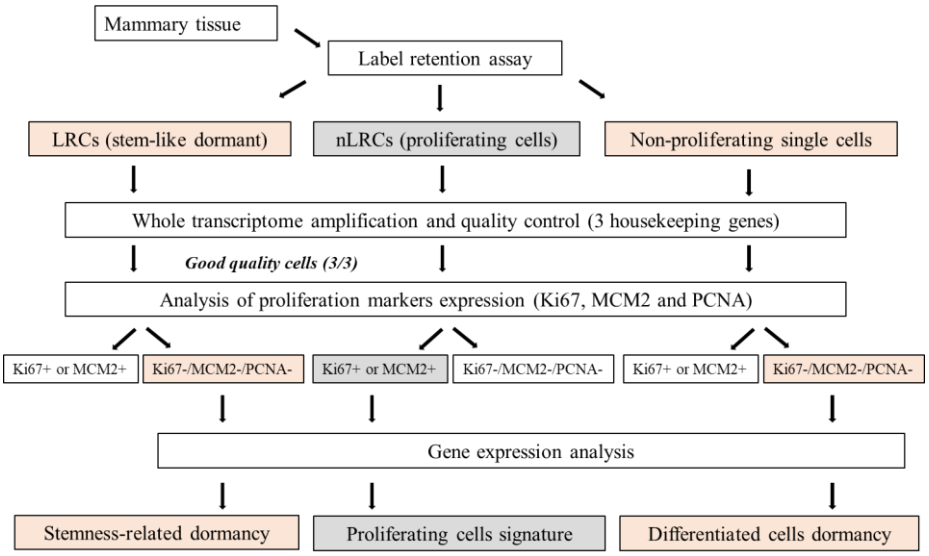

Figure 45: Workflow depicting the selection of patient derived HMECs from different proliferation states (proliferating and non-proliferating cells) for gene expression analysis. Red highlighting labels the cells classified as non-proliferating and grey highlighting labels the cells classified as proliferating cells. Cells whose proliferation status from the label-retention assay was confirmed by proliferation analysis were taken for gene expression analysis.

After this selection process, we had 26 QSCs, 8 LRCs and 5 nLRCs from three patients fulfilling the requirements (Table 10). From these 9 QSCs, 8 LRCs and 5 nLRCs were subjected to gene expression analysis using microarray analysis. Additionally, we analyzed three QSCs expressing only PCNA.

Table 10: Number of selected cells for gene expression analysis representing different states of proliferation and quiescence in cells.

Patient	Patient 1	Patient 2	Patient 3	Total
QSCs	**7**	**9**	**10**	**26**
Non-proliferating LRCs	**4**	**1**	**3**	**8**
Proliferating nLRCs	**3**	**2**	**2**	**5**

3.8.1 Gene expression profiling discriminates 5 groups within HMECs

Proliferating and non-proliferating cells have gene expression profiles specific to the state in which they reside. Therefore, different gene expression would enable us to discriminate proliferating from non-proliferating cells.

Unsupervised k-means clustering classified cells into 5 distinct groups (Figure 46). All proliferating nLRCs were classified in the same group (g1) and separated from non-cycling cells. Two distinct subpopulations within each of the QSC and LRC populations were identified. LRCs grouped into groups g2 and g4, and QSCs into groups g3 and g5. Interestingly, three PCNA+ QSCs (QSC1, QSC5

and QSC9) grouped together with other Ki67-/MCM2-/PCNA- QSCs, confirming that PCNA is not the optimal marker to determine the proliferative status of the cell.

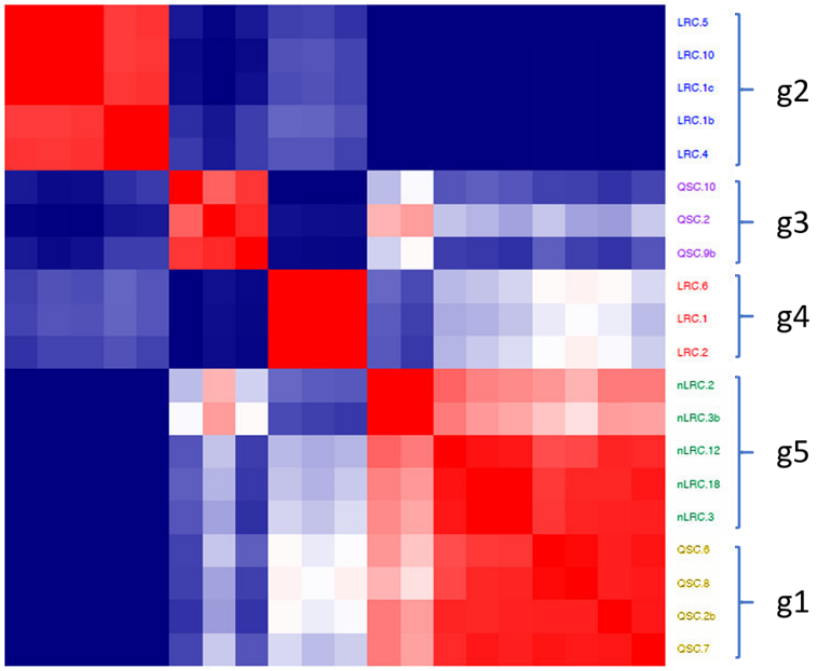

Figure 46: K-means clustering following microarray analysis of HMECs classifies cells into 5 separate groups. QSCs – g3 and g5 - non-proliferative differentiated cells; LRCs – g2 and g4 - stem-like, non-proliferative cells; nLRCs – g1 - proliferative, progenitor cells.

3.8.2 QSCs, LRCs, and nLRCs belong to the populations of distinct differentiation states in mammary gland

Next, we wanted to profile the stem-like cells (LRCs), progenitor cells (nLRCs), and EpCAM+ QSCs isolated from the stem cell model. Data coming from the gene expression profiles of these groups were transformed using quantile normalization and compared pairwise. Differentially expressed genes (DEG) represented the group of activated genes needed for transition (shift) of the cell from one state to another (or one population to another).

We searched the literature for the analysis of mammary cells from distinct differentiation states and found that Lim and colleagues (Lim et al., 2009) isolated mammary cells (blood lineage marker negative cells) from a tissue of a healthy donor and sorted them based on EpCAM and CD49f expression in the following subpopulations: $CD49f^{+}EpCAM^{-}$ mammary stem cells, $CD49f^{+}EpCAM^{+}$ luminal progenitors and $CD49f^{-}EpCAM^{+}$ mature luminal cells. These subpopulations were subjected to gene expression analysis. We compared their findings with ours and learned that LRCs from our analysis mostly correspond to mammary stem cell hierarchical level in the work of Lim and colleagues, nLRCs correspond to the progenitors and QSCs to mature luminal cells (Table 11). Additional confirmation of

the relevance of this approach was displayed the comparison of two groups of the same hierarchical level (Table 11, Column 5) in which no difference (hierarchical shift) was detected.

Table 11: Accuracy of comparison of different groups (g1-g5) with cells from different hierarchical level. Accuracy higher than 50% indicates true similarity (50% accuracy is a result of randomized gene distribution) in comparison of the "shifts" between the groups. Highlighted field are the comparison that showed highest statistical significance. For simplicity, only representative comparisons between the groups of distinct differentiation states are shown.

nLRC -> LRC1	nLRC -> QSC1	LRC2 -> QSC2	QSC1 -> LRC2	LRC1 -> LRC2
ML -> MaSC; 67%; p= 5,54e-13	MaSC -> ML; 50%; p= 0,9253	MaSC -> ML; 72%; p= 2,606e-19	ML -> MaSC; 62%; p= 1,283e-10	ML -> MaSC; 53%; p= 0,264
LP -> ML; 57%; p= 0,052	LP -> ML; 58%; p= 0,008	ML -> LP; 53%; p= 0,185	ML -> LP; 56%; p= 0,006	ML -> LP; 52%; p= 0,385
LP -> MaSC; 72%; p= 2,23e-20	LP -> MaSC; 55%; p= 0,049	MaSC -> LP; 75%; p= 1,679e-24	LP -> MaSC; 61%; p= 6,181e-07	LP -> MaSC; 53%; p= 0,585

3.8.3 Pathway analysis determines signaling profiles of defined groups

Next, we performed bioinformatical analysis of the activated cell signaling pathways and defined the profiles of deregulated signaling pathways in each of the previously defined five groups of cells. Pathway analysis resulted in a list of up- and downregulated pathways for each of the groups (Figure 47). Both groups of LRCs expressed some of the stemness related pathways, such as non-canonical Wnt, PI3K/AKT, MAPK family (LRC1), PI3K/AKT, Wnt, Notch (LRC2). Interestingly, in nLRC group p38 signaling mediated by MAP kinases, MAP kinases signaling, TGF-β, and Hippo pathways were upregulated, as well as many pathways related to progression through cell cycle. Unexpectedly, Wnt pathway, a signaling pathway connected to stemness, was upregulated in QSCs, which also overexpressed apoptotic pathways. One of the signaling pathways that was associated to stemness (upregulated in both LRC1 in LRC2 groups compared to others) was the IL-6 signaling pathway (Figure 47). We decided to further investigate the mechanism of this pathway in regulation of stemness and dormancy in mammary cells.

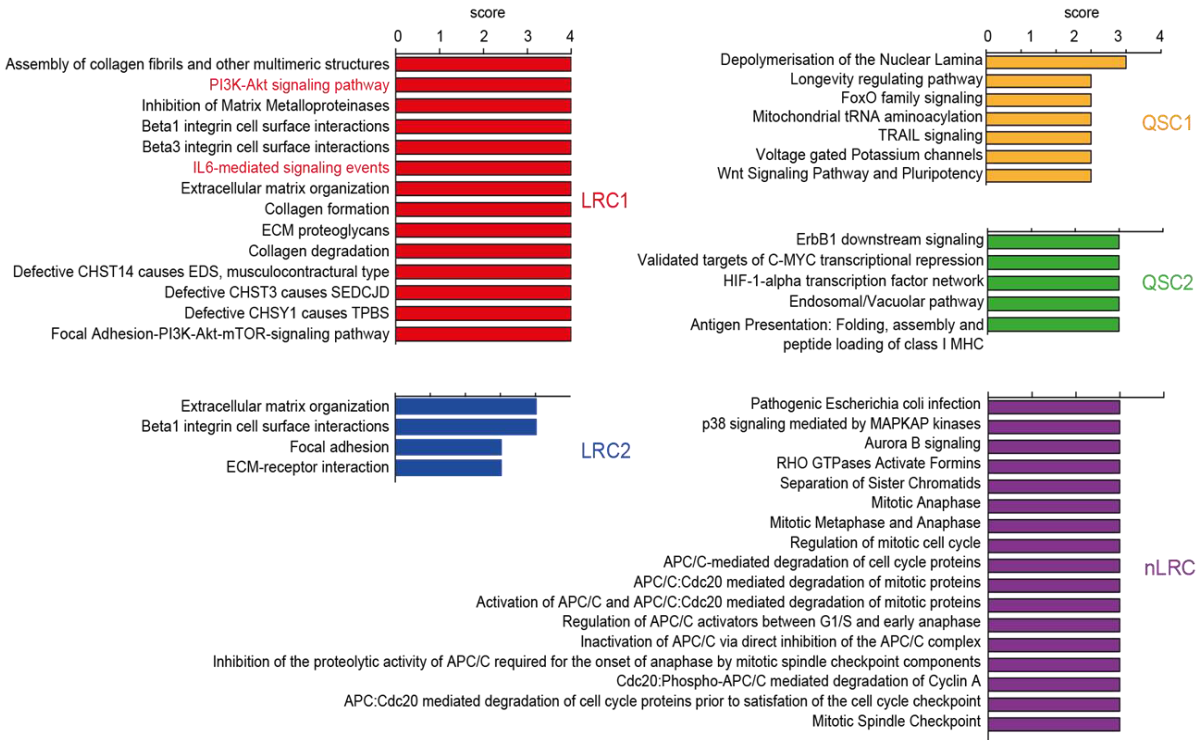

Figure 47: Summarized cell-signaling pathway analysis of QSCs, LRCs and nLRCs isolated from mammary specimens of healthy individuals. Each bar indicates the number of comparisons in which that specific pathway was upregulated, i.e. PI3K-Akt and IL-6 signaling pathway are upregulated in LRC1 group in 4 comparisons, meaning they are upregulated in this group compared to all others.

3.8.4 IL-6 signaling in patient derived MC-DCCs

Having found that IL-6 signaling plays a role in stem like cells (LRCs), we wanted to see how it is reflected in our DCC collective. We generated a “gene signature” consisting of the genes upregulated upon stimulation of IL-6 signaling in MCF10A cells (Figure 61) and IL-6 regulated genes that we found by mining the literature. We used this “gene signature” to analyze 21 MC-DCCs (15 M0-DCCs and 6 M1-DCCs) with aberrant mCGH profiles that we subjected to deep transcriptome sequencing. The supervised clustering discriminated three DCCs clusters, one comprising of a majority of M1-DCCs and two M0-DCCs subgroups with one M1-DCC each. IL-6 signaling pathway was activated in eight of 15 M0-DCCs, while seven of 15 M0-DCCs did not show an active IL-6 signaling pathway (Figure 48).

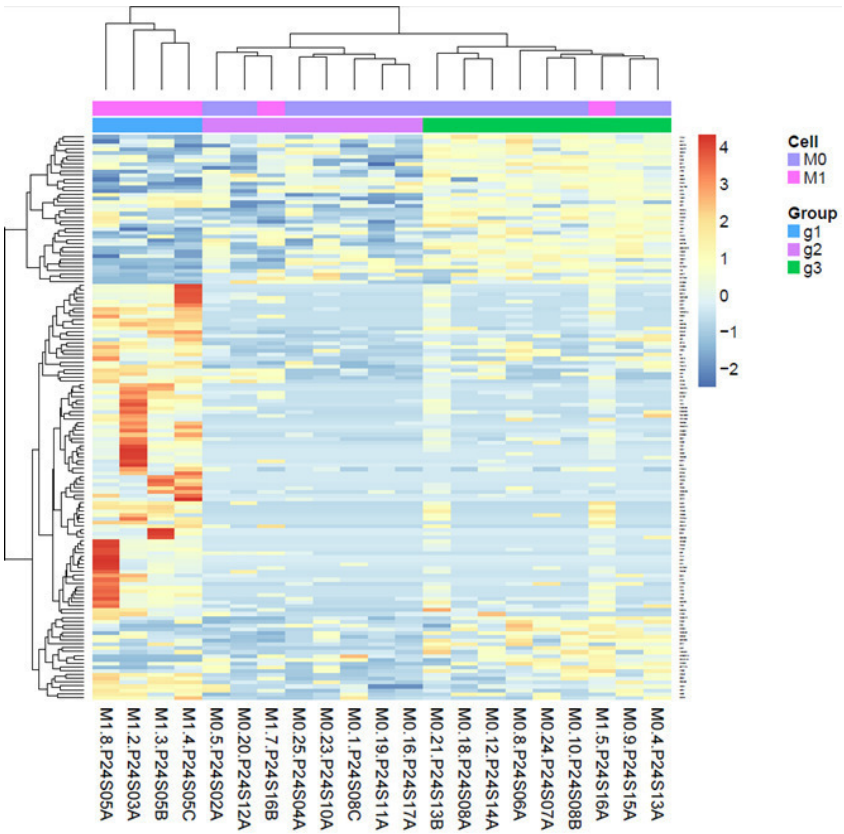

Figure 48: Heatmap demonstrates selective IL-6 activation in subsets of aberrant MC-DCCs. M1-DCCs form separate group, while M0-DCCs comprise of two subpopulations, one with active and one with non-activated IL-6 signaling pathway.

Ki67 and MCM2 expression, determined by qPCR, was significantly higher in group of cells with activated IL-6 signaling (Table 12) supporting our hypothesis that IL-6 signaling is one of the signals that plays a role in controlling the proliferation of DCCs in the bone marrow of breast cancer patients.

Table 12: Expression of proliferation markers (Ki67 or MCM2) in M0-DCC subgroups with active/non-active IL-6 signaling. Number of proliferative (Ki67+ or MCM2+) cells is significantly higher in M0-DCCs with active IL-6 signaling pathway (Fisher's Exact test, p=0,0406).

	$Ki67^{+}$ or $MCM2^{+}$	$Ki67^{-}$ and $MCM2^{-}$
IL-6 active	7	1
IL-6 non-active	2	5

3.9 IL-6 signaling in the mammary gland

Our finding that majority of breast DCCs are non-proliferating fits well to the data that most of breast cancers never become metastatic. Only 15% of analyzed aberrant DCCs (4/26) were classified in a group of proliferating nLRCs. From all women diagnosed with early-stage breast cancer 30% develop metastatic disease (Redig and McAllister, 2013). A half of that number can be women with DCCs with proliferating profile. We asked whether the rest of cells with potential for metastatic outgrowth lie among LRCs, while 15% of analyzed DCCs were classified into this group. Accumulating evidence suggests that a subpopulation of stem-like cancer cells possess the capability to disseminate to distant organs (Liu et al., 2010; Liu et al., 2011). This prompted us to further explore IL-6 signaling pathway, which is activated in non-proliferating LRCs (stem-like cells).

3.9.1 MCF10A cells express IL-6 and IL-6Ra

To receive the IL-6 signal in a classical manner, the cell must express the membrane bound IL-6Ra. We therefore examined IL-6Ra protein expression in MCF10A cells. To analyze whether IL-6Ra expression is confined to the stem cell state, we examined its expression in a bulk of cells from 2D culture and in a cell pool from disaggregated mammospheres, which is enriched with stem cells (Dontu et al., 2003). Expression of IL-6Ra on the cell membrane (mIL-6Ra) of single MCF10A cells was examined by flow cytometry both in 2D and 3D cultures. We found that detection of the IL-6Ra protein was dependent on the proteolytic cleavage by trypsin for cell isolation (Figure 49). Trypsinization of 8 minutes negatively affected the detection of IL-6Ra indicating that this receptor is cleaved by trypsinization period. Therefore, 3 minutes incubation with trypsin, which did not affect IL-6Ra detection was used for further experiments.

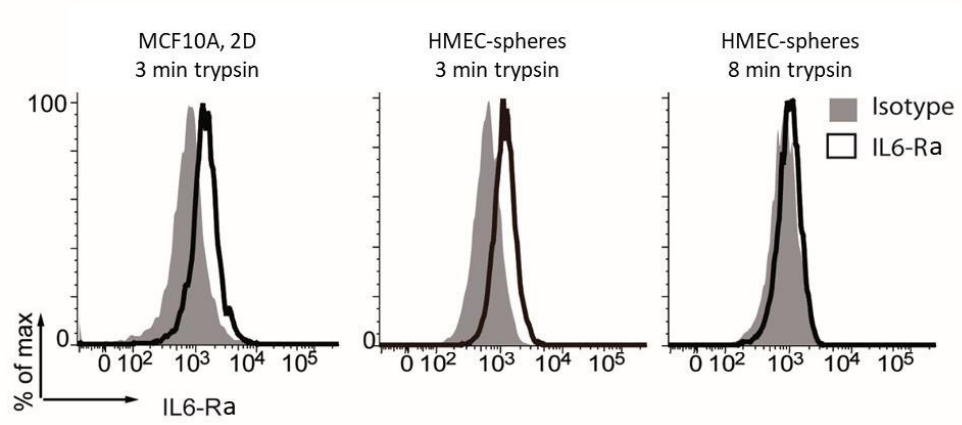

Figure 49: Flow cytometric analysis of IL6-Ra surface expression on MCF10A cells cultured under adherent conditions (2D) and in anchorage independent conditions as mammospheres (3D). Mammospheres were collected and disaggregated using trypsin. A 40mm cell strainer was used to separate single cells from remaining parts of non-disaggregated spheres. The data is representative of three independently performed experiments.

Next, we disaggregated patient-derived HMECs mammospheres and isolated single cells which were then subjected to analysis of IL-6Ra by flow cytometry. IL-6Ra was detected in single cells derived from HMEC-spheres neither after 3 nor 8 minutes trypsinization (Figure 50).

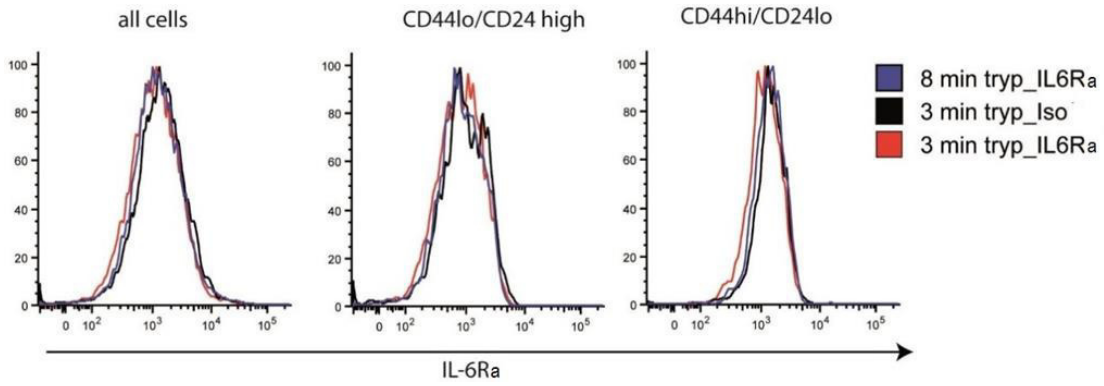

Figure 50: Flow cytometric analysis of membrane bound IL-6Ra expression on HMEC cells cultured in anchorage independent conditions as mammospheres (3D). To avoid technical artefacts result was confirmed with different trypsinization time points (3 and 8 minutes).

The IL-6 cascade can be activated even in cells that do not express IL-6Ra, if soluble IL-6Ra (sIL-6Ra) is present in the surrounding environment (Rose-John and Heinrich, 1994). Therefore, we investigated the presence of IL-6 and sIL-6Ra in adherent MCF10A cell cultures by ELISA. Both, IL-6 and sIL-6Ra were found in the supernatant of MCF10A cultures (Figure 51), showing that these cells fulfil the prerequisites to be stimulated not only by classical, but also by IL-6 trans-signaling. sIL-6Ra can be produced in two different manners, by alternative splicing (spliced IL-6Ra in further text) or by shedding. We further investigated which of the mechanisms are responsible for the production of different isoforms of IL-6Ra.

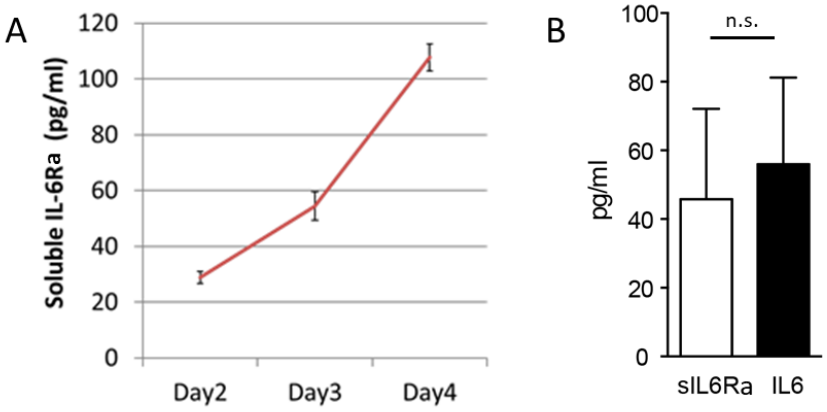

Figure 51: IL6 and the soluble IL-6Ra were measured in cell culture supernatants of MCF10A cells cultured under adherent conditions (n=4 experiments, Mean +/- SD) on days 2, 3 and 4. A) Concentration of sIL6-R is elevated with increasing confluence. B) IL-6 and sIL-6Ra concentration in the supernatant of MCF10A cells at day 2, average of three independent experiments.

To analyze whether expression of IL-6 and any isoform of IL-6Ra was confined to the same cell, we analyzed individually isolated single MCF10A cells (n=46 single cells) from adherent cultures (2D) using a unique primer pair for mIL6-Ra and spliced IL-6Ra analysis. The PCR-product of the spliced IL-6Ra transcript is shorter than of mIL-6Ra transcript (Figure 52A). We observed a heterogeneous

expression profile, with expression of IL-6 and IL-6Ra transcript in 0% (0/29) and 41% (12/29) of the cells, respectively (Figure 52B). Of the 41% IL-6Ra expressing cells, most cells expressed the membrane-bound form, 38% (11/29), with only 7% (2/29) expressing the splice-variant for the secreted receptor from which one cell expressed both mIL-6Ra and splice IL-6Ra and one expressed only splice IL-6R mRNA. The expression of the mediator of IL-6 signaling, gp130 was detected in 97% (28/29) of cells. Hence, only a small fraction of MCF10A cells is amenable to classical IL-6 signaling, but they can all be stimulated by IL-6 (via gp130) if sIL-6Ra is present in the environment.

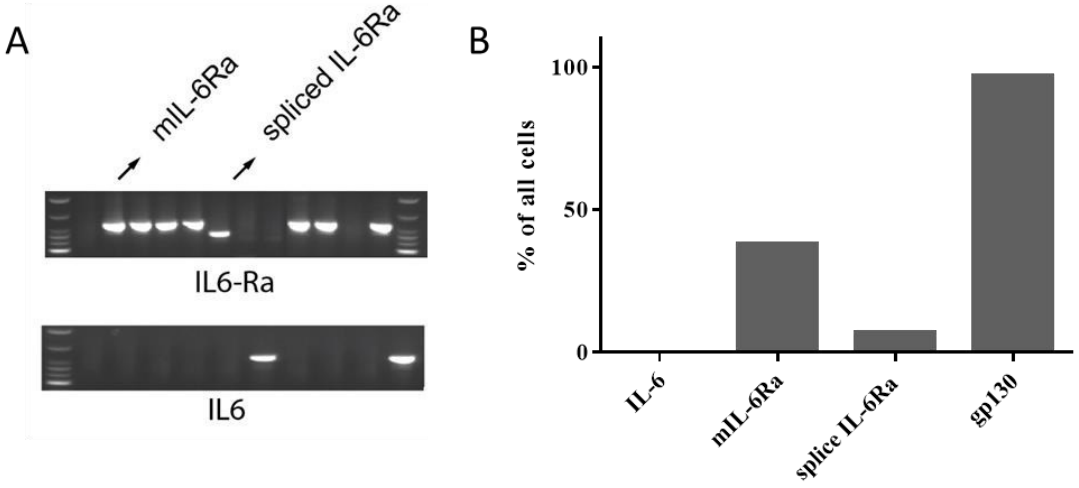

Figure 52: Expression of IL-6 and IL-6Ra mRNA in individually isolated MCF10A cells from adherent culture-conditions. A. The membrane-bound and spliced mRNA-form of IL6-R were discriminated according to the size of the specific PCR band. B. Y-axis represents the percentage of all cells expressing corresponding marker determined through end-point PCR (n=46 for IL-6 and IL-6Ra; n=29 for gp130 analysis).

Next, we analyzed whether these cells co-express some of examined markers and found that 36% (10/28) of gp130 expressing cells co-express mIL-6Ra, both cells that express spliced IL-6Ra also express gp130.

Since spliced variant of the receptor contributes only to a minor extent to the pool of sIL-6Ra, we concluded that majority of sIL-6Ra is produced by limited proteolysis through "a disintegrin and metalloproteinases" (ADAM proteases), ADAM-10 and ADAM-17 (Riethmueller et al., 2016). ADAM proteases shed the extracellular region of the transmembrane proteins. To investigate the role of limited proteolysis, we used TAPI-2, a potent inhibitor of matrix metalloproteinases, ADAM10 and ADAM17 among the others. TAPI-2 mediated inhibition of ADAM-proteases reduced the level of sIL-6Ra, but not of IL-6 (Figure 53), confirming that both alternative splicing and limited proteolysis are the sources of the soluble form of IL-6Ra (sIL-6Ra).

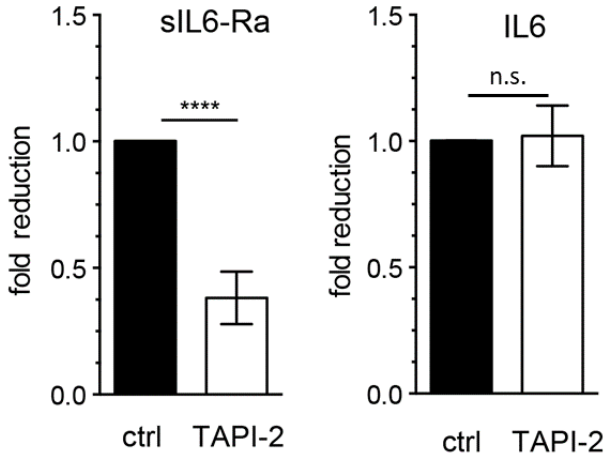

Figure 53: MCF10A cultured under adherent conditions with or without 2 µM TAPI-2. Protein levels of soluble IL6-Ra and IL6 in the supernatant were determined by ELISA (n = 3 experiments, **** p<0,0001, two-sided student's t-test, Mean ±SD).

Taken together, the data show that non-tumorigenic mammary epithelial cells such as MCF10A cells express the membrane-bound IL-6Ra and therefore have potential to respond to classical IL-6 signaling, what we wanted to investigate next. IL-6 and sIL-6Ra detection in the environment confirms existence of a certain level of endogenous activation of IL-6 trans-signaling in these cells.

3.9.2 IL-6 signaling regulates the frequency of stem-like MCF10A cells

To test the effect of IL-6 signaling on the self-renewal capacity of MCF10A cells (i.e. their stem-cell like phenotype) we subjected these cells to a sphere-forming assay. Under these culture conditions, stem/progenitor cells from non-transformed mammary tissue can be expanded and generate mammospheres, which have a clonal origin (Dontu et al., 2003). In line with this, mammosphere-derived cells from both, mouse and human mammary gland, were shown to have the highest ability to repopulate the cleared mammary fat pad *in vivo* (Cicalese et al., 2009; Pece et al., 2010). To elucidate the impact of classical and trans-signaling on mammosphere-formation, which is a stem cell function, we added activators of both pathways: (i) IL-6 to activate both, classical and trans-signaling and (ii) Hyper IL-6 (HIL-6) to activate trans-signaling only. In control cultures, the number of spheres at day 7 represented 0,3% +/- 0,16% (Mean +/- SD) of the input number of MCF10A cells. In the presence of IL-6 and HIL-6 the sphere forming ability was significantly increased (Figure 54) indicating that IL-6 signaling plays a role in the regulation of the stem cell pool not only in cancer (Marotta et al., 2011; Sansone et al., 2007) but also in non-transformed mammary epithelial cells.

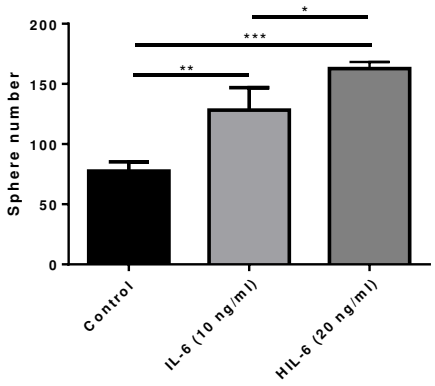

Figure 54: MCF10A cells were cultured as mammospheres (30.000 per plate) in the presence of IL-6 or Hyper-IL6. Each group analyzed in triplicates (one-way ANOVA, * p<0,05, ** p<0,01, all error bars correspond to standard deviation (Mean ±SD))

To discriminate between the influence of classical and trans- IL-6 signaling on the sphere-forming ability of the cells, we inhibited trans-signaling with the soluble form of gp130 (sgp130-Fc), which was shown to specifically inhibit IL-6 trans-signaling at a concentration of up to 100 ng/ml (Scheller et al., 2005) with a suggested effective concentration of 0,1 ng/ml. At both tested concentrations (0,1 ng/ml and 10 ng/ml), the enhanced sphere formation was abolished, showing that all IL-6 effect on sphere formation goes via trans-signaling (Figure 55).

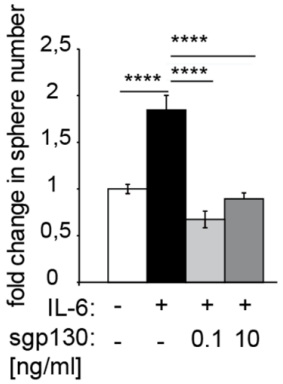

Figure 55: MCF10A cells were cultured in anchorage independent conditions, with or without IL-6 and IL-6 plus sgp130-Fc at the indicated concentrations. Spheres were counted at d7 (n = 2 experiments, each group in triplicates, one-way ANOVA, adjusted p-value **** <0,0001, all error bars correspond to standard deviation (Mean ±SD)). One representative experiment displayed.

3.9.3 Expression of IL-6 and IL-6Ra in stem-like and progenitor cells from MCF10A-spheres

To further elucidate the role of IL-6Ra expression by stem and progenitor cells, we analyzed expression of IL-6 and IL-6Ra mRNA in label-retaining (LRCs) and non-label-retaining cells (nLRCs) isolated from disaggregated MCF10A-spheres. Prior to seeding cells in mammosphere conditions, they were labeled using CFSE (proliferation tracking dye) which is being diluted upon every division. Spliced IL-

6Ra was not expressed by any of analyzed cells, IL-6 mRNA was detected in very few samples, while mIL-6Ra and gp130 were detected in more samples (Table 13), corresponding to expression detected in MCF10A cells from adherent cultures (Figure 52).

Table 13: Expression of IL-6, IL-6Ra (membrane and spliced) and gp130 mRNA in single LRC and nLRC isolated from MCF10A spheres at day 7 (LRC: n=16; nLRC: n=48) determined by end point PCR. Neither IL-6 nor IL-6Ra expression was confined to LRCs or nLRCs.

LRCs	IL-6	mIL-6Ra	Splice IL-6Ra	gp130
Number	0/16	1/16	0/16	12/16
%	0%	6%	0%	75%

nLRCs	IL-6	mIL-6Ra	Splice IL-6Ra	gp130
Number	1/48	7/48	0/48	36/48
%	2%	15%	0%	75%

Another approach to study the expression of IL-6 and its receptor in stem-like and non-stem cells is utilization of the stemness markers, CD44 and CD24 expression. Stem-like cell function has been attributed to mammary epithelial cells expressing high levels of CD44 and low levels of CD24 ($CD44^{hi}/CD24^{lo}$). We analyzed the percentage of $CD44^{hi}/CD24^{lo}$ stem-like cells in MCF10A spheres at day 7 and observed that exogenous IL-6 stimulation significantly increased the percentage of these cells (Figure 56), with HIL-6 stimulated cultures showing the highest increase. In contrast to the results of the mammosphere assay (Figure 55) where increase in the sphere number indicates increase in number of cells with ability to give rise to mammospheres in non-adherent conditions (stem-like cells), no significant difference was observed in the percentage of $CD44^{hi}/CD24^{lo}$ (markers of stem-like cells) cells between IL-6 and IL-6+sgp130 treated cultures. We concluded that stem cell markers do not define stem cells faithfully as sphere formation (function of stem cells).

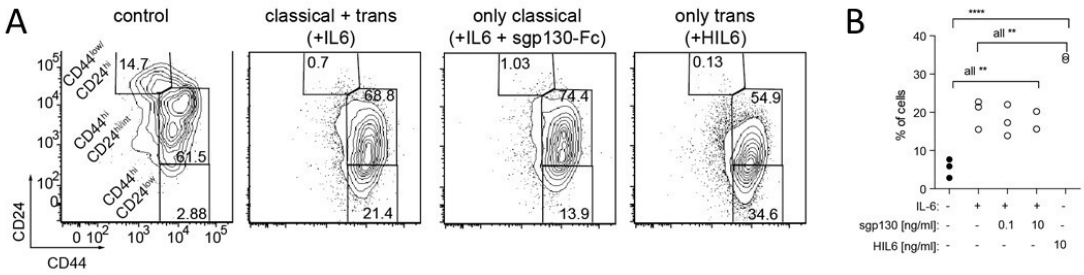

Figure 56: MCF10A spheres were analyzed by flow cytometry at day 7 for the expression of CD44 and CD24. The percentage of $CD44^{hi}CD24^{lo}$ (stem-like) and $CD44^{low/int}CD24^{hi}$ (non-stem) expressing cells was determined. B) Quantification of the data from A. The data represents the cumulative results of three independently performed experiments (n=3 experiments with pooled analysis of triplicates, one-way ANOVA, **p<0,01, ****p<0,0001)

3.9.4 Effect of IL-6 classical- and trans-signaling on proliferation and survival of cells

In the mammosphere assays with the same activators of IL-6 signaling cascade as in Figure 56, we observed the increase in the size of mammospheres in IL-6, IL-6+sgp130 and HIL-6 treated cultures compared to control spheres (Figure 57).

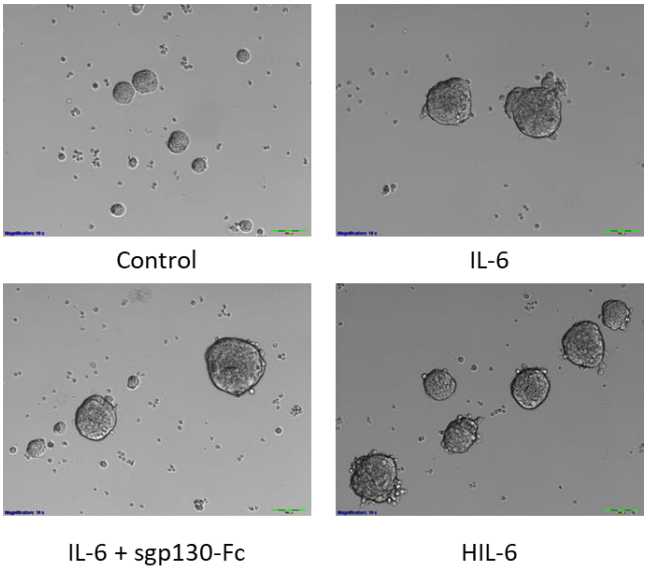

Figure 57: MCF10A mammospheres after 7 days cultivation in anchorage independent conditions with or without IL-6, IL-6 plus sgp130 and Hyper-IL6. Scale bar 100 µm.

Next, we assessed cell proliferation of CFSE labelled MCF10A mammospheres, cultured without or with IL-6, IL-6 + sgp130-Fc and HIL-6. After 4 days, proliferation as function of CFSE-dilution was determined by flow cytometry. Interestingly, $CD44^{hi}/CD24^{lo}$ cells proliferated faster than $CD44^{lo}/CD24^{hi}$ cells (Figure 58), and irrespective of the signaling-pathway, i.e. classical or trans, IL-6 showed a tendency to increase the percentage of living cells in MCF10A-spheres (Figure 59).

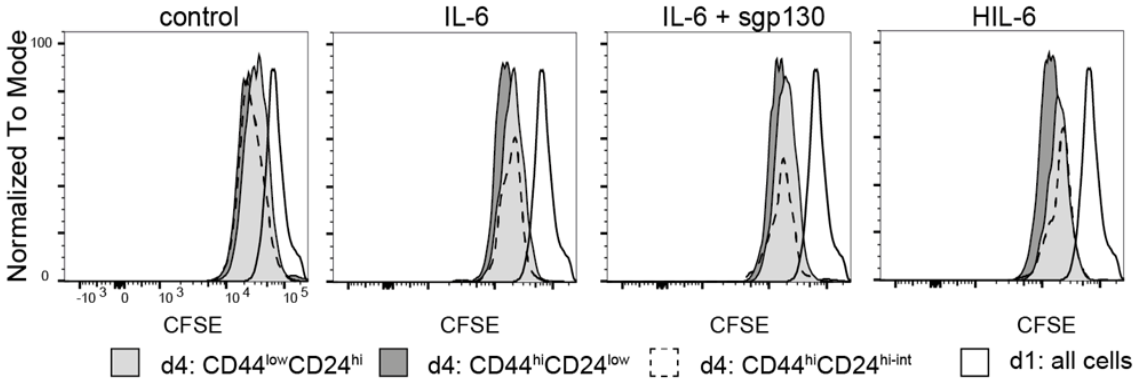

Figure 58: CFSE-labelled MCF10A cells were cultured in anchorage independent conditions with or without activators of classical and trans-signaling and in presence of inhibitor of trans-signaling. At day 4, mammospheres were collected, disaggregated and analyzed. CFSE-dilution of $CD44^{hi}CD24^{lo}$ and $CD44^{low}CD24^{hi}$ was determined at day 4 by flow cytometry. Data is representative for 3 independently performed experiments.

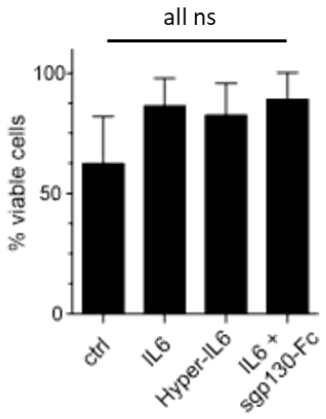

Figure 59: The percentage of viable cells was determined at day 4 by flow cytometry (n=3 experiments, pooled analysis of triplicates in each group).

To examine the population that was mostly affected by IL-6 stimulated proliferation, we needed a reference population, i.e. latex beads. Therefore, after disaggregation of the mammospheres and staining markers for the markers CD44 and CD24, we added the same number of beads to every sample to determine the absolute numbers of $CD44^{hi}/CD24^{lo}$ and $CD44^{lo}/CD24^{hi}$ expression and compare their number in response to stimulation with IL6, IL6-spg130, HIL6. The percentage of LRCs (mainly comprising of $CD44^{hi}/CD24^{lo}$ cells) in the analyzed population was not decreased upon activation of IL-6 signaling (both, only classical or trans) indicating that IL-6 stimulation does not activate proliferation of stem-like cells, but rather of progenitor cells (nLRCs). (Figure 60).

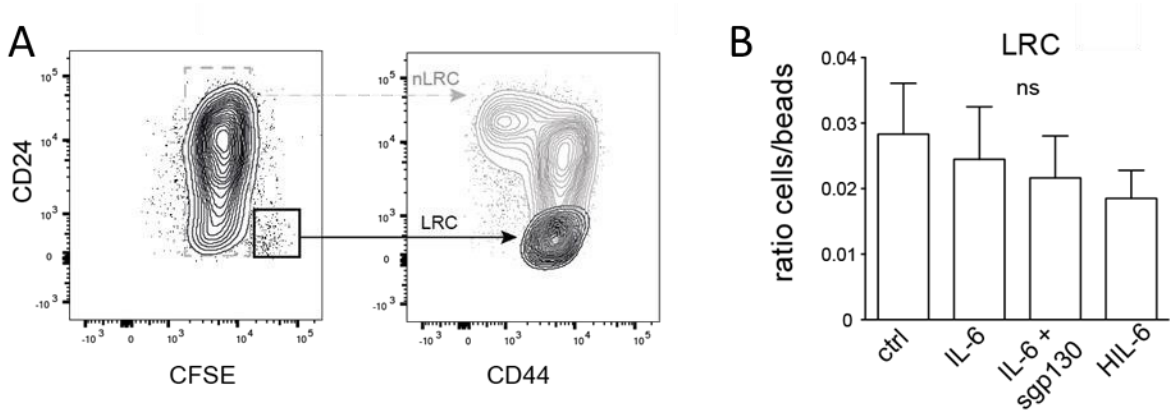

Figure 60: A) CFSE-labelled MCF10A cells were cultured in anchorage independent conditions with or without activators of classical and trans-signaling and in presence of inhibitor of trans-signaling. $CFSE^{hi}$ cells were mostly comprised of $CD44^{hi}CD24^{lo}$ cells. B) The percentage of stem-like LRCs upon IL-6 stimulation showed as ratio of the absolute number of LRCs in control and stimulated cultures to the constant number of beads. Data is representative for 3 independently performed experiments.

These findings corroborate the observed increase in sphere size in IL-6 (classical + trans), IL-6 +sgp130 (only classical) and HIL-6 (only trans) treated cultures (Figure 57), is not achieved by activation of LRCs, meaning the pool of stem-like cells is not changed upon IL-6 stimulation.

3.9.5 Signaling pathway analysis in MCF10A cells upon stimulation of IL-6 signaling

The finding that IL-6 trans-signaling is responsible for stem-cell function prompted us to further investigate differences in signaling cascades activated by only classical, only trans and both pathways. For that purpose we cultured MCF10A cells in anchorage independent conditions alone (group A) or supplemented with IL-6 (group B, activation of both pathways), IL-6 + sgp130-Fc (group C, classical signaling only) and HIL-6 (group D, trans-signaling only) for 12h and 24h. After that we collected the whole cultures, isolated mRNA, and performed a gene expression analysis using microarray. Despite phenotypical differences (Figure 55) we did not detect any other signaling pathways activated by different IL-6 signaling components (classical or trans). Gene expression analysis of the microarray data showed that activation of Jak-STAT, MAPK, inflammatory genes was consistent across all stimulated groups (Figure 61) implying that all IL-6 signaling branches activate the same cascade, but with different signal strength.

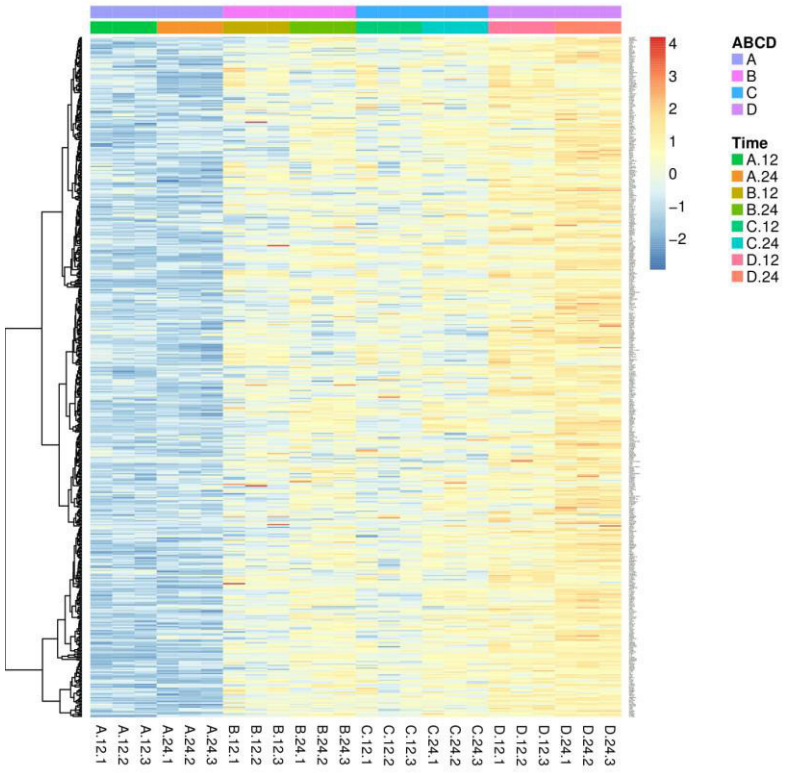

Figure 61: Heatmap depicting the differentially expressed gene (DEG) signature upon activation of IL-6 signaling pathway in MCF10A cells. Non-treated cells (group A) were analyzed at 12h and 24h upon seeding and compared to cells stimulated using activator of both classical and trans signaling (IL-6, group B), only classical signaling (IL-6+sgp130, group C) and only trans-signaling (HIL-6, group D) at 12h and 24h after seeding. The same genes are activated irrespective of the stimulation, but with different strength of the signal.

3.9.6 IL-6 trans-signaling increases sphere formation of HMECs

As we found that IL-6 mediates an increase in stem-like properties among mammary epithelial MCF10A cells, we decided to test primary mammary epithelial cells, HMECs, isolated from reduction mammoplasties of three healthy women and subjected them to the mammosphere-assay in the presence of anti-IL-6, IL-6, and HIL-6. In line with the data from MCF10A cells, HIL-6 significantly increased the sphere-forming ability of primary mammary epithelial cells and the diameter of individual spheres (Figure 62). In contrast, IL-6 did not induce a significant increase in the number of spheres, suggesting that sIL-6Ra was a limiting factor (these findings were presented in the PhD thesis of Dr. Milan Obradovic).

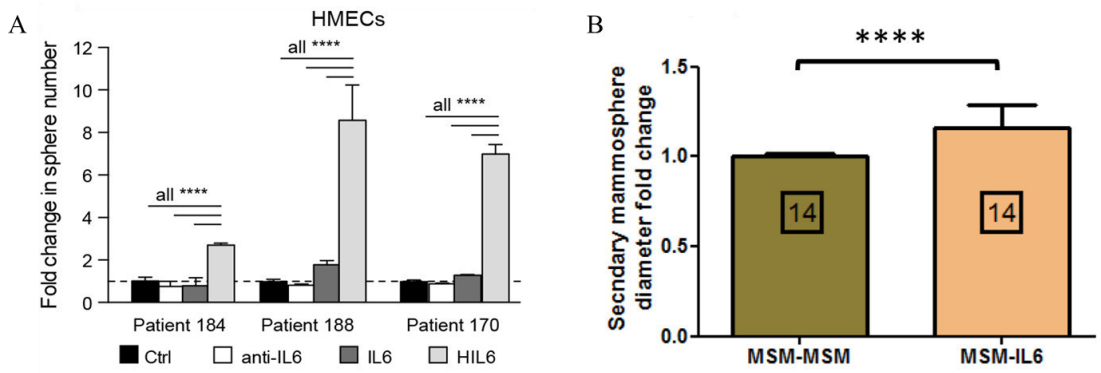

Figure 62: (A) HMECs were cultured with or without IL6, an IL6 blocking antibody or Hyper-IL6. (n = 3 patients, each group in triplicates). One-way ANOVA; **** p<0,0001. All error bars correspond to standard deviation (Mean ±SD). (B) IL6 influenced proliferation of single mammosphere measured by the fold change of the mammosphere diameter (p< 0,0001, two-tailed unpaired t-test). Results are obtained from 7 independent tissue specimens (n=7).

3.9.7 Expression of IL-6 and IL-6Ra in LRCs and nLRCs from HMEC-spheres

To find out whether the expression of IL-6 or IL-6Ra was confined to any cell population within mammospheres, we analyzed the mRNA expression of IL-6 and IL-6Ra in individually isolated QSCs as well as in LRCs and nLRCs from disaggregated spheres. From 3 patients we tested 30 QSCs, 30 LRCs and 30 nLRCs with for the expression of IL-6 and IL-6Ra. Like in MCF10A cells, we found that neither IL-6 nor IL-6Ra expression was confined exclusively to QSCs, nLRCs or LRCs (Table 14). Instead, in all the populations a similar percentage of cells were expressing IL-6 (QSC/LRC/nLRC: 16,7%/20%/33%) and IL-6Ra (QSC/LRC/nLRC: 6,7%/10%/6,7%). Co-expression of IL-6Ra and IL-6 was detected in only one nLRC (3,3%). Majority of cells from all the groups expressed gp130 (QSC/LRC/nLRC: 83,3%/73,3%/66,7%).

Table 14: IL-6 and IL-6Ra mRNA expression was determined in QSCs, LRCs and nLRCs (n=30 in each group) isolated as single cells from secondary HMEC-mammospheres. Expression of neither IL-6 nor IL-6Ra was confined to QSCs, LRCs, or nLRCs.

QSCs		IL-6	IL-6Ra	gp130
Number	30	5	2	25
	%	16,7	6,7	83,3

LRC		IL-6	IL-6Ra	gp130
Number	30	6	3	22
	%	20	10	73,3

nLRC		IL-6	IL-6Ra	gp130
Number	30	10	2	20
	%	33,3	6,7	66,7

3.9.8 Expression of IL-6 and IL-6Ra in DCCs from breast cancer patients

Further, we wanted to examine whether the IL-6 signaling pathway is activated in DCCs isolated from breast cancer patients. Early disseminated cancer cells show very few genomic changes, which makes them more similar to normal than to aberrant cancer cells deriving from late stage primary tumors. We chose 25 DCCs with an aberrant profile in mCGH analysis, isolated from bone marrow of the patients without metastases at the time of surgery (M0-DCCs) and 10 DCCs with an aberrant profile in mCGH analysis from patients with detectable metastases at the time of surgery (M1-DCCs). In line with the restricted expression of IL-6 and IL-6Ra in MCF10A cells and patient derived HMECs, we did not detect expression of IL-6 and IL-6Ra in 25 M0-DCCs (Figure 63) or 10 M1-DCCs indicating that classical IL-6 signaling cannot be activated in these cells.

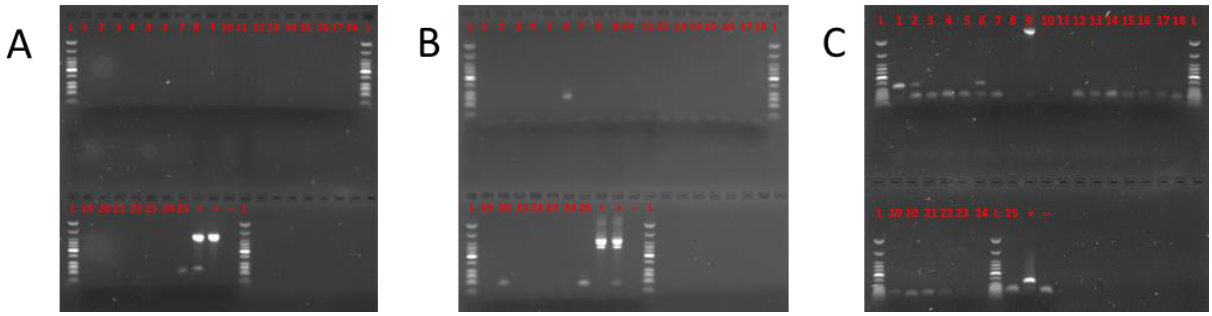

Figure 63: Visualization of IL-6 (A), IL-6Ra (B) and gp130 (C) gene expression in aberrant M0-DCCs from breast cancer patients. Size marker (L): 2-Log-DNA-ladder, WTA-control (+), Negative control (-) of WTA

Gp130 primer pair specifically amplifies the fragment of 125 bp. All analyzed MCF10A single cells (10/10) were positive in this analysis confirming maximal sensitivity of primers. Analysis of the M0- and M1-DCCs showed that 16% (4/25) M0-DCCs and 30% (3/10) M1-DCCs express gp130 mRNA.

3.9.9 Quantitative PCR analysis of gp130 in DCCs from patients with breast cancer

To precisely assess the expression level of target genes, we developed a quantitative PCR (qPCR) method enabling expression analysis of selected genes in a single-cell. The new protocol enabled the use of either primary or re-amplified single-cell whole transcriptome amplification (WTA) products, providing re-usable source of material for downstream analyses. The method was established and tested in a proof-of-concept study on HER2 expression and presented in a bachelor thesis of Franziska Durst. Since this method is more sensitive than end point PCR, we repeated the expression analysis in M0-DCCs using the second primer pair for gp130. In 40% (10/25 cells) of aberrant M0-DCCs the specific amplicon with Ct values lower than 33 was detected. Two cells in which the specific amplicon was detected by end-point PCR did not show a specific melting curve, indicating the absence of a specific amplicon. Overall gp130 expression was detected using either end-point or qPCR in 48% (12/25) of aberrant M0-DCCs and in 40% (4/10) of aberrant M1-DCCs.

Next, we expanded the analysis to a bigger collective of 147 M0-DCCs and 49 M1-DCCs whose mCGH status was not determined, but their gene expression profiles classified them to a group of "true DCCs" (PhD thesis of Nina Patwary). In total we detected the gp130 amplicon (Cp<33) in 84% (123/147) of M0-DCCs and 86% (42/49) of M1-DCCs, indicating that mammary DCCs rarely downregulate gp130 after dissemination. For comparison, we employed the same sensitive method to assess the expression level of gp130 in non-tumorigenic mammary cells, MCF10A. Additionally, we included the MCF7 cell line originating from pleural effusion of breast cancer patient. Although present, the level of gp130 expression was significantly lower in MC-DCCs compared to both, MCF10A and MCF7 cells (Figure 64) indicating that the bone marrow environment can have an impact on the expression level of gp130 in mammary DCCs.

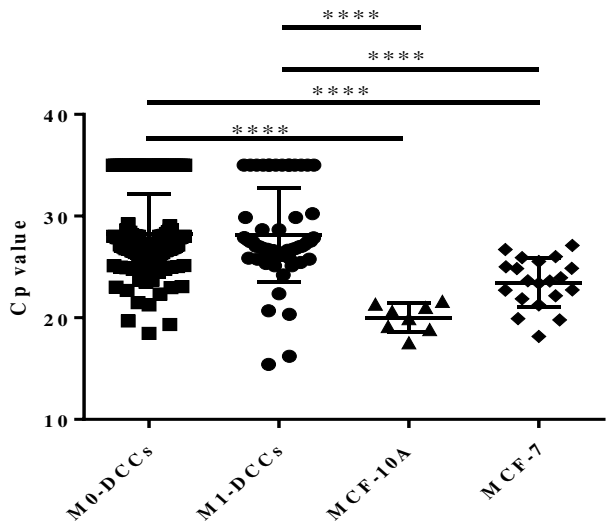

Figure 64: gp130 mRNA expression in MCF10A, MCF-7 and DCCs from breast cancer patients with (M1) and without (M0) distant metastases (M0-DCCs, n=122; M1-DCCs, n=40; MCF7, n=22; MCF10A, n=8). One-way ANOVA, **** p<0,0001.

3.9.10 Regulation of the gp130 expression in DCCs by the bone marrow environment

The bone marrow environment is mostly comprised of mesenchymal stromal (stem) cells (MSCs), osteoblasts (OBs), endothelial cells (HUVECs) and hematopoietic cells. To test whether bone marrow stromal cells modulate the ability of mammary cells to receive IL-6 signals, we co-cultured MCF10A cells with (i) primary human MSCs isolated from the bone marrow aspirates of non-metastasized breast cancer patients or healthy volunteers, (ii) OBs differentiated from these MSCs or (iii) primary human umbilical cord endothelial cells (HUVECs) and genetically manipulated to prolong their life *in vitro* (Ghajar et al., 2013). On day five, flow cytometric analysis revealed cell-surface downregulation of gp130 on MCF10A cells co-cultured with MSCs and OBs, but not with HUVECs (Figure 65).

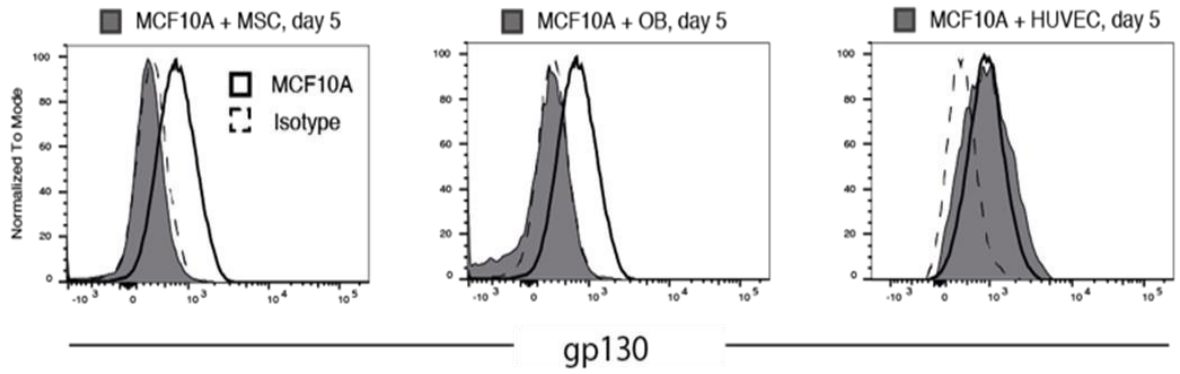

Figure 65: Surface gp130 expression of MCF10A analyzed by flow cytometry analysis after 5 days of co-culture with primary mesenchymal stem cells (MSCs) from a breast cancer patient, primary osteoblasts (OBs) derived thereof and primary human umbilical endothelial cells (HUVECs). MCF10A – cells cultured alone (positive control of gp130 expression).

The regulation of the gp130 protein expression can be a result of cell-cell contact or contact independent. We further investigated the mechanism how MSCs impact expression in mammary cells. To examine this we cultivated cells in co-cultures with MSCs and also in a transwell set up, in which MCF10A cells are separated from MSCs resulting in an inhibition of the contact, but enabling transfer of the secreted soluble factors. Downregulation of the gp130 protein was independent from cell-cell contact as it was also detected when MCF10A and MSCs were separated by a transwell membrane (Figure 66), indicating that gp130 protein downregulation in mammary cells it occurs via a soluble factor secreted by MSCs.

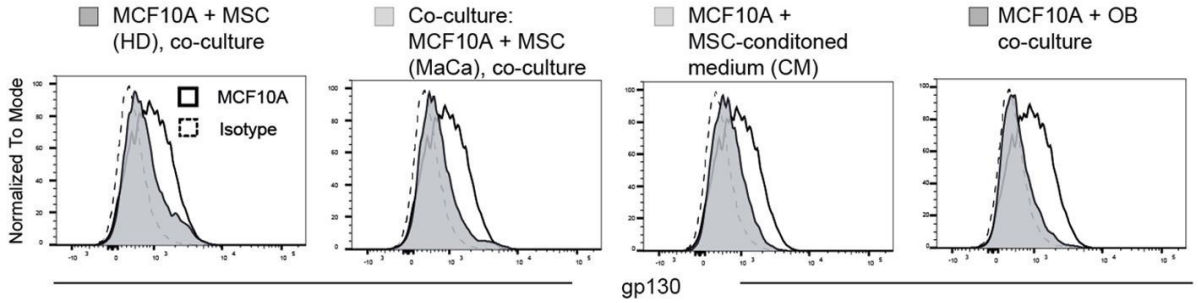

Figure 66: Surface gp130 expression of MCF10A by flow cytometry analysis after 14 hours of co-culture with MSCs from a healthy control (HD) or breast cancer patient (MaCa), OBs (co-culture) or MSC-conditioned medium. Grey filled histograms indicate MCF10A co-cultures with MSCs, MSC-conditoned medium (CM) or OBs. White filled histograms indicate MCF10A cell cultured alone, and dashed histograms isotype control staining for gp130.

Next, we wanted to examine whether this effect of MSCs on gp130 expression is instant in mammary cells or it requires longer stimulation. To answer this question we co-cultured MCF10A cells with MSCs and examined expression of gp130 protein in MCF10A cells from these co-cultures after 6, 14, 24, 38 and 48 hours of cultivation (Figure 67). Downregulation of gp130 from the cell surface was not instantly detected, but observed between 6 and 14 hours after initiation of the co-culture with MSCs and remained stable until the last analyzed time point. This effect is consistent with constitutive endocytosis of gp130 that is independent of binding the IL-6/IL-6R ligand complex (Thiel et al., 1998).

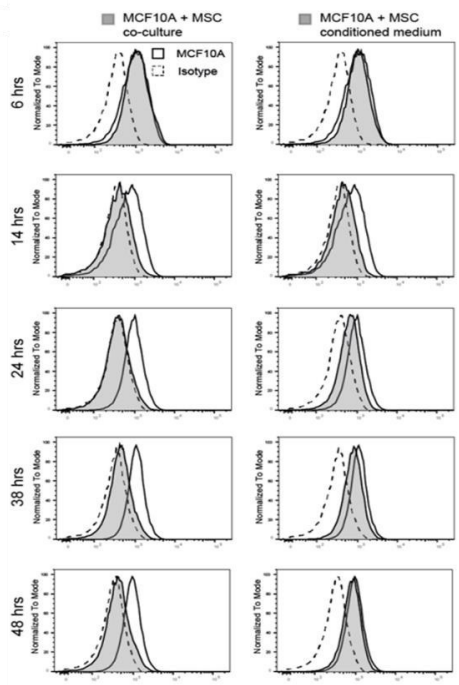

Figure 67: Surface gp130 expression of MCF 10A after 6, 14, 24, 38 and 48 hours of co-culture with MSCs or MSC-conditioned medium). Grey filled histograms indicate MCF 10A co-cultures with MSCs or MSC-conditoned medium (CM). White filled histograms indicate MCF10A cells cultured alone, and dashed histograms show isotype control staining for gp130.

To explore whether this MSC-induced phenotype is stable once when achieved, we cultivated the MCF10A cells and MSCs in transwell plates, removed MSCs after 5 days and analyzed gp130 expression on day 6. Persistent downregulation of gp130 after 5 days in the presence of MSCs or CM from MSCs (transwell) was rescued by removal of the transwell with the MSCs indicating that gp130 expression in mammary cells is reversible and dependent on the continuous presence of MSCs as removing the MSC-containing transwell restored the gp130 expression level in comparison to MCF10A cells co-cultured with MSCs for all 6 days (Figure 68).

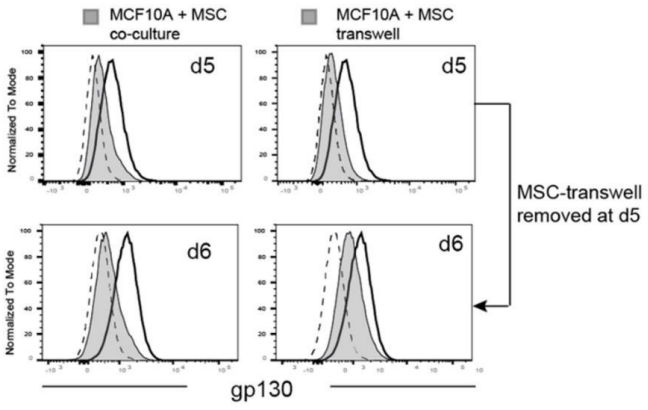

Figure 68: gp130 surface expression on MCF10A cells after 5 and 6 days of co-culture with MSCs or MSCs and MCF10A separated by a transwell.membrane. Removal of transwell containing inhibiting MSCs retrieves gp130 expression (right panel in bottom row). Grey filled histograms indicate MCF 10A co-cultures with MSCs or MSC-conditoned medium (CM). White filled histograms indicate MCF10A cells cultured alone, and dashed histograms show isotype control staining for gp130.

Finally, we asked whether gp130 cell-surface downregulation had functional consequences and therefore tested MCF10A cells pre-treated for 14 hours with conditioned medium (CM) from patient derived MSC for their sphere-forming ability in the presence or absence of HIL-6. Compared to control cultures, the ones pre-treated with MSC-CM showed an increase in the number of single cells and significantly reduced number of spheres, reflecting the impaired IL-6 signaling by endogenously produced IL-6/IL-6Ra (Figure 69). Adding HIL-6 restored sphere-numbers only in the range of control-cultures and failed to reach the level of cultures supplemented only with HIL-6. Taken together, our data indicate that the ability of early DCCs to react to IL-6 signaling and trans-signaling is dependent on the microenvironment in which they reside, with mesenchymal stem cells and osteoblasts disabling IL-6 trans-signaling and consequently also the number of DCCs with a stem-like phenotype and function.

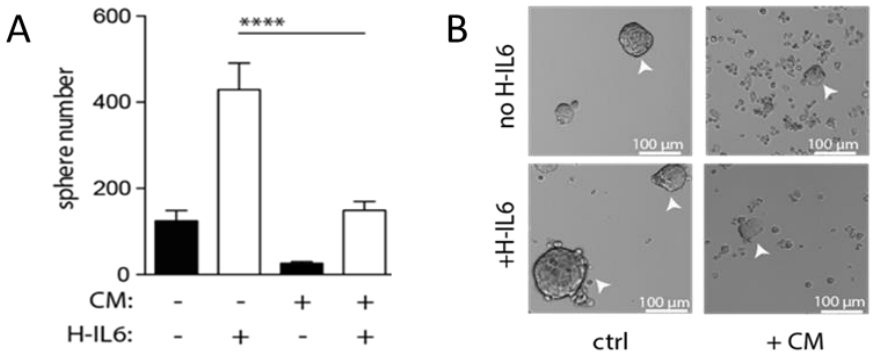

Figure 69: MCF10A were pre-treated for 14 hrs with MSC-conditioned medium, washed and then tested for their ability to form spheres in the presence or absence of exogenously added H-IL6. A) Quantification of sphere-formation assessed after 7 days. **** p<0,0001 B) Images of the spheres of the cells treated as described. Arrowheads point to a typical mammospheres from given condition. Scale bar 100µm.

4 Discussion

In this study we investigated whether the BM-DCCs originating from breast cancer patients are dormant, and consequently in which type of dormancy. Our aims were to i) find the best model(s) of mammary cell dormancy, ii) explore mechanisms that regulate dormancy of breast DCCs in the bone marrow and apply this knowledge on early DCCs, putative precursors of metastases. Early DCCs display significantly fewer chromosomal aberrations than primary tumor cells or DCCs from metastatic patients. In that regard, early DCCs are much closer to normal (non-transformed) cells than to advanced tumor cells (Schardt et al., 2005; Schmidt-Kittler et al., 2003). Therefore, we chose mammary cells isolated from the tissue originating from healthy donors and a non-tumorigenic mammary cell line as a model of early DCCs. In search for best model of dormancy we used previously established *in vitro* models and adapted them to our needs Single mammary cells of different proliferation states could be isolated from the established models of dormancy and utilized for further analysis. The adapted stem cell model enabled isolation and subsequent analysis of the proliferation state of mammary cells and was chosen for further analysis. In this model mammary cells were cultured in anchorage independent conditions, enabling discrimination of the single quiescent (surviving non-proliferating) cells and mammospheres (originating from activated stem-like cells) from which single cells were isolated after disaggregation. To determine the proliferation status of isolated cells, we established a PCR-based assay which examines the expression of proliferation markers Ki67 and MCM2 in single cells. PKH26-label retention assay was combined with PCR analysis to select proliferative and non-proliferative cells for gene expression analysis. For analysis of the proliferation markers we isolated (i) sphere-derived LRCs, (ii) sphere derived nLRCs and (iii) single cells that had not divided over time and remained single cells after one week of sphere culture and therefore were termed quiescent single cells (QSCs). Proliferation status of these cells was validated by Ki67 and MCM2 expression giving three groups of cells (sphere-derived non-proliferating LRCs, sphere derived proliferating nLRCs and non-proliferating QSCs) that were subjected to whole gene expression analysis on microarray. K-means clustering following microarray analysis divided these three cell phenotypes into 5 groups, with LRCs and QSCs comprising two subgroups each. Among several signaling pathways characteristic for stem-like cells (LRC), IL-6-related signaling events were identified as one of the most prominent. Therefore, we further investigated the role of IL-6 signaling in stem cells and DCCs isolated from bone marrow of breast cancer patients. Gene expression analysis of human samples using microarray and sequencing, showed that both, proliferative and quiescent cells can be found among DCCs in the bone marrow. In further analysis of different BM compartments (niches) we learned that mammary cells residing in the mesenchymal or osteoblastic niches enter a quiescent state, whereas mammary cells can be activated to enter cell cycle if they reside in the vascular niche.

In studying dormancy in DCCs derived from breast cancer patients we faced many challenges, among which the biggest is lack of the appropriate human DCC-derived models. Therefore we decided to employ the Her2-driven mouse model.

4.1 Balb-NeuT as *in vivo* model of dormancy

Balb-NeuT model, in which tumor development closely resembles this process in women (Di Carlo et al., 1999) has been intensively used to study breast cancer. Previous findings indicated existence of DCCs, which give rise to lung metastases in lung, but do not give rise to metastases in bones. These cells are able to proliferate in the BM in the conditions existing upon bone marrow transplantation (Husemann et al., 2008). We aimed to isolate these cells from BM and for that purpose engaged different labeling methods, such as labeling using cell tracking dye and GFP-genetic labeling. Inability to detect any DCC in the bone marrow suspension of recipient mice by any of these approaches prompted us to use EpCAM as a selection marker for DCC detection and isolation, which showed us existence of EpCAM+ cells both among CD45- and CD45+ (hematopoietic) cells. Although we initially thought that inability to detect GFP+ cells was due to immune rejection (Ansari et al., 2016; Gambotto et al., 2000), experiments with NSG recipient mice and cell labeling using PKH26 pointed to a possibility that in these mice dissemination did not occur. EpCAM is regularly used as a marker for DCCs in bone marrow. Knowing that EpCAM is also expressed by some of the cells from the erythroid lineage, we separated hematopoietic cells (CD45+ cells) from the rest of the BM cells and isolated EpCAM+ cells from both fractions. Profiling of these cells will enable discrimination of the true DCCs from the confounding population of erythroid cells.

Having an approach that enables detection of DCCs among bone marrow cells (EpCAM+ cells in CD45- fraction) we tested in Balb-NeuT mice the effect of progesterone, steroid hormone that was found to affect the migration of Her2+ mammary cells (Hosseini et al., 2016a; Johnson et al., 2010). However, we did not detect any change in the number of DCCs in the BM of Balb-NeuT mice, which could also be a consequence of an impaired dissemination of mammary cancer cells. Since the number of DCCs, we are aiming to isolate, is very low in tested models, we tried to employ the model where transplantation of the BM of the young transgenic mice to the wild type recipients resulted in expansion of DCCs (Husemann et al., 2008) with 10-30% of DCCs in the whole BM cell population. In the experiments of Hüsemann and colleagues, BM transplantation stimulated the outgrowth of DCCs, but in our experiments neither recipient mice developed any symptoms of disease nor could we detect DCCs in their BM.

All these results with different models and in different experiments raise the question whether dissemination of the mammary cells to BM is impaired. The reason for detected change in dissemination in the models can be effect of the environment since the lab was changed in previous years and the

conditions in these laboratories differ. That influences the complete gut microbiota of the laboratory animals, which is shown to differ in healthy women from the women with breast cancer (Erdman and Poutahidis, 2017; Fernandez et al., 2018; Rea et al., 2018). Therefore, microbiota of the animal model in different conditions, as well as its impact on breast cancer development is now intensively studied in our laboratory.

4.2 Establishment of the *in vitro* models of dormancy

After failing to establish *in vivo* model of dormancy, we searched for good *in vitro* models. Since we wanted to study dormancy in early BM-DCCs, which display close-to-normal genomes (Hosseini et al., 2016a; Schardt et al., 2005) existing cancer cell lines carrying many aberrations were not good as a potential model. Therefore, we decided to use mammary epithelial cells *ex vivo* isolated from reduction mammoplasties as a model and MCF10A, immortalized pre-malignant mammary cell line, for functional testing. The bone marrow is a very complex organ consisting of hematopoietic cells, fibroblasts, macrophages, adipocytes, osteoblasts, osteoclasts and endothelial cells which form organized niches with specific roles (Tamma and Ribatti, 2017) among which are endosteal (osteoblastic) and vascular (endothelial) are the most important for the function of bone marrow. Therefore, we tried to establish these two niches and culture mammary cells in them. The main function of the bone marrow is production and lodging of hematopoietic stem cells (HSCs) why we also cultivated cells in anchorage independent conditions (mammosphere assay) which favor the growth of stem cells. Analysis of the mammary cells cultured in established osteoblastic (Kim et al., 2013a) and endothelial (Ghajar et al., 2013) niches showed that they just slow the growth of mammary cells on population level, but do not induce dormancy in single cells, which we aimed to study. Contrary, in the mammosphere assay we were able to detect and isolate the single cells that did not proliferate for 7-10 days. Besides that, we could isolated stem-like and proliferating mammary cells. Therefore, we decided to proceed with the mammosphere assay as the model for studying dormancy in closest-to-DCCs cells.

4.3 Studying dormancy and proliferation in BM-DCCs

To analyze the proliferation status of the DCCs we established assay based on analysis of expression of the proliferation markers MKi67 and MCM2 using non-activated and activated CD8+ T-cells. Using PKH26 labeling (Cicalese et al., 2009; Pece et al., 2010) and analysis of the expression of proliferation markers, we classified mammary cells isolated from human mammary gland and cultured in anchorage independent conditions in three groups: (i) non-proliferating quiescent single cells (QSCs), (ii) non-proliferating stem-like cells (LRCs) and (iii) proliferating progenitor cells (nLRCs). These cells were subjected to gene expression analysis using micro arrays and identified “gene signatures” were applied to 21 aberrant BM-DCCs (15 M0-DCCs and 6 M1-DCCs), as confirmed by mCGH. This analysis

revealed us subgroups in the groups of QSCs and LRCs, pointing to heterogeneity existing both among stem and differentiated mammary cells.

4.3.1 Mammary stem cells

One of the type of dormancy widely known in literature is dormancy of the stem cells. Cultivation of cells in ultra-low attachment conditions in serum free medium results in enrichment of stem and progenitor cells (Dontu et al., 2003; Ponti et al., 2005; Rappa et al., 2008; Rybak et al., 2011) which correlates to the findings that at least a fraction of DCCs (Bartkowiak et al., 2010) and CTCs express stem cell markers, such as CD44, ALDH and Bmi1 (Baccelli et al., 2013; Barriere et al., 2012). Additionally, these conditions enable purifying the population of epithelial cells, since fibroblasts cannot survive these hostile conditions (Kulkarni and McCulloch, 1994; Wei et al., 2003). Subgrouping of the LRCs into two subgroups, was not surprising, since heterogeneity within mammary stem cells has already been described, indicating existence of both multipotent basal and luminal MaSCs (Fu et al., 2014; Van Keymeulen et al., 2017; Visvader and Stingl, 2014). Whether defined LRC1 and LRC2 groups fit to this phenotype is to be done. Also, during mammary gland development one can discriminate two types of MaSCs, fetal and adult. In adult mammary gland distinct types of stem cells exist, long-term and short-term repopulating cells. They are responsible for intensive transient alveologenesis during pregnancy, but their self-renewal capacity is lower than of fMaSCs (Asselin-Labat et al., 2010; Tiede and Kang, 2011). Numerous studies identified different stem cell markers. For instance, basal cells display an $EpCAM^{lo}CD49f^{hi}$ phenotype (Eirew et al., 2008; Lim et al., 2009; Stingl et al., 2001), and express c-Kit (Lim et al., 2009; Stingl et al., 2001). ALDH1 is also often used as mammary stem cell marker since ALDH1+ cells show multilineage potential both *in vitro* and *in vivo* (Ginestier et al., 2007; Liu et al., 2014), but some studies also show its controversial expression and demonstrate that these cells are restricted to a luminal subpopulation in *in vitro* and *in vivo* experiments where they do not provide long-term engraftment (Eirew et al., 2012; Shehata et al., 2012). All these methods determine different subpopulations with stem-cell character, but they all emphasize the existence of more than one type of stem cell in the mammary gland, going in line with our results where we defined different subgroups of stem cells, LRC1 and LRC2. The relevance of our method was additionally examined by comparing gene expression profiles of LRCs, nLRCs and QSCs. isolated based on label retention, with the gene expression profiles obtained in the study of Lim et al, on stem, progenitor and differentiated mammary cells, isolated based on expression of EpCAM and CD49f (Lim et al., 2009). Differentiation of cells in our study shows statistically significant correlation to the one in above mentioned study with accuracy of 58% - 75%, pointing to a differentiation in a LRC→nLRC→QSC direction. Although the selection based on expression of stem-cell related markers was not applied here, we could isolate stem population based on retention of the labeling dye. These cells were further analyzed for expression of a distinct set of stem-cell markers using gene expression

microarrays. We found MUC1 to be upregulated in the LRC population correlating with the data of other groups where MUC1 was found to be expressed by stem/progenitor MCF-7 cells (Engelmann et al., 2008), but also is an oncogene involved in cancer progression (Nath and Mukherjee, 2014) and further by stem cells among CTCs of breast cancer patients (Kasimir-Bauer et al., 2012). Also, we detected upregulation of CD24 in QSCs compared to sphere-derived LRCs and nLRCs indicating these are more differentiated cells (Schabath et al., 2006; Spike et al., 2012).

4.3.2 Signaling pathways in mammary stem cells

Analysis of the activated signaling pathways in defined groups of mammary cells (QSCs, LRCs and nLRCs) detected that different signaling pathways which were already known to be associated to stem cells were also activated in LRCs. Involvement of Wnt (Merrill, 2012; Sokol, 2011; Xu et al., 2016), PI3K/AKT (Dubrovska et al., 2009; He et al., 2017; Romorini et al., 2016), MAPK and Notch (Woo et al., 2009; Yu et al., 2008) signaling pathways in stem cells is already known. Notch is also involved in maintaining the quiescence in adult muscle stem cells and hematopoietic stem cells (Bjornson et al., 2012; Wang et al., 2015b) while Wnt is also necessary for differentiation of human embryonic stem cells, mouse neurons, myocytes and embryonic stem cells, (Atlasi et al., 2013; Davidson et al., 2012; Newman et al., 2018; Prakash and Wurst, 2007; Suzuki et al., 2015). Not surprisingly, nLRCs which represent actively dividing progenitors mostly overexpress pathways involved in the regulation of the cell cycle. The role of IL-6 signaling in mammary gland and breast cancer is not completely elucidated. Our data suggest that this pathway is one of the regulators of the stem cell function in mammary cells, but its role in stem cells is not yet so intensively studied like the roles of the other pathways which were upregulated in stem-like cells. To increase the knowledge of less studied signaling pathway in mammary stem cells we further focused on studying IL-6 signaling in the mammary gland.

4.4 IL-6 signaling in the mammary gland

IL-6 activates its signaling cascade through binding to its receptor, IL-6R and then the IL-6/IL-6R complex induces homodimerization of gp130 which then triggers a downstream activation of Janus (JAK) kinases, and the downstream effectors STAT3, SHP-2/Ras, and PI3K/Akt (Kishimoto, 2005; Murakami et al., 1993). To investigate the role of IL-6 in normal mammary gland and DCCs from breast cancer patients, we started with an analysis of a non-tumorigenic mammary cell line, MCF10A where we detected the presence of IL-6R on the surface of cells grown in adherent conditions and cells grown as mammospheres. However, we did not detect IL-6R on the surface of patient derived HMECs grown as mammospheres. Jiang and colleagues showed that down-regulation of IL-6/IL-6R expression results in growth inhibition of MCF-7 cells (Jiang et al., 2011) which is in line with our finding that addition of extracellular IL-6 increases the size of the mammospheres, a consequence of increased proliferation

of progenitor cells. Besides that, IL-6 induced an increase in the number of mammospheres, stimulating stem cell function in mammary cells, as already shown for different cell types, such as hepatic cancer, lung and ovarian cancer cells (Ding et al., 2016; Lee et al., 2016; Sansone et al., 2007; Wang et al., 2016). Lee and colleagues found that in lung cancer this effect is confined to a CD133+ positive population (Lee et al., 2016).

Mammosphere derived patient HMECs do not express IL-6R protein, but still react to IL-6 stimulation. An alternative mechanism to activate IL-6 signaling cascade is trans signaling, activated through soluble IL-6R that can bind IL-6, bridge binding to the gp130 and activate the signaling cascade, even in cells that do not express mIL-6R (Mitsuyama et al., 2006). Soluble IL-6R is in mammary cells mostly produced by limited proteolysis of mIL-6R by ADAM proteases (Briso et al., 2008; Holub et al., 1999; Horiuchi et al., 1994; Mullberg et al., 1993). Due to the low frequency of cells co-expressing IL-6 and IL-6R (membrane or soluble), as detected by transcriptomic analysis, we concluded that IL-6 signaling (both classical, conducted via mIL-6R or trans, conducted via sIL-6R) in mammary cells is rather maintained in a paracrine than autocrine manner. Different cell types found in mammary gland, such as adipocytes (Gyamfi et al., 2018a; Gyamfi et al., 2018b), normal and tumor associated fibroblasts (Adams et al., 1991; Subramaniam et al., 2016), but also mesenchymal stem cells (Cortini et al., 2016; Ding et al., 2016) secrete IL-6, that fuels the sources of necessary ligand for mammary cells activation. The inability to detect IL-6R on the membrane of cells isolated from patient derived mammospheres pointed to the trans-signaling as a potential mechanism regulating stem cell function in the mammary gland. Therefore, we tested HIL-6, a fusion protein of IL-6 and sIL-6R that directly binds to ubiquitously expressed gp130 and activates the signaling cascade (Adam et al., 2009b; Peters et al., 1998), and found that this triggers trans signaling and confers stem cell features to mammary cells (increased number of sphere forming cells, increased CD44+/CD24- fraction), in a significantly higher manner than IL-6 alone. Selective inhibition of sIL-6R using sgp130-Fc confirmed that IL-6 trans-signaling confers stem cell features to mammary cells. This was unknown as trans-signaling was so far connected to pathological conditions, such as chronic inflammatory diseases (Scheller et al., 2006) and cancers (Becker et al., 2004; Brooks et al., 2016; Matsumoto et al., 2010). Interestingly, progression of IL-6 trans-signaling driven colon cancer can be suppressed by TGF-β activity (Becker et al., 2004). In line with our data are the findings that IL-6 signaling triggers conversion of prostate, breast and lung cancer non-stem cells to cancer stem cells (Iliopoulos et al., 2011; Kim et al., 2013b; Rodrigues et al., 2018). However, in these studies different roles of classical and trans signaling were not examined. Although sgp130-Fc inhibits both, classical and trans-signaling at extremely high concentrations (Garbers et al., 2011), which cannot be found in physiological conditions, the concentration we used (0,1 ng/ml) was very low and selectively affected only the trans-signaling (Jostock et al., 2001; Scheller et al., 2005), confirming trans signaling is the responsible factor in maintaining stemness in mammary cells. Gene expression analysis of populations in which separate IL-6 signaling pathways were

activated/blocked did not indicate different pathways activated by classical or trans-signaling, corroborating findings that they share major functions, but the strength of the signal may differ. This could also be a consequence of the technical limitation as the stem cell population is quite rare and their contribution in whole mRNA samples taken from a bulk of cells might be diluted, and therefore fine differences present in that small population are lost.

The present cell hierarchy we found in the mammary gland raises the question of the population in which IL-6 exerts its function. As we found that IL-6R expression is not confined to any of the defined subpopulation of HMECs (LRCs, nLRCs or QSCs) we further examined the effect of trans-signaling. End point and qPCR analysis confirmed ubiquitous expression of gp130 (Scheller et al., 2014; Xu and Neamati, 2013) in patient derived HMECs indicating that IL-6 signaling in these cells depends on the presence of mIL-6R or excess of sIL-6R. In our analysis IL-6 signaling, irrespective classical or trans, showed the trend to increase the percentage of living cells in MCF10A-spheres, as well as an increase in the size of mammospheres as a phenotypic manifestation of increased proliferation. Since the percentage of LRCs was unaffected we concluded that the major target population for increased proliferation were the progenitor cells. Among the three analyzed subpopulations of cells (QSCs, LRCs, and nLRCs), IL-6R was expressed in a similar percentage of cells, with or without sIL-6R. Most of the IL-6 expressing cells were found among nLRCs. Although this difference was not statistically significant, it confirmed that activation of the endogenous IL-6 signaling could be confined to the progenitor cell population enabling them to actively proliferate in mammosphere cultures.

After we found that the majority of cells isolated from HMEC-spheres (67-83%) express gp130, we investigated its expression in DCCs isolated from the bone marrow of breast cancer patients and learned that only 48% of aberrant M0-DCCs express this IL-6 signaling transducer, suggesting a gp130 downregulation upon dissemination to bone marrow. Further we examined the regulation of gp130 expression in MCF10A cells by the cells comprising the bone marrow microenvironment and found that osteoblasts and mesenchymal stromal cells downregulate gp130, opposite to endothelial cells. Although this downregulation is contact independent (exists also in the presence of transwell membrane), it is also transient, indicating that stimuli dictating downregulation must be constantly produced by the environment of the DCCs. Although transient, this downregulation has a long term effect since the sphere cultures after 7 days produce significantly lower number of mammospheres, reflecting decreased stem cell and proliferating capacity. Proliferation analysis (Ki67 and MCM2 expression) showed that the number of proliferating cells was significantly higher in group of cells with activated IL-6 signaling than in the group where IL-6 signaling was downregulated. Overall, this all indicates that IL-6 signaling is at least one of the important pathways that play a role in regulation of BM-DCCs quiescence in breast cancer patients. In line with our data, another recent study showed that endothelial IL-6 confers tumorigenic (CSC) potential to primary head and neck squamous cell

carcinoma cells (Krishnamurthy et al., 2014). Therefore, our findings of IL-6 regulating dormancy of BM-DCCs in breast cancer patients is of great importance for further therapeutical approaches.

4.5 Cancer cell dormancy in the bone marrow niche

Of advanced breast cancer patients 65-75% develop bone metastases (Langley and Fidler, 2011). In our study we aimed to investigate the effect of some of these niches on the proliferation of tumor cells. Endosteal (osteoblastic) and vascular niches are the two main types of organized lodges in the bone marrow environment (Oh and Kwon, 2010; Tamma and Ribatti, 2017), but very close proximity of these niches complicates studying of their role in metastasis. Complex cooperation of these niches with mesenchymal stromal cells results in specific stem cell niches as most important functional unit for homing of the hematopoietic stem cells (HSC) (Morrison and Scadden, 2014; Yin and Li, 2006). In last years it was shown that cancer cells home to the epiphyseal osteoblastic surface of the endosteum (Nwajei and Konopleva, 2013) or to metaphysis (Bussard et al., 2008), but they were also found in the proximity of blood vessels, with specifically dormant DCCs occupying the regions of stable vasculature (Ghajar et al., 2013) or E-selectin- and stromal cell-derived factor 1 (SDF-1)-rich perisinusoidal vascular regions (Price et al., 2016). We found that the proliferation rate of mammary cells is decreased in co-cultures with osteoblasts, which is in line with earlier findings that the majority of disseminated prostate cancer cells in mice occupy the same (osteoblastic) niche as quiescent HSCs (Shiozawa et al., 2011; Wang et al., 2014) where they reside in a non-proliferative state at least 7 days after injection (Wang et al., 2014). A recent study showed that prostate DCCs in the osteoblastic niche take on stem cell markers, such as CD133+/CD44+ and increased levels of KLF 4, Bmi-1, and Nanog mRNA, which justifies comparison of DCCs with HSCs in this sense (Shiozawa et al., 2016). Osteoblasts have been shown to play a role in maintaining HSC quiescence partly through the interactions of CXCR4/CXCL12 that also regulates homing of tumor cells to the bone (Wang et al., 2014). Quiescence in prostate cancer cells is regulated by expression of engaging factors, such as Gas6 and its receptors Axl/Tyro/Mer (Shiozawa et al., 2010), whose ratio in disseminated cell determines whether a cell will proliferate or be quiescent (Taichman et al., 2013). In lung metastases, activation of the bone morphogenic factor (BMP) signaling inhibits colonization, while its inhibitor, Coco, reverses that effect and reactivates cells (Gao et al., 2012), as well as expression of VCAM-1. In bones, VCAM-1 promotes osteolytic metastasis of breast cancer by activation of α4β1-positive osteoclast progenitors. Interaction of VCAM-1 and α4β1 integrin activates the PI3K/Akt pathway enabling prolonged survival and potential for metastatic outgrowth of the cells (Lu et al., 2011). As HSCs move towards the vasculature and the oxygenated endothelial niche, cells acquire a more proliferative phenotype (Ehninger and Trumpp, 2011). In co-culture of mammary cells with HUVECs we showed that the endothelial niche did not affect the proliferation rate of mammary cells. But we must emphasize that our assays were all performed at the same oxygen concentration (7% O_2). This is in accordance to previously published studies that more

oxygenated endothelial niche induces proliferation of the HSCs (Ehninger and Trumpp, 2011). Opposite to these findings, a recent study showed that dormant DCCs preferentially reside in E-selectin rich vascular niches (Price et al., 2016). A possible explanation of this paradox is existence of distinct subniches in the vascular niche and depending whether the cancer cell lodges in the proximity of the trunk or the neovascular tip of the endothelial net it will enter a dormant or proliferative state, respectively (Ghajar et al., 2013). Endothelial-derived thrombospondin-1 (TSP-1) was defined as a mediator of dormancy of breast cancer cells in vascular niches, while periostin (POSTN) and TGF-β1 were found to activate cell cycle (Ghajar et al., 2013). Leukemia inhibitory factor receptor (LIFR) was defined as a factor activating the dormancy program and suppressing metastases in breast cancer (Chen et al., 2012; Johnson et al., 2016). LIFR levels are lower in bone metastasis and inversely correlate with hypoxia gene activity. Hypoxia reduces the LIFR:STAT3:SOCS3 signaling and enables reactivation of the dormant breast cancer cells and bone colonization, suggesting that LIFR:STAT3 signaling confers a dormancy phenotype to breast cancer cells disseminated to the bone (Johnson et al., 2016). These contradictory results just emphasize the difference in the models, but also points to the involvement of these signaling pathways in regulation of dormancy. Therefore, further research in this direction and clarification is necessary.

We identified an activated IL6 pathway in half of the single DCCs and found in mammary stem/progenitor cells the pathway being activated via trans signaling. Trans-signaling makes cells dependent on the microenvironment, however, bone marrow represents an IL-6 rich environment. In the context of breast cancer it is noteworthy that serum levels of IL-6 and sIL-6R and their local production in bone marrow by osteoblasts depends on sex-steroids, change with the menstrual cycle, are negatively regulated by estrogen and hormone replacement therapy and increase during menopause (Abrahamsen et al., 2000; Girasole et al., 1999; Giuliani et al., 2001). Therefore, systemic microenvironmental changes may provide a mechanism by which DCCs become activated in post-menopausal breast cancer patients. Consistently, bone-only metastasis is significantly associated with higher age at primary diagnosis in HR-positive breast cancer patients (Diessner et al., 2016).

4.6 Conclusions

Among the pre-established *in vitro* models we identified the adapted stem cell model to be the best fitting model in inducing dormancy in single cells. Using this model for further molecular analyses we determined pathways involved in the regulation of the state of cellular dormancy and cellular hierarchy in the mammary gland. This novel gene expression profile of cellular dormancy was utilized to distinguish proliferating and non-proliferating DCCs isolated from breast cancer patients. Pathway analysis of the profiles of proliferating and non-proliferating human mammary epithelial cells pointed to IL-6 as one of the key players in controlling the differentiation state of the cells in the mammary

gland. Therefore, the mechanisms of IL-6 signaling pathway in the human mammary gland were further examined. Functional analyses confirmed that the IL-6 signaling plays an important role in stem cell function of mammary cells, as well as colonizing behavior of disseminated human breast cancer cells, while IL-6 signaling was activated in cells with proliferating phenotype.

The findings presented in this thesis enabled us to propose the following mechanism depicted in Figure 70: breast cancer cells that disseminate in the early phases during cancer development reach the bone marrow and occupy distinct niches (mesenchymal, endothelial or osteoblastic). Depending on the niche that DCC occupies gp130 will be downregulated (osteoblastic or mesenchymal niche) or expressed on the membrane (endothelial niche) and cells will acquire a dormant or proliferative phenotype, respectively. IL-6 which is enriched in bone marrow environment and binds sIL-6R, which is also present in physiological conditions in BM (Cho et al., 2013), triggers proliferation of DCCs which regain gp130 expression. Cells downregulating gp130 lose the ability to react to IL-6 stimulation and re/-enter a dormant state.

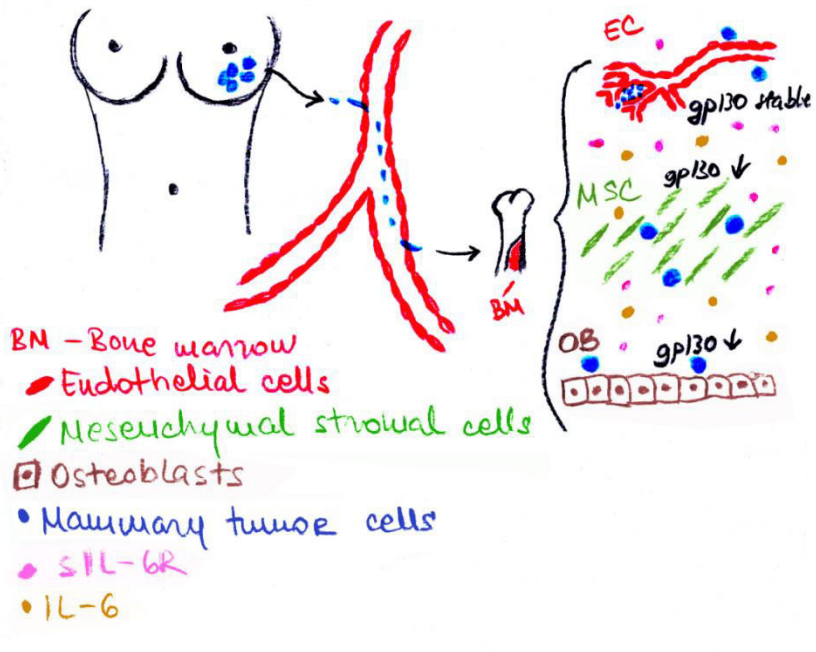

Figure 70: Mechanism of the metastasis outgrowth in bone marrow. Breast cancer cells disseminate form the primary site through the vascular net and extravasate to the bone marrow. There they come in contact with MSCs or OBs that induce gp130 downregulation or with endothelial cells that do not have effect on gp130 expression. Gp130 downregulation leads to cell quiescence.

5 Summary

Metastasis is the major cause of death of cancer patients. In breast cancer dissemination from the primary site occurs preferentially in early tumor stages, long before the clinical manifestation of metastasis, with cases of metastases detected 25 years after removal of the primary tumor. Early dissemination and prolonged clinical latency at distant sites raise the question about the identity and nature of signals that confer survival, persistence in dormant state over extended periods of time and finally, the outgrowth of DCCs. DCCs are extremely rare and detected in bone marrow of about 30% of breast cancer patients with no evidence of manifest metastasis at very low frequency (1-2 DCCs per 10^6 BM cells). Genomic studies showed that early DCCs often lack critical genetic alterations and need to acquire them at the distant site in breast and other cancers.

Studying dormancy in patient derived DCCs is challenging due to the lack of human DCC-derived models, as well as spontaneous or transgenic mouse models that generate bone metastases. Therefore, to identify signals that support survival or outgrowth of dormant DCCs in patients, we profiled *ex vivo* rare bone marrow-derived DCCs (BM-DCCs) that were isolated long before manifestation of metastasis and identified IL-6 signaling as a candidate pathway for DCC activation. Since early DCCs often display "close-to-normal" genomes we used mammary epithelial cells *ex vivo* isolated from reduction mammoplasties and available immortalized pre-malignant mammary cell lines as a model for *in vitro* functional testing. We identified IL-6 trans-signaling (mediated by sIL-6R), but not the classical IL-6 signaling (mediated by mIL-6R), as a pathway to activate stem-like and progenitor traits underlying colony formation in anchorage independent conditions. Further we explored that activation of this pathway in DCCs depends on a special cell population present within the bone marrow niche. Expression of gp130, which is a pre-requisite for IL-6 trans-signaling, was down-regulated by bone marrow stromal and endosteal, but not vascular niche cells, ensuring that only DCCs in vascular niches display a possible responsiveness to IL-6 trans-signaling. The bone marrow represents an IL-6 rich environment and data from other studies have also shown increased serum levels of sIL-6R in breast cancer patients. Furthermore, serum levels of IL-6 and sIL-6R and their local production by osteoblasts in the bone marrow depends on sex-steroids. Expression levels change with the menstrual cycle therefore providing a mechanism for activation of DCCs in the bone marrow and outgrowth of metastasis.

Our data suggest that the initial steps of metastasis formation depend on microenvironmental signals and are not cell-autonomous. They also shed light into early phases of metastasis formation and may inform about potential novel adjuvant therapies as a way to delay or prevent development of the metachronous metastasis in patients diagnosed only with locally confined breast cancer.

6 Literature

Abbas, H., Elyamany, A., Salem, M., Salem, A., Binziad, S., and Gamal, B. (2011). The optimal sequence of radiotherapy and chemotherapy in adjuvant treatment of breast cancer. Int Arch Med *4*, 35.

Abrahamsen, B., Bonnevie-Nielsen, V., Ebbesen, E.N., Gram, J., and Beck-Nielsen, H. (2000). Cytokines and bone loss in a 5-year longitudinal study--hormone replacement therapy suppresses serum soluble interleukin-6 receptor and increases interleukin-1-receptor antagonist: the Danish Osteoporosis Prevention Study. J Bone Miner Res *15*, 1545-1554.

Adam, A.P., George, A., Schewe, D., Bragado, P., Iglesias, B.V., Ranganathan, A.C., Kourtidis, A., Conklin, D.S., and Aguirre-Ghiso, J.A. (2009a). Computational identification of a p38SAPK-regulated transcription factor network required for tumor cell quiescence. Cancer Res *69*, 5664-5672.

Adam, N., Rabe, B., Suthaus, J., Grotzinger, J., Rose-John, S., and Scheller, J. (2009b). Unraveling viral interleukin-6 binding to gp130 and activation of STAT-signaling pathways independently of the interleukin-6 receptor. J Virol *83*, 5117-5126.

Adams, E.F., Rafferty, B., and White, M.C. (1991). Interleukin 6 is secreted by breast fibroblasts and stimulates 17 beta-oestradiol oxidoreductase activity of MCF-7 cells: possible paracrine regulation of breast 17 beta-oestradiol levels. Int J Cancer *49*, 118-121.

Aden, K., Breuer, A., Rehman, A., Geese, H., Tran, F., Sommer, J., Waetzig, G.H., Reinheimer, T.M., Schreiber, S., Rose-John, S., *et al.* (2016). Classic IL-6R signalling is dispensable for intestinal epithelial proliferation and repair. Oncogenesis *5*, e270.

Aguirre-Ghiso, J.A. (2007). Models, mechanisms and clinical evidence for cancer dormancy. Nat Rev Cancer *7*, 834-846.

Aguirre-Ghiso, J.A., Estrada, Y., Liu, D., and Ossowski, L. (2003). ERK(MAPK) activity as a determinant of tumor growth and dormancy; regulation by p38(SAPK). Cancer Res *63*, 1684-1695.

Aguirre-Ghiso, J.A., Liu, D., Mignatti, A., Kovalski, K., and Ossowski, L. (2001). Urokinase receptor and fibronectin regulate the ERK(MAPK) to p38(MAPK) activity ratios that determine carcinoma cell proliferation or dormancy in vivo. Mol Biol Cell *12*, 863-879.

Anbazhagan, R., Bartek, J., Monaghan, P., and Gusterson, B.A. (1991). Growth and development of the human infant breast. Am J Anat *192*, 407-417.

Ansari, A.M., Ahmed, A.K., Matsangos, A.E., Lay, F., Born, L.J., Marti, G., Harmon, J.W., and Sun, Z. (2016). Cellular GFP Toxicity and Immunogenicity: Potential Confounders in in Vivo Cell Tracking Experiments. Stem Cell Rev *12*, 553-559.

Asselin-Labat, M.L., Vaillant, F., Sheridan, J.M., Pal, B., Wu, D., Simpson, E.R., Yasuda, H., Smyth, G.K., Martin, T.J., Lindeman, G.J., *et al.* (2010). Control of mammary stem cell function by steroid hormone signalling. Nature *465*, 798-802.

Atlasi, Y., Noori, R., Gaspar, C., Franken, P., Sacchetti, A., Rafati, H., Mahmoudi, T., Decraene, C., Calin, G.A., Merrill, B.J., *et al.* (2013). Wnt signaling regulates the lineage differentiation potential of mouse embryonic stem cells through Tcf3 down-regulation. PLoS Genet *9*, e1003424.

Baccelli, I., Schneeweiss, A., Riethdorf, S., Stenzinger, A., Schillert, A., Vogel, V., Klein, C., Saini, M., Bauerle, T., Wallwiener, M., *et al.* (2013). Identification of a population of blood circulating tumor cells from breast cancer patients that initiates metastasis in a xenograft assay. Nat Biotechnol *31*, 539-544.

Bachelot, T., Ray-Coquard, I., Menetrier-Caux, C., Rastkha, M., Duc, A., and Blay, J.Y. (2003). Prognostic value of serum levels of interleukin 6 and of serum and plasma levels of vascular endothelial growth factor in hormone-refractory metastatic breast cancer patients. Br J Cancer *88*, 1721-1726.

Baeuerle, P.A., and Gires, O. (2007). EpCAM (CD326) finding its role in cancer. Br J Cancer *96*, 417-423.

Baillo, A., Giroux, C., and Ethier, S.P. (2011). Knock-down of amphiregulin inhibits cellular invasion in inflammatory breast cancer. J Cell Physiol *226*, 2691-2701.

Balogh, G.A., Heulings, R., Mailo, D.A., Russo, P.A., Sheriff, F., Russo, I.H., Moral, R., and Russo, J. (2006). Genomic signature induced by pregnancy in the human breast. Int J Oncol *28*, 399-410.

Barkan, D., Kleinman, H., Simmons, J.L., Asmussen, H., Kamaraju, A.K., Hoenorhoff, M.J., Liu, Z.Y., Costes, S.V., Cho, E.H., Lockett, S., *et al.* (2008). Inhibition of metastatic outgrowth from single dormant tumor cells by targeting the cytoskeleton. Cancer Res *68*, 6241-6250.

Barriere, G., Riouallon, A., Renaudie, J., Tartary, M., and Rigaud, M. (2012). Mesenchymal and stemness circulating tumor cells in early breast cancer diagnosis. BMC Cancer *12*, 114.

Bartkowiak, K., Effenberger, K.E., Harder, S., Andreas, A., Buck, F., Peter-Katalinic, J., Pantel, K., and Brandt, B.H. (2010). Discovery of a novel unfolded protein response phenotype of cancer stem/progenitor cells from the bone marrow of breast cancer patients. J Proteome Res *9*, 3158-3168.

Becker, C., Fantini, M.C., Schramm, C., Lehr, H.A., Wirtz, S., Nikolaev, A., Burg, J., Strand, S., Kiesslich, R., Huber, S., *et al.* (2004). TGF-beta suppresses tumor progression in colon cancer by inhibition of IL-6 trans-signaling. Immunity *21*, 491-501.

Behrens, A., van Deursen, J.M., Rudolph, K.L., and Schumacher, B. (2014). Impact of genomic damage and ageing on stem cell function. Nat Cell Biol *16*, 201-207.

Bhat, K., Sarkissyan, M., Wu, Y., and Vadgama, J.V. (2017). GROalpha overexpression drives cell migration and invasion in triple negative breast cancer cells. Oncol Rep *38*, 21-30.

Bill, R., and Christofori, G. (2015). The relevance of EMT in breast cancer metastasis: Correlation or causality? FEBS Lett *589*, 1577-1587.

Bjerkvig, R., Tysnes, B.B., Aboody, K.S., Najbauer, J., and Terzis, A.J. (2005). Opinion: the origin of the cancer stem cell: current controversies and new insights. Nat Rev Cancer *5*, 899-904.

Bjornson, C.R., Cheung, T.H., Liu, L., Tripathi, P.V., Steeper, K.M., and Rando, T.A. (2012). Notch signaling is necessary to maintain quiescence in adult muscle stem cells. Stem Cells *30*, 232-242.
Bliss, S.A., Paul, S., Pobiarzyn, P.W., Ayer, S., Sinha, G., Pant, S., Hilton, H., Sharma, N., Cunha, M.F., Engelberth, D.J.*, et al.* (2018). Evaluation of a developmental hierarchy for breast cancer cells to assess risk-based patient selection for targeted treatment. Sci Rep *8*, 367.
Bloom, A.B., and Zaman, M.H. (2014). Influence of the microenvironment on cell fate determination and migration. Physiol Genomics *46*, 309-314.
Braun, S., Vogl, F.D., Naume, B., Janni, W., Osborne, M.P., Coombes, R.C., Schlimok, G., Diel, I.J., Gerber, B., Gebauer, G.*, et al.* (2005). A pooled analysis of bone marrow micrometastasis in breast cancer. N Engl J Med *353*, 793-802.
Brisken, C., Park, S., Vass, T., Lydon, J.P., O'Malley, B.W., and Weinberg, R.A. (1998). A paracrine role for the epithelial progesterone receptor in mammary gland development. Proc Natl Acad Sci U S A *95*, 5076-5081.
Briso, E.M., Dienz, O., and Rincon, M. (2008). Cutting edge: soluble IL-6R is produced by IL-6R ectodomain shedding in activated CD4 T cells. J Immunol *180*, 7102-7106.
Brooks, G.D., McLeod, L., Alhayyani, S., Miller, A., Russell, P.A., Ferlin, W., Rose-John, S., Ruwanpura, S., and Jenkins, B.J. (2016). IL6 Trans-signaling Promotes KRAS-Driven Lung Carcinogenesis. Cancer Res *76*, 866-876.
Browning, L., Patel, M.R., Horvath, E.B., Tawara, K., and Jorcyk, C.L. (2018). IL-6 and ovarian cancer: inflammatory cytokines in promotion of metastasis. Cancer Manag Res *10*, 6685-6693.
Bussard, K.M., Gay, C.V., and Mastro, A.M. (2008). The bone microenvironment in metastasis; what is special about bone? Cancer Metastasis Rev *27*, 41-55.
Chambers, A.F., Groom, A.C., and MacDonald, I.C. (2002). Dissemination and growth of cancer cells in metastatic sites. Nat Rev Cancer *2*, 563-572.
Chaterjee, M., and van Golen, K.L. (2011). Breast cancer stem cells survive periods of farnesyl-transferase inhibitor-induced dormancy by undergoing autophagy. Bone Marrow Res *2011*, 362938.
Chen, D., Sun, Y., Wei, Y., Zhang, P., Rezaeian, A.H., Teruya-Feldstein, J., Gupta, S., Liang, H., Lin, H.K., Hung, M.C.*, et al.* (2012). LIFR is a breast cancer metastasis suppressor upstream of the Hippo-YAP pathway and a prognostic marker. Nat Med *18*, 1511-1517.
Chen, X., Liu, Q., and Song, E. (2017). Mammary stem cells: angels or demons in mammary gland? Signal Transduct Target Ther *2*, 16038.
Cheung, T.H., and Rando, T.A. (2013). Molecular regulation of stem cell quiescence. Nat Rev Mol Cell Biol *14*, 329-340.
Cho, S.W., Pirih, F.Q., Koh, A.J., Michalski, M., Eber, M.R., Ritchie, K., Sinder, B., Oh, S., Al-Dujaili, S.A., Lee, J.*, et al.* (2013). The soluble interleukin-6 receptor is a mediator of hematopoietic and skeletal actions of parathyroid hormone. J Biol Chem *288*, 6814-6825.
Choesmel, V., Anract, P., Hoifodt, H., Thiery, J.P., and Blin, N. (2004). A relevant immunomagnetic assay to detect and characterize epithelial cell adhesion molecule-positive cells in bone marrow from patients with breast carcinoma: immunomagnetic purification of micrometastases. Cancer *101*, 693-703.
Chu, J.E., and Allan, A.L. (2012). The Role of Cancer Stem Cells in the Organ Tropism of Breast Cancer Metastasis: A Mechanistic Balance between the "Seed" and the "Soil"? Int J Breast Cancer *2012*, 209748.
Cicalese, A., Bonizzi, G., Pasi, C.E., Faretta, M., Ronzoni, S., Giulini, B., Brisken, C., Minucci, S., Di Fiore, P.P., and Pelicci, P.G. (2009). The tumor suppressor p53 regulates polarity of self-renewing divisions in mammary stem cells. Cell *138*, 1083-1095.
Cimino, A., Halushka, M., Illei, P., Wu, X., Sukumar, S., and Argani, P. (2010). Epithelial cell adhesion molecule (EpCAM) is overexpressed in breast cancer metastases. Breast Cancer Res Treat *123*, 701-708.
Clarke, M.F., Dick, J.E., Dirks, P.B., Eaves, C.J., Jamieson, C.H., Jones, D.L., Visvader, J., Weissman, I.L., and Wahl, G.M. (2006). Cancer stem cells--perspectives on current status and future directions: AACR Workshop on cancer stem cells. Cancer Res *66*, 9339-9344.
Colacino, J.A., Azizi, E., Brooks, M.D., Harouaka, R., Fouladdel, S., McDermott, S.P., Lee, M., Hill, D., Madden, J., Boerner, J.*, et al.* (2018). Heterogeneity of Human Breast Stem and Progenitor Cells as Revealed by Transcriptional Profiling. Stem Cell Reports *10*, 1596-1609.
Coppe, J.P., Patil, C.K., Rodier, F., Krtolica, A., Beausejour, C.M., Parrinello, S., Hodgson, J.G., Chin, K., Desprez, P.Y., and Campisi, J. (2010). A human-like senescence-associated secretory phenotype is conserved in mouse cells dependent on physiological oxygen. PLoS One *5*, e9188.
Cornelissen, B., Able, S., Kartsonaki, C., Kersemans, V., Allen, P.D., Cavallo, F., Cazier, J.B., Iezzi, M., Knight, J., Muschel, R.*, et al.* (2014). Imaging DNA damage allows detection of preneoplasia in the BALB-neuT model of breast cancer. J Nucl Med *55*, 2026-2031.
Cortini, M., Massa, A., Avnet, S., Bonuccelli, G., and Baldini, N. (2016). Tumor-Activated Mesenchymal Stromal Cells Promote Osteosarcoma Stemness and Migratory Potential via IL-6 Secretion. PLoS One *11*, e0166500.
D'Cruz, C.M., Moody, S.E., Master, S.R., Hartman, J.L., Keiper, E.A., Imielinski, M.B., Cox, J.D., Wang, J.Y., Ha, S.I., Keister, B.A.*, et al.* (2002). Persistent parity-induced changes in growth factors, TGF-beta3, and differentiation in the rodent mammary gland. Mol Endocrinol *16*, 2034-2051.
da Silveira, W.A., Palma, P.V.B., Sicchieri, R.D., Villacis, R.A.R., Mandarano, L.R.M., Oliveira, T.M.G., Antonio, H.M.R., Andrade, J.M., Muglia, V.F., Rogatto, S.R.*, et al.* (2017). Transcription Factor Networks derived from Breast Cancer Stem Cells control the immune response in the Basal subtype. Sci Rep *7*, 2851.
Davidson, K.C., Adams, A.M., Goodson, J.M., McDonald, C.E., Potter, J.C., Berndt, J.D., Biechele, T.L., Taylor, R.J., and Moon, R.T. (2012). Wnt/beta-catenin signaling promotes differentiation, not self-renewal, of human embryonic stem cells and is repressed by Oct4. Proc Natl Acad Sci U S A *109*, 4485-4490.
Dhankhar, R., Vyas, S.P., Jain, A.K., Arora, S., Rath, G., and Goyal, A.K. (2010). Advances in novel drug delivery strategies for breast cancer therapy. Artif Cells Blood Substit Immobil Biotechnol *38*, 230-249.

Di Carlo, E., Diodoro, M.G., Boggio, K., Modesti, A., Modesti, M., Nanni, P., Forni, G., and Musiani, P. (1999). Analysis of mammary carcinoma onset and progression in HER-2/neu oncogene transgenic mice reveals a lobular origin. Lab Invest *79*, 1261-1269.
Dienz, O., Eaton, S.M., Bond, J.P., Neveu, W., Moquin, D., Noubade, R., Briso, E.M., Charland, C., Leonard, W.J., Ciliberto, G.*, et al.* (2009). The induction of antibody production by IL-6 is indirectly mediated by IL-21 produced by CD4+ T cells. J Exp Med *206*, 69-78.
Diessner, J., Wischnewsky, M., Stuber, T., Stein, R., Krockenberger, M., Hausler, S., Janni, W., Kreienberg, R., Blettner, M., Schwentner, L.*, et al.* (2016). Evaluation of clinical parameters influencing the development of bone metastasis in breast cancer. BMC Cancer *16*, 307.
Ding, D.C., Liu, H.W., and Chu, T.Y. (2016). Interleukin-6 from Ovarian Mesenchymal Stem Cells Promotes Proliferation, Sphere and Colony Formation and Tumorigenesis of an Ovarian Cancer Cell Line SKOV3. J Cancer *7*, 1815-1823.
Dontu, G., Abdallah, W.M., Foley, J.M., Jackson, K.W., Clarke, M.F., Kawamura, M.J., and Wicha, M.S. (2003). In vitro propagation and transcriptional profiling of human mammary stem/progenitor cells. Genes Dev *17*, 1253-1270.
Du, J., Wu, Y., Ai, Z., Shi, X., Chen, L., and Guo, Z. (2014). Mechanism of SB431542 in inhibiting mouse embryonic stem cell differentiation. Cell Signal *26*, 2107-2116.
Dubrovska, A., Kim, S., Salamone, R.J., Walker, J.R., Maira, S.M., Garcia-Echeverria, C., Schultz, P.G., and Reddy, V.A. (2009). The role of PTEN/Akt/PI3K signaling in the maintenance and viability of prostate cancer stem-like cell populations. Proc Natl Acad Sci U S A *106*, 268-273.
Ehninger, A., and Trumpp, A. (2011). The bone marrow stem cell niche grows up: mesenchymal stem cells and macrophages move in. J Exp Med *208*, 421-428.
Eirew, P., Kannan, N., Knapp, D.J., Vaillant, F., Emerman, J.T., Lindeman, G.J., Visvader, J.E., and Eaves, C.J. (2012). Aldehyde dehydrogenase activity is a biomarker of primitive normal human mammary luminal cells. Stem Cells *30*, 344-348.
Eirew, P., Stingl, J., Raouf, A., Turashvili, G., Aparicio, S., Emerman, J.T., and Eaves, C.J. (2008). A method for quantifying normal human mammary epithelial stem cells with in vivo regenerative ability. Nat Med *14*, 1384-1389.
Elston, C.W., and Ellis, I.O. (1991). Pathological prognostic factors in breast cancer. I. The value of histological grade in breast cancer: experience from a large study with long-term follow-up. Histopathology *19*, 403-410.
Engelmann, K., Shen, H., and Finn, O.J. (2008). MCF7 side population cells with characteristics of cancer stem/progenitor cells express the tumor antigen MUC1. Cancer Res *68*, 2419-2426.
Erdman, S.E., and Poutahidis, T. (2017). Gut microbiota modulate host immune cells in cancer development and growth. Free Radic Biol Med *105*, 28-34.
Eto, D., Lao, C., DiToro, D., Barnett, B., Escobar, T.C., Kageyama, R., Yusuf, I., and Crotty, S. (2011). IL-21 and IL-6 are critical for different aspects of B cell immunity and redundantly induce optimal follicular helper CD4 T cell (Tfh) differentiation. PLoS One *6*, e17739.
Eyles, J., Puaux, A.L., Wang, X., Toh, B., Prakash, C., Hong, M., Tan, T.G., Zheng, L., Ong, L.C., Jin, Y.*, et al.* (2010). Tumor cells disseminate early, but immunosurveillance limits metastatic outgrowth, in a mouse model of melanoma. J Clin Invest *120*, 2030-2039.
Fernandez, M.F., Reina-Perez, I., Astorga, J.M., Rodriguez-Carrillo, A., Plaza-Diaz, J., and Fontana, L. (2018). Breast Cancer and Its Relationship with the Microbiota. Int J Environ Res Public Health *15*.
Ferrone, S., and Marincola, F.M. (1995). Loss of HLA class I antigens by melanoma cells: molecular mechanisms, functional significance and clinical relevance. Immunol Today *16*, 487-494.
Fidler, I.J. (2003). The pathogenesis of cancer metastasis: the 'seed and soil' hypothesis revisited. Nat Rev Cancer *3*, 453-458.
Fischer, M., Goldschmitt, J., Peschel, C., Brakenhoff, J.P., Kallen, K.J., Wollmer, A., Grotzinger, J., and Rose-John, S. (1997). I. A bioactive designer cytokine for human hematopoietic progenitor cell expansion. Nat Biotechnol *15*, 142-145.
Forsyth, I.A. (1991). The mammary gland. Baillieres Clin Endocrinol Metab *5*, 809-832.
Fu, N., Lindeman, G.J., and Visvader, J.E. (2014). The mammary stem cell hierarchy. Curr Top Dev Biol *107*, 133-160.
Gambotto, A., Dworacki, G., Cicinnati, V., Kenniston, T., Steitz, J., Tuting, T., Robbins, P.D., and DeLeo, A.B. (2000). Immunogenicity of enhanced green fluorescent protein (EGFP) in BALB/c mice: identification of an H2-Kd-restricted CTL epitope. Gene Ther *7*, 2036-2040.
Gao, H., Chakraborty, G., Lee-Lim, A.P., Mo, Q., Decker, M., Vonica, A., Shen, R., Brogi, E., Brivanlou, A.H., and Giancotti, F.G. (2012). The BMP inhibitor Coco reactivates breast cancer cells at lung metastatic sites. Cell *150*, 764-779.
Gao, H., Chakraborty, G., Zhang, Z., Akalay, I., Gadiya, M., Gao, Y., Sinha, S., Hu, J., Jiang, C., Akram, M.*, et al.* (2016). Multi-organ Site Metastatic Reactivation Mediated by Non-canonical Discoidin Domain Receptor 1 Signaling. Cell *166*, 47-62.
Garbers, C., Thaiss, W., Jones, G.W., Waetzig, G.H., Lorenzen, I., Guilhot, F., Lissilaa, R., Ferlin, W.G., Grotzinger, J., Jones, S.A.*, et al.* (2011). Inhibition of classic signaling is a novel function of soluble glycoprotein 130 (sgp130), which is controlled by the ratio of interleukin 6 and soluble interleukin 6 receptor. J Biol Chem *286*, 42959-42970.
Ghajar, C.M., Chen, X., Harris, J.W., Suresh, V., Hughes, C.C., Jeon, N.L., Putnam, A.J., and George, S.C. (2008). The effect of matrix density on the regulation of 3-D capillary morphogenesis. Biophys J *94*, 1930-1941.
Ghajar, C.M., Peinado, H., Mori, H., Matei, I.R., Evason, K.J., Brazier, H., Almeida, D., Koller, A., Hajjar, K.A., Stainier, D.Y.*, et al.* (2013). The perivascular niche regulates breast tumour dormancy. Nat Cell Biol *15*, 807-817.
Ginestier, C., Hur, M.H., Charafe-Jauffret, E., Monville, F., Dutcher, J., Brown, M., Jacquemier, J., Viens, P., Kleer, C.G., Liu, S.*, et al.* (2007). ALDH1 is a marker of normal and malignant human mammary stem cells and a predictor of poor clinical outcome. Cell Stem Cell *1*, 555-567.
Girasole, G., Giuliani, N., Modena, A.B., Passeri, G., and Pedrazzoni, M. (1999). Oestrogens prevent the increase of human serum soluble interleukin-6 receptor induced by ovariectomy in vivo and decrease its release in human osteoblastic cells in vitro. Clin Endocrinol (Oxf) *51*, 801-807.

Giuliani, N., Sansoni, P., Girasole, G., Vescovini, R., Passeri, G., Passeri, M., and Pedrazzoni, M. (2001). Serum interleukin-6, soluble interleukin-6 receptor and soluble gp130 exhibit different patterns of age- and menopause-related changes. Exp Gerontol *36*, 547-557.
Goss, P.E., and Chambers, A.F. (2010). Does tumour dormancy offer a therapeutic target? Nat Rev Cancer *10*, 871-877.
Grivennikov, S., Karin, E., Terzic, J., Mucida, D., Yu, G.Y., Vallabhapurapu, S., Scheller, J., Rose-John, S., Cheroutre, H., Eckmann, L.*, et al.* (2009). IL-6 and Stat3 are required for survival of intestinal epithelial cells and development of colitis-associated cancer. Cancer Cell *15*, 103-113.
Guo, W. (2014). Concise review: breast cancer stem cells: regulatory networks, stem cell niches, and disease relevance. Stem Cells Transl Med *3*, 942-948.
Guo, W., Pylayeva, Y., Pepe, A., Yoshioka, T., Muller, W.J., Inghirami, G., and Giancotti, F.G. (2006). Beta 4 integrin amplifies ErbB2 signaling to promote mammary tumorigenesis. Cell *126*, 489-502.
Guzvic, M., Braun, B., Ganzer, R., Burger, M., Nerlich, M., Winkler, S., Werner-Klein, M., Czyz, Z.T., Polzer, B., and Klein, C.A. (2014). Combined genome and transcriptome analysis of single disseminated cancer cells from bone marrow of prostate cancer patients reveals unexpected transcriptomes. Cancer Res *74*, 7383-7394.
Gyamfi, J., Eom, M., Koo, J.S., and Choi, J. (2018a). Multifaceted Roles of Interleukin-6 in Adipocyte-Breast Cancer Cell Interaction. Transl Oncol *11*, 275-285.
Gyamfi, J., Lee, Y.H., Eom, M., and Choi, J. (2018b). Interleukin-6/STAT3 signalling regulates adipocyte induced epithelial-mesenchymal transition in breast cancer cells. Sci Rep *8*, 8859.
Hartmann, C.H., and Klein, C.A. (2006). Gene expression profiling of single cells on large-scale oligonucleotide arrays. Nucleic Acids Res *34*, e143.
Hartwell, K.A., Muir, B., Reinhardt, F., Carpenter, A.E., Sgroi, D.C., and Weinberg, R.A. (2006). The Spemann organizer gene, Goosecoid, promotes tumor metastasis. Proc Natl Acad Sci U S A *103*, 18969-18974.
Hassiotou, F., Hepworth, A.R., Beltran, A.S., Mathews, M.M., Stuebe, A.M., Hartmann, P.E., Filgueira, L., and Blancafort, P. (2013). Expression of the Pluripotency Transcription Factor OCT4 in the Normal and Aberrant Mammary Gland. Front Oncol *3*, 79.
He, D., Wang, R.X., Mao, J.P., Xiao, B., Chen, D.F., and Tian, W. (2017). Three-dimensional spheroid culture promotes the stemness maintenance of cranial stem cells by activating PI3K/AKT and suppressing NF-kappaB pathways. Biochem Biophys Res Commun *488*, 528-533.
He, J.Y., Wei, X.H., Li, S.J., Liu, Y., Hu, H.L., Li, Z.Z., Kuang, X.H., Wang, L., Shi, X., Yuan, S.T.*, et al.* (2018). Adipocyte-derived IL-6 and leptin promote breast Cancer metastasis via upregulation of Lysyl Hydroxylase-2 expression. Cell Commun Signal *16*, 100.
Hens, J.R., and Wysolmerski, J.J. (2005). Key stages of mammary gland development: molecular mechanisms involved in the formation of the embryonic mammary gland. Breast Cancer Res *7*, 220-224.
Herlyn, M., Steplewski, Z., Herlyn, D., and Koprowski, H. (1979). Colorectal carcinoma-specific antigen: detection by means of monoclonal antibodies. Proc Natl Acad Sci U S A *76*, 1438-1442.
Hinck, L., and Silberstein, G.B. (2005). Key stages in mammary gland development: the mammary end bud as a motile organ. Breast Cancer Res *7*, 245-251.
Hogg, N.A., Harrison, C.J., and Tickle, C. (1983). Lumen formation in the developing mouse mammary gland. J Embryol Exp Morphol *73*, 39-57.
Holub, M.C., Szalai, C., Polgar, A., Toth, S., and Falus, A. (1999). Generation of 'truncated' interleukin-6 receptor (IL-6R) mRNA by alternative splicing; a possible source of soluble IL-6R. Immunol Lett *68*, 121-124.
Horiuchi, S., Koyanagi, Y., Zhou, Y., Miyamoto, H., Tanaka, Y., Waki, M., Matsumoto, A., Yamamoto, M., and Yamamoto, N. (1994). Soluble interleukin-6 receptors released from T cell or granulocyte/macrophage cell lines and human peripheral blood mononuclear cells are generated through an alternative splicing mechanism. Eur J Immunol *24*, 1945-1948.
Hosseini, H., Obradovic, M.M., Hoffmann, M., Harper, K.L., Sosa, M.S., Werner-Klein, M., Nanduri, L.K., Werno, C., Ehrl, C., Maneck, M.*, et al.* (2016a). Early dissemination seeds metastasis in breast cancer. Nature.
Hosseini, H., Obradovic, M.M.S., Hoffmann, M., Harper, K.L., Sosa, M.S., Werner-Klein, M., Nanduri, L.K., Werno, C., Ehrl, C., Maneck, M.*, et al.* (2016b). Early dissemination seeds metastasis in breast cancer. Nature *540*, 552-558.
Howard, B.A., and Gusterson, B.A. (2000). Human breast development. J Mammary Gland Biol Neoplasia *5*, 119-137.
Hughes, E.S. (1950). The Development of the Mammary Gland: Arris and Gale Lecture, delivered at the Royal College of Surgeons of England on 25th October, 1949. Ann R Coll Surg Engl *6*, 99-119.
Husemann, Y., Geigl, J.B., Schubert, F., Musiani, P., Meyer, M., Burghart, E., Forni, G., Eils, R., Fehm, T., Riethmuller, G.*, et al.* (2008). Systemic spread is an early step in breast cancer. Cancer Cell *13*, 58-68.
Ibrahim, T., Leong, I., Sanchez-Sweatman, O., Khokha, R., Sodek, J., Tenenbaum, H.C., Ganss, B., and Cheifetz, S. (2000). Expression of bone sialoprotein and osteopontin in breast cancer bone metastases. Clin Exp Metastasis *18*, 253-260.
Iliopoulos, D., Hirsch, H.A., Wang, G., and Struhl, K. (2011). Inducible formation of breast cancer stem cells and their dynamic equilibrium with non-stem cancer cells via IL6 secretion. Proc Natl Acad Sci U S A *108*, 1397-1402.
Inman, J.L., Robertson, C., Mott, J.D., and Bissell, M.J. (2015). Mammary gland development: cell fate specification, stem cells and the microenvironment. Development *142*, 1028-1042.
Jacob, K., Webber, M., Benayahu, D., and Kleinman, H.K. (1999). Osteonectin promotes prostate cancer cell migration and invasion: a possible mechanism for metastasis to bone. Cancer Res *59*, 4453-4457.
Janni, W., Vogl, F.D., Wiedswang, G., Synnestvedt, M., Fehm, T., Juckstock, J., Borgen, E., Rack, B., Braun, S., Sommer, H.*, et al.* (2011). Persistence of disseminated tumor cells in the bone marrow of breast cancer patients predicts increased risk for relapse--a European pooled analysis. Clin Cancer Res *17*, 2967-2976.
Javed, A., and Lteif, A. (2013). Development of the human breast. Semin Plast Surg *27*, 5-12.
Jiang, X.P., Yang, D.C., Elliott, R.L., and Head, J.F. (2011). Down-regulation of expression of interleukin-6 and its receptor results in growth inhibition of MCF-7 breast cancer cells. Anticancer Res *31*, 2899-2906.

Jin, K., Gao, W., Lu, Y., Lan, H., Teng, L., and Cao, F. (2012). Mechanisms regulating colorectal cancer cell metastasis into liver (Review). Oncol Lett *3*, 11-15.
Jin, L., Han, B., Siegel, E., Cui, Y., Giuliano, A., and Cui, X. (2018). Breast cancer lung metastasis: Molecular biology and therapeutic implications. Cancer Biol Ther *19*, 858-868.
Johnson, E., Seachrist, D.D., DeLeon-Rodriguez, C.M., Lozada, K.L., Miedler, J., Abdul-Karim, F.W., and Keri, R.A. (2010). HER2/ErbB2-induced breast cancer cell migration and invasion require p120 catenin activation of Rac1 and Cdc42. J Biol Chem *285*, 29491-29501.
Johnson, R.W., Finger, E.C., Olcina, M.M., Vilalta, M., Aguilera, T., Miao, Y., Merkel, A.R., Johnson, J.R., Sterling, J.A., Wu, J.Y., *et al.* (2016). Induction of LIFR confers a dormancy phenotype in breast cancer cells disseminated to the bone marrow. Nat Cell Biol *18*, 1078-1089.
Jostock, T., Mullberg, J., Ozbek, S., Atreya, R., Blinn, G., Voltz, N., Fischer, M., Neurath, M.F., and Rose-John, S. (2001). Soluble gp130 is the natural inhibitor of soluble interleukin-6 receptor transsignaling responses. Eur J Biochem *268*, 160-167.
Jung, H., Lee, K.P., Park, S.J., Park, J.H., Jang, Y.S., Choi, S.Y., Jung, J.G., Jo, K., Park, D.Y., Yoon, J.H., *et al.* (2008). TMPRSS4 promotes invasion, migration and metastasis of human tumor cells by facilitating an epithelial-mesenchymal transition. Oncogene *27*, 2635-2647.
Kareva, I. (2016). Primary and metastatic tumor dormancy as a result of population heterogeneity. Biol Direct *11*, 37.
Kasimir-Bauer, S., Hoffmann, O., Wallwiener, D., Kimmig, R., and Fehm, T. (2012). Expression of stem cell and epithelial-mesenchymal transition markers in primary breast cancer patients with circulating tumor cells. Breast Cancer Res *14*, R15.
Kim, J.K., Jung, Y., Wang, J., Joseph, J., Mishra, A., Hill, E.E., Krebsbach, P.H., Pienta, K.J., Shiozawa, Y., and Taichman, R.S. (2013a). TBK1 regulates prostate cancer dormancy through mTOR inhibition. Neoplasia *15*, 1064-1074.
Kim, M.Y., Oskarsson, T., Acharyya, S., Nguyen, D.X., Zhang, X.H., Norton, L., and Massague, J. (2009). Tumor self-seeding by circulating cancer cells. Cell *139*, 1315-1326.
Kim, S.Y., Kang, J.W., Song, X., Kim, B.K., Yoo, Y.D., Kwon, Y.T., and Lee, Y.J. (2013b). Role of the IL-6-JAK1-STAT3-Oct-4 pathway in the conversion of non-stem cancer cells into cancer stem-like cells. Cell Signal *25*, 961-969.
Kimura, H., Kato, H., Faried, A., Sohda, M., Nakajima, M., Fukai, Y., Miyazaki, T., Masuda, N., Fukuchi, M., and Kuwano, H. (2007). Prognostic significance of EpCAM expression in human esophageal cancer. Int J Oncol *30*, 171-179.
Kishimoto, T. (2005). Interleukin-6: from basic science to medicine--40 years in immunology. Annu Rev Immunol *23*, 1-21.
Klein, C.A. (2009). Parallel progression of primary tumours and metastases. Nat Rev Cancer *9*, 302-312.
Klein, C.A. (2011). Framework models of tumor dormancy from patient-derived observations. Curr Opin Genet Dev *21*, 42-49.
Klein, C.A., Seidl, S., Petat-Dutter, K., Offner, S., Geigl, J.B., Schmidt-Kittler, O., Wendler, N., Passlick, B., Huber, R.M., Schlimok, G., *et al.* (2002). Combined transcriptome and genome analysis of single micrometastatic cells. Nat Biotechnol *20*, 387-392.
Kleinberg, D.L., and Ruan, W. (2008). IGF-I, GH, and sex steroid effects in normal mammary gland development. J Mammary Gland Biol Neoplasia *13*, 353-360.
Kobayashi, A., Okuda, H., Xing, F., Pandey, P.R., Watabe, M., Hirota, S., Pai, S.K., Liu, W., Fukuda, K., Chambers, C., *et al.* (2011). Bone morphogenetic protein 7 in dormancy and metastasis of prostate cancer stem-like cells in bone. J Exp Med *208*, 2641-2655.
Koebel, C.M., Vermi, W., Swann, J.B., Zerafa, N., Rodig, S.J., Old, L.J., Smyth, M.J., and Schreiber, R.D. (2007). Adaptive immunity maintains occult cancer in an equilibrium state. Nature *450*, 903-907.
Koechli, O.R., Sevin, B.U., Perras, J.P., Angioli, R., Steren, A., Rodriguez, M., Ganjei, P., and Averette, H.E. (1994). Growth characteristics of nonmalignant cells in the ATP cell viability assay. Oncology *51*, 35-41.
Koscielny, S., Tubiana, M., Le, M.G., Valleron, A.J., Mouriesse, H., Contesso, G., and Sarrazin, D. (1984). Breast cancer: relationship between the size of the primary tumour and the probability of metastatic dissemination. Br J Cancer *49*, 709-715.
Kozlowski, L., Zakrzewska, I., Tokajuk, P., and Wojtukiewicz, M.Z. (2003). Concentration of interleukin-6 (IL-6), interleukin-8 (IL-8) and interleukin-10 (IL-10) in blood serum of breast cancer patients. Rocz Akad Med Bialymst *48*, 82-84.
Krishnamurthy, S., Warner, K.A., Dong, Z., Imai, A., Nor, C., Ward, B.B., Helman, J.I., Taichman, R.S., Bellile, E.L., McCauley, L.K., *et al.* (2014). Endothelial interleukin-6 defines the tumorigenic potential of primary human cancer stem cells. Stem Cells *32*, 2845-2857.
Kulkarni, G.V., and McCulloch, C.A. (1994). Serum deprivation induces apoptotic cell death in a subset of Balb/c 3T3 fibroblasts. J Cell Sci *107 (Pt 5)*, 1169-1179.
Kuperwasser, C., Chavarria, T., Wu, M., Magrane, G., Gray, J.W., Carey, L., Richardson, A., and Weinberg, R.A. (2004). Reconstruction of functionally normal and malignant human breast tissues in mice. Proc Natl Acad Sci U S A *101*, 4966-4971.
LaBarge, M.A., Petersen, O.W., and Bissell, M.J. (2007). Of microenvironments and mammary stem cells. Stem Cell Rev *3*, 137-146.
Langley, R.R., and Fidler, I.J. (2011). The seed and soil hypothesis revisited--the role of tumor-stroma interactions in metastasis to different organs. Int J Cancer *128*, 2527-2535.
Lawson, D.A., Bhakta, N.R., Kessenbrock, K., Prummel, K.D., Yu, Y., Takai, K., Zhou, A., Eyob, H., Balakrishnan, S., Wang, C.Y., *et al.* (2015). Single-cell analysis reveals a stem-cell program in human metastatic breast cancer cells. Nature *526*, 131-135.
Lee, J.W., Stone, M.L., Porrett, P.M., Thomas, S.K., Komar, C.A., Li, J.H., Delman, D., Graham, K., Gladney, W.L., Hua, X., *et al.* (2019). Hepatocytes direct the formation of a pro-metastatic niche in the liver. Nature *567*, 249-252.
Lee, S.O., Yang, X., Duan, S., Tsai, Y., Strojny, L.R., Keng, P., and Chen, Y. (2016). IL-6 promotes growth and epithelial-mesenchymal transition of CD133+ cells of non-small cell lung cancer. Oncotarget *7*, 6626-6638.
Lim, E., Vaillant, F., Wu, D., Forrest, N.C., Pal, B., Hart, A.H., Asselin-Labat, M.L., Gyorki, D.E., Ward, T., Partanen, A., *et al.* (2009). Aberrant luminal progenitors as the candidate target population for basal tumor development in BRCA1 mutation carriers. Nat Med *15*, 907-913.

Lim, P.K., Bliss, S.A., Patel, S.A., Taborga, M., Dave, M.A., Gregory, L.A., Greco, S.J., Bryan, M., Patel, P.S., and Rameshwar, P. (2011). Gap junction-mediated import of microRNA from bone marrow stromal cells can elicit cell cycle quiescence in breast cancer cells. Cancer Res *71*, 1550-1560.
Liu, H., Patel, M.R., Prescher, J.A., Patsialou, A., Qian, D., Lin, J., Wen, S., Chang, Y.F., Bachmann, M.H., Shimono, Y.*, et al.* (2010). Cancer stem cells from human breast tumors are involved in spontaneous metastases in orthotopic mouse models. Proc Natl Acad Sci U S A *107*, 18115-18120.
Liu, S., Cong, Y., Wang, D., Sun, Y., Deng, L., Liu, Y., Martin-Trevino, R., Shang, L., McDermott, S.P., Landis, M.D.*, et al.* (2014). Breast cancer stem cells transition between epithelial and mesenchymal states reflective of their normal counterparts. Stem Cell Reports *2*, 78-91.
Liu, S., Ginestier, C., Ou, S.J., Clouthier, S.G., Patel, S.H., Monville, F., Korkaya, H., Heath, A., Dutcher, J., Kleer, C.G.*, et al.* (2011). Breast cancer stem cells are regulated by mesenchymal stem cells through cytokine networks. Cancer Res *71*, 614-624.
Lu, X., and Kang, Y. (2007). Organotropism of breast cancer metastasis. J Mammary Gland Biol Neoplasia *12*, 153-162.
Lu, X., Mu, E., Wei, Y., Riethdorf, S., Yang, Q., Yuan, M., Yan, J., Hua, Y., Tiede, B.J., Lu, X.*, et al.* (2011). VCAM-1 promotes osteolytic expansion of indolent bone micrometastasis of breast cancer by engaging alpha4beta1-positive osteoclast progenitors. Cancer Cell *20*, 701-714.
Luker, K.E., and Luker, G.D. (2006). Functions of CXCL12 and CXCR4 in breast cancer. Cancer Lett *238*, 30-41.
Luo, M., Clouthier, S.G., Deol, Y., Liu, S., Nagrath, S., Azizi, E., and Wicha, M.S. (2015). Breast cancer stem cells: current advances and clinical implications. Methods Mol Biol *1293*, 1-49.
Luo, Y., and Zheng, S.G. (2016). Hall of Fame among Pro-inflammatory Cytokines: Interleukin-6 Gene and Its Transcriptional Regulation Mechanisms. Front Immunol *7*, 604.
Macias, H., and Hinck, L. (2012). Mammary gland development. Wiley Interdiscip Rev Dev Biol *1*, 533-557.
MacKie, R.M., Reid, R., and Junor, B. (2003). Fatal melanoma transferred in a donated kidney 16 years after melanoma surgery. N Engl J Med *348*, 567-568.
Mani, S.A., Yang, J., Brooks, M., Schwaninger, G., Zhou, A., Miura, N., Kutok, J.L., Hartwell, K., Richardson, A.L., and Weinberg, R.A. (2007). Mesenchyme Forkhead 1 (FOXC2) plays a key role in metastasis and is associated with aggressive basal-like breast cancers. Proc Natl Acad Sci U S A *104*, 10069-10074.
Mansi, J.L., Gogas, H., Bliss, J.M., Gazet, J.C., Berger, U., and Coombes, R.C. (1999). Outcome of primary-breast-cancer patients with micrometastases: a long-term follow-up study. Lancet *354*, 197-202.
Marotta, L.L., Almendro, V., Marusyk, A., Shipitsin, M., Schemme, J., Walker, S.R., Bloushtain-Qimron, N., Kim, J.J., Choudhury, S.A., Maruyama, R.*, et al.* (2011). The JAK2/STAT3 signaling pathway is required for growth of CD44(+)CD24(-) stem cell-like breast cancer cells in human tumors. J Clin Invest *121*, 2723-2735.
Marshall, W.A., and Tanner, J.M. (1969). Variations in pattern of pubertal changes in girls. Arch Dis Child *44*, 291-303.
Martin, G.S. (2003). Cell signaling and cancer. Cancer Cell *4*, 167-174.
Massoner, P., Thomm, T., Mack, B., Untergasser, G., Martowicz, A., Bobowski, K., Klocker, H., Gires, O., and Puhr, M. (2014). EpCAM is overexpressed in local and metastatic prostate cancer, suppressed by chemotherapy and modulated by MET-associated miRNA-200c/205. Br J Cancer *111*, 955-964.
Mathiesen, R.R., Borgen, E., Renolen, A., Lokkevik, E., Nesland, J.M., Anker, G., Ostenstad, B., Lundgren, S., Risberg, T., Mjaaland, I.*, et al.* (2012). Persistence of disseminated tumor cells after neoadjuvant treatment for locally advanced breast cancer predicts poor survival. Breast Cancer Res *14*, R117.
Matsumoto, S., Hara, T., Mitsuyama, K., Yamamoto, M., Tsuruta, O., Sata, M., Scheller, J., Rose-John, S., Kado, S., and Takada, T. (2010). Essential roles of IL-6 trans-signaling in colonic epithelial cells, induced by the IL-6/soluble-IL-6 receptor derived from lamina propria macrophages, on the development of colitis-associated premalignant cancer in a murine model. J Immunol *184*, 1543-1551.
Mattern, J., Koomagi, R., and Volm, M. (1996). Association of vascular endothelial growth factor expression with intratumoral microvessel density and tumour cell proliferation in human epidermoid lung carcinoma. Br J Cancer *73*, 931-934.
McGill, G., Shimamura, A., Bates, R.C., Savage, R.E., and Fisher, D.E. (1997). Loss of matrix adhesion triggers rapid transformation-selective apoptosis in fibroblasts. J Cell Biol *138*, 901-911.
Medina, D. (1996). The mammary gland: a unique organ for the study of development and tumorigenesis. J Mammary Gland Biol Neoplasia *1*, 5-19.
Merrill, B.J. (2012). Wnt pathway regulation of embryonic stem cell self-renewal. Cold Spring Harb Perspect Biol *4*, a007971.
Milovanovic, I.S., Stjepanovic, M., and Mitrovic, D. (2017). Distribution patterns of the metastases of the lung carcinoma in relation to histological type of the primary tumor: An autopsy study. Ann Thorac Med *12*, 191-198.
Mitsuyama, K., Sata, M., and Rose-John, S. (2006). Interleukin-6 trans-signaling in inflammatory bowel disease. Cytokine Growth Factor Rev *17*, 451-461.
Monaghan, P., Perusinghe, N.P., Cowen, P., and Gusterson, B.A. (1990). Peripubertal human breast development. Anat Rec *226*, 501-508.
Morrison, B.J., Schmidt, C.W., Lakhani, S.R., Reynolds, B.A., and Lopez, J.A. (2008). Breast cancer stem cells: implications for therapy of breast cancer. Breast Cancer Res *10*, 210.
Morrison, S.J., and Scadden, D.T. (2014). The bone marrow niche for haematopoietic stem cells. Nature *505*, 327-334.
Mullberg, J., Dittrich, E., Graeve, L., Gerhartz, C., Yasukawa, K., Taga, T., Kishimoto, T., Heinrich, P.C., and Rose-John, S. (1993). Differential shedding of the two subunits of the interleukin-6 receptor. FEBS Lett *332*, 174-178.
Muller, A., Homey, B., Soto, H., Ge, N., Catron, D., Buchanan, M.E., McClanahan, T., Murphy, E., Yuan, W., Wagner, S.N.*, et al.* (2001). Involvement of chemokine receptors in breast cancer metastasis. Nature *410*, 50-56.
Murakami, M., Hibi, M., Nakagawa, N., Nakagawa, T., Yasukawa, K., Yamanishi, K., Taga, T., and Kishimoto, T. (1993). IL-6-induced homodimerization of gp130 and associated activation of a tyrosine kinase. Science *260*, 1808-1810.
Murray, P.J. (2007). The JAK-STAT signaling pathway: input and output integration. J Immunol *178*, 2623-2629.

Naccarato, A.G., Viacava, P., Vignati, S., Fanelli, G., Bonadio, A.G., Montruccoli, G., and Bevilacqua, G. (2000). Bio-morphological events in the development of the human female mammary gland from fetal age to puberty. Virchows Arch *436*, 431-438.
Nakashima, Y., and Omasa, T. (2016). What Kind of Signaling Maintains Pluripotency and Viability in Human-Induced Pluripotent Stem Cells Cultured on Laminin-511 with Serum-Free Medium? Biores Open Access *5*, 84-93.
Nath, S., and Mukherjee, P. (2014). MUC1: a multifaceted oncoprotein with a key role in cancer progression. Trends Mol Med *20*, 332-342.
Newman, E.A., Wu, D., Taketo, M.M., Zhang, J., and Blackshaw, S. (2018). Canonical Wnt signaling regulates patterning, differentiation and nucleogenesis in mouse hypothalamus and prethalamus. Dev Biol *442*, 236-248.
Nwajei, F., and Konopleva, M. (2013). The bone marrow microenvironment as niche retreats for hematopoietic and leukemic stem cells. Adv Hematol *2013*, 953982.
O'Shaughnessy, J. (2005). Extending survival with chemotherapy in metastatic breast cancer. Oncologist *10 Suppl 3*, 20-29.
Oh, I.H., and Kwon, K.R. (2010). Concise review: multiple niches for hematopoietic stem cell regulations. Stem Cells *28*, 1243-1249.
Osisami, M., and Keller, E.T. (2013). Mechanisms of Metastatic Tumor Dormancy. J Clin Med *2*, 136-150.
Osta, W.A., Chen, Y., Mikhitarian, K., Mitas, M., Salem, M., Hannun, Y.A., Cole, D.J., and Gillanders, W.E. (2004). EpCAM is overexpressed in breast cancer and is a potential target for breast cancer gene therapy. Cancer Res *64*, 5818-5824.
Paez, D., Labonte, M.J., Bohanes, P., Zhang, W., Benhanim, L., Ning, Y., Wakatsuki, T., Loupakis, F., and Lenz, H.J. (2012). Cancer dormancy: a model of early dissemination and late cancer recurrence. Clin Cancer Res *18*, 645-653.
Paget, S. (1989). The distribution of secondary growths in cancer of the breast. 1889. Cancer Metastasis Rev *8*, 98-101.
Paine, I.S., and Lewis, M.T. (2017). The Terminal End Bud: the Little Engine that Could. J Mammary Gland Biol Neoplasia *22*, 93-108.
Pannellini, T., Forni, G., and Musiani, P. (2004). Immunobiology of her-2/neu transgenic mice. Breast Dis *20*, 33-42.
Pasic, L., Eisinger-Mathason, T.S., Velayudhan, B.T., Moskaluk, C.A., Brenin, D.R., Macara, I.G., and Lannigan, D.A. (2011). Sustained activation of the HER1-ERK1/2-RSK signaling pathway controls myoepithelial cell fate in human mammary tissue. Genes Dev *25*, 1641-1653.
Pece, S., Tosoni, D., Confalonieri, S., Mazzarol, G., Vecchi, M., Ronzoni, S., Bernard, L., Viale, G., Pelicci, P.G., and Di Fiore, P.P. (2010). Biological and molecular heterogeneity of breast cancers correlates with their cancer stem cell content. Cell *140*, 62-73.
Peters, M., Blinn, G., Solem, F., Fischer, M., Meyer zum Buschenfelde, K.H., and Rose-John, S. (1998). In vivo and in vitro activities of the gp130-stimulating designer cytokine Hyper-IL-6. J Immunol *161*, 3575-3581.
Pollina, E.A., and Brunet, A. (2011). Epigenetic regulation of aging stem cells. Oncogene *30*, 3105-3126.
Ponti, D., Costa, A., Zaffaroni, N., Pratesi, G., Petrangolini, G., Coradini, D., Pilotti, S., Pierotti, M.A., and Daidone, M.G. (2005). Isolation and in vitro propagation of tumorigenic breast cancer cells with stem/progenitor cell properties. Cancer Res *65*, 5506-5511.
Prakash, N., and Wurst, W. (2007). A Wnt signal regulates stem cell fate and differentiation in vivo. Neurodegener Dis *4*, 333-338.
Price, T.T., Burness, M.L., Sivan, A., Warner, M.J., Cheng, R., Lee, C.H., Olivere, L., Comatas, K., Magnani, J., Kim Lyerly, H.*, et al.* (2016). Dormant breast cancer micrometastases reside in specific bone marrow niches that regulate their transit to and from bone. Sci Transl Med *8*, 340ra373.
Qian, T., Liu, Y., Dong, Y., Zhang, L., Dong, Y., Sun, Y., and Sun, D. (2018). CXCR7 regulates breast tumor metastasis and angiogenesis in vivo and in vitro. Mol Med Rep *17*, 3633-3639.
Quesnel, B. (2008). Tumor dormancy and immunoescape. APMIS *116*, 685-694.
Rakha, E.A., Reis-Filho, J.S., Baehner, F., Dabbs, D.J., Decker, T., Eusebi, V., Fox, S.B., Ichihara, S., Jacquemier, J., Lakhani, S.R.*, et al.* (2010). Breast cancer prognostic classification in the molecular era: the role of histological grade. Breast Cancer Res *12*, 207.
Ranganathan, A.C., Adam, A.P., Zhang, L., and Aguirre-Ghiso, J.A. (2006). Tumor cell dormancy induced by p38SAPK and ER-stress signaling: an adaptive advantage for metastatic cells? Cancer Biol Ther *5*, 729-735.
Rappa, G., Mercapide, J., Anzanello, F., Prasmickaite, L., Xi, Y., Ju, J., Fodstad, O., and Lorico, A. (2008). Growth of cancer cell lines under stem cell-like conditions has the potential to unveil therapeutic targets. Exp Cell Res *314*, 2110-2122.
Rea, D., Coppola, G., Palma, G., Barbieri, A., Luciano, A., Del Prete, P., Rossetti, S., Berretta, M., Facchini, G., Perdona, S.*, et al.* (2018). Microbiota effects on cancer: from risks to therapies. Oncotarget *9*, 17915-17927.
Redig, A.J., and McAllister, S.S. (2013). Breast cancer as a systemic disease: a view of metastasis. J Intern Med *274*, 113-126.
Reichert, M., Bakir, B., Moreira, L., Pitarresi, J.R., Feldmann, K., Simon, L., Suzuki, K., Maddipati, R., Rhim, A.D., Schlitter, A.M.*, et al.* (2018). Regulation of Epithelial Plasticity Determines Metastatic Organotropism in Pancreatic Cancer. Dev Cell *45*, 696-711 e698.
Reyal, F., Hamy, A.S., and Piccart, M.J. (2018). Neoadjuvant treatment: the future of patients with breast cancer. ESMO Open *3*, e000371.
Reymond, N., d'Agua, B.B., and Ridley, A.J. (2013). Crossing the endothelial barrier during metastasis. Nat Rev Cancer *13*, 858-870.
Riethmueller, S., Ehlers, J.C., Lokau, J., Dusterhoft, S., Knittler, K., Dombrowsky, G., Grotzinger, J., Rabe, B., Rose-John, S., and Garbers, C. (2016). Cleavage Site Localization Differentially Controls Interleukin-6 Receptor Proteolysis by ADAM10 and ADAM17. Sci Rep *6*, 25550.
Rodrigues, C.F.D., Serrano, E., Patricio, M.I., Val, M.M., Albuquerque, P., Fonseca, J., Gomes, C.M.F., Abrunhosa, A.J., Paiva, A., Carvalho, L.*, et al.* (2018). Stroma-derived IL-6, G-CSF and Activin-A mediated dedifferentiation of lung carcinoma cells into cancer stem cells. Sci Rep *8*, 11573.

Roland, N., Porter, G., Fish, B., and Makura, Z. (2016). Tumour assessment and staging: United Kingdom National Multidisciplinary Guidelines. J Laryngol Otol *130*, S53-S58.
Romorini, L., Garate, X., Neiman, G., Luzzani, C., Furmento, V.A., Guberman, A.S., Sevlever, G.E., Scassa, M.E., and Miriuka, S.G. (2016). AKT/GSK3beta signaling pathway is critically involved in human pluripotent stem cell survival. Sci Rep *6*, 35660.
Rose-John, S., and Heinrich, P.C. (1994). Soluble receptors for cytokines and growth factors: generation and biological function. Biochem J *300 (Pt 2)*, 281-290.
Russo, J., and Russo, I.H. (2004). Development of the human breast. Maturitas *49*, 2-15.
Rybak, A.P., He, L., Kapoor, A., Cutz, J.C., and Tang, D. (2011). Characterization of sphere-propagating cells with stem-like properties from DU145 prostate cancer cells. Biochim Biophys Acta *1813*, 683-694.
Sakakura, T., Nishizuka, Y., and Dawe, C.J. (1976). Mesenchyme-dependent morphogenesis and epithelium-specific cytodifferentiation in mouse mammary gland. Science *194*, 1439-1441.
Sansone, P., Storci, G., Tavolari, S., Guarnieri, T., Giovannini, C., Taffurelli, M., Ceccarelli, C., Santini, D., Paterini, P., Marcu, K.B.*, et al.* (2007). IL-6 triggers malignant features in mammospheres from human ductal breast carcinoma and normal mammary gland. J Clin Invest *117*, 3988-4002.
Schabath, H., Runz, S., Joumaa, S., and Altevogt, P. (2006). CD24 affects CXCR4 function in pre-B lymphocytes and breast carcinoma cells. J Cell Sci *119*, 314-325.
Schaper, F., and Rose-John, S. (2015). Interleukin-6: Biology, signaling and strategies of blockade. Cytokine Growth Factor Rev *26*, 475-487.
Schardt, J.A., Meyer, M., Hartmann, C.H., Schubert, F., Schmidt-Kittler, O., Fuhrmann, C., Polzer, B., Petronio, M., Eils, R., and Klein, C.A. (2005). Genomic analysis of single cytokeratin-positive cells from bone marrow reveals early mutational events in breast cancer. Cancer Cell *8*, 227-239.
Scheller, J., Chalaris, A., Schmidt-Arras, D., and Rose-John, S. (2011). The pro- and anti-inflammatory properties of the cytokine interleukin-6. Biochim Biophys Acta *1813*, 878-888.
Scheller, J., Garbers, C., and Rose-John, S. (2014). Interleukin-6: from basic biology to selective blockade of pro-inflammatory activities. Semin Immunol *26*, 2-12.
Scheller, J., Ohnesorge, N., and Rose-John, S. (2006). Interleukin-6 trans-signalling in chronic inflammation and cancer. Scand J Immunol *63*, 321-329.
Scheller, J., Schuster, B., Holscher, C., Yoshimoto, T., and Rose-John, S. (2005). No inhibition of IL-27 signaling by soluble gp130. Biochem Biophys Res Commun *326*, 724-728.
Schewe, D.M., and Aguirre-Ghiso, J.A. (2008). ATF6alpha-Rheb-mTOR signaling promotes survival of dormant tumor cells in vivo. Proc Natl Acad Sci U S A *105*, 10519-10524.
Schmidt-Kittler, O., Ragg, T., Daskalakis, A., Granzow, M., Ahr, A., Blankenstein, T.J., Kaufmann, M., Diebold, J., Arnholdt, H., Muller, P.*, et al.* (2003). From latent disseminated cells to overt metastasis: genetic analysis of systemic breast cancer progression. Proc Natl Acad Sci U S A *100*, 7737-7742.
Scully, O.J., Bay, B.H., Yip, G., and Yu, Y. (2012). Breast cancer metastasis. Cancer Genomics Proteomics *9*, 311-320.
Seandel, M., Butler, J.M., Kobayashi, H., Hooper, A.T., White, I.A., Zhang, F., Vertes, E.L., Kobayashi, M., Zhang, Y., Shmelkov, S.V.*, et al.* (2008). Generation of a functional and durable vascular niche by the adenoviral E4ORF1 gene. Proc Natl Acad Sci U S A *105*, 19288-19293.
Shackleton, M., Vaillant, F., Simpson, K.J., Stingl, J., Smyth, G.K., Asselin-Labat, M.L., Wu, L., Lindeman, G.J., and Visvader, J.E. (2006). Generation of a functional mammary gland from a single stem cell. Nature *439*, 84-88.
Sheffield, L.G. (1988). Organization and growth of mammary epithelia in the mammary gland fat pad. J Dairy Sci *71*, 2855-2874.
Shehata, M., Teschendorff, A., Sharp, G., Novcic, N., Russell, I.A., Avril, S., Prater, M., Eirew, P., Caldas, C., Watson, C.J.*, et al.* (2012). Phenotypic and functional characterisation of the luminal cell hierarchy of the mammary gland. Breast Cancer Res *14*, R134.
Shiozawa, Y., Berry, J.E., Eber, M.R., Jung, Y., Yumoto, K., Cackowski, F.C., Yoon, H.J., Parsana, P., Mehra, R., Wang, J.*, et al.* (2016). The marrow niche controls the cancer stem cell phenotype of disseminated prostate cancer. Oncotarget *7*, 41217-41232.
Shiozawa, Y., Pedersen, E.A., Havens, A.M., Jung, Y., Mishra, A., Joseph, J., Kim, J.K., Patel, L.R., Ying, C., Ziegler, A.M.*, et al.* (2011). Human prostate cancer metastases target the hematopoietic stem cell niche to establish footholds in mouse bone marrow. J Clin Invest *121*, 1298-1312.
Shiozawa, Y., Pedersen, E.A., Patel, L.R., Ziegler, A.M., Havens, A.M., Jung, Y., Wang, J., Zalucha, S., Loberg, R.D., Pienta, K.J.*, et al.* (2010). GAS6/AXL axis regulates prostate cancer invasion, proliferation, and survival in the bone marrow niche. Neoplasia *12*, 116-127.
Smith, G.H., Sharp, R., Kordon, E.C., Jhappan, C., and Merlino, G. (1995). Transforming growth factor-alpha promotes mammary tumorigenesis through selective survival and growth of secretory epithelial cells. Am J Pathol *147*, 1081-1096.
Sokol, S.Y. (2011). Maintaining embryonic stem cell pluripotency with Wnt signaling. Development *138*, 4341-4350.
Sorlie, T., Perou, C.M., Tibshirani, R., Aas, T., Geisler, S., Johnsen, H., Hastie, T., Eisen, M.B., van de Rijn, M., Jeffrey, S.S.*, et al.* (2001). Gene expression patterns of breast carcinomas distinguish tumor subclasses with clinical implications. Proc Natl Acad Sci U S A *98*, 10869-10874.
Sotiriou, C., Neo, S.Y., McShane, L.M., Korn, E.L., Long, P.M., Jazaeri, A., Martiat, P., Fox, S.B., Harris, A.L., and Liu, E.T. (2003). Breast cancer classification and prognosis based on gene expression profiles from a population-based study. Proc Natl Acad Sci U S A *100*, 10393-10398.
Spike, B.T., Engle, D.D., Lin, J.C., Cheung, S.K., La, J., and Wahl, G.M. (2012). A mammary stem cell population identified and characterized in late embryogenesis reveals similarities to human breast cancer. Cell Stem Cell *10*, 183-197.

Spizzo, G., Went, P., Dirnhofer, S., Obrist, P., Simon, R., Spichtin, H., Maurer, R., Metzger, U., von Castelberg, B., Bart, R., *et al.* (2004). High Ep-CAM expression is associated with poor prognosis in node-positive breast cancer. Breast Cancer Res Treat *86*, 207-213.
Stingl, J., Eaves, C.J., Zandieh, I., and Emerman, J.T. (2001). Characterization of bipotent mammary epithelial progenitor cells in normal adult human breast tissue. Breast Cancer Res Treat *67*, 93-109.
Stingl, J., Raouf, A., Eirew, P., and Eaves, C.J. (2006). Deciphering the mammary epithelial cell hierarchy. Cell Cycle *5*, 1519-1522.
Stoecklein, N.H., Siegmund, A., Scheunemann, P., Luebke, A.M., Erbersdobler, A., Verde, P.E., Eisenberger, C.F., Peiper, M., Rehders, A., Esch, J.S., *et al.* (2006). Ep-CAM expression in squamous cell carcinoma of the esophagus: a potential therapeutic target and prognostic marker. BMC Cancer *6*, 165.
Streetz, K.L., Tacke, F., Leifeld, L., Wustefeld, T., Graw, A., Klein, C., Kamino, K., Spengler, U., Kreipe, H., Kubicka, S., *et al.* (2003). Interleukin 6/gp130-dependent pathways are protective during chronic liver diseases. Hepatology *38*, 218-229.
Subramaniam, K.S., Omar, I.S., Kwong, S.C., Mohamed, Z., Woo, Y.L., Mat Adenan, N.A., and Chung, I. (2016). Cancer-associated fibroblasts promote endometrial cancer growth via activation of interleukin-6/STAT-3/c-Myc pathway. Am J Cancer Res *6*, 200-213.
Suzuki, A., Pelikan, R.C., and Iwata, J. (2015). WNT/beta-Catenin Signaling Regulates Multiple Steps of Myogenesis by Regulating Step-Specific Targets. Mol Cell Biol *35*, 1763-1776.
Taichman, R.S., Patel, L.R., Bedenis, R., Wang, J., Weidner, S., Schumann, T., Yumoto, K., Berry, J.E., Shiozawa, Y., and Pienta, K.J. (2013). GAS6 receptor status is associated with dormancy and bone metastatic tumor formation. PLoS One *8*, e61873.
Tamma, R., and Ribatti, D. (2017). Bone Niches, Hematopoietic Stem Cells, and Vessel Formation. Int J Mol Sci *18*.
Tanaka, T., and Kishimoto, T. (2014). The biology and medical implications of interleukin-6. Cancer Immunol Res *2*, 288-294.
Tanaka, T., Narazaki, M., and Kishimoto, T. (2014). IL-6 in inflammation, immunity, and disease. Cold Spring Harb Perspect Biol *6*, a016295.
Tang, H., Bai, Y., Shen, W., and Zhao, J. (2018). [Research progress on interleukin-6 in lung cancer]. Zhejiang Da Xue Xue Bao Yi Xue Ban *47*, 659-664.
Tanner, K., Mori, H., Mroue, R., Bruni-Cardoso, A., and Bissell, M.J. (2012). Coherent angular motion in the establishment of multicellular architecture of glandular tissues. Proc Natl Acad Sci U S A *109*, 1973-1978.
Thiel, S., Dahmen, H., Martens, A., Muller-Newen, G., Schaper, F., Heinrich, P.C., and Graeve, L. (1998). Constitutive internalization and association with adaptor protein-2 of the interleukin-6 signal transducer gp130. FEBS Lett *441*, 231-234.
Thobe, M.N., Clark, R.J., Bainer, R.O., Prasad, S.M., and Rinker-Schaeffer, C.W. (2011). From prostate to bone: key players in prostate cancer bone metastasis. Cancers (Basel) *3*, 478-493.
Tiede, B., and Kang, Y. (2011). From milk to malignancy: the role of mammary stem cells in development, pregnancy and breast cancer. Cell Res *21*, 245-257.
Timp, W., and Feinberg, A.P. (2013). Cancer as a dysregulated epigenome allowing cellular growth advantage at the expense of the host. Nat Rev Cancer *13*, 497-510.
Udagawa, N., Takahashi, N., Katagiri, T., Tamura, T., Wada, S., Findlay, D.M., Martin, T.J., Hirota, H., Taga, T., Kishimoto, T., *et al.* (1995). Interleukin (IL)-6 induction of osteoclast differentiation depends on IL-6 receptors expressed on osteoblastic cells but not on osteoclast progenitors. J Exp Med *182*, 1461-1468.
Valastyan, S., and Weinberg, R.A. (2011). Tumor metastasis: molecular insights and evolving paradigms. Cell *147*, 275-292.
Van Keymeulen, A., Fioramonti, M., Centonze, A., Bouvencourt, G., Achouri, Y., and Blanpain, C. (2017). Lineage-Restricted Mammary Stem Cells Sustain the Development, Homeostasis, and Regeneration of the Estrogen Receptor Positive Lineage. Cell Rep *20*, 1525-1532.
Vesely, M.D., Kershaw, M.H., Schreiber, R.D., and Smyth, M.J. (2011). Natural innate and adaptive immunity to cancer. Annu Rev Immunol *29*, 235-271.
Visvader, J.E., and Stingl, J. (2014). Mammary stem cells and the differentiation hierarchy: current status and perspectives. Genes Dev *28*, 1143-1158.
Wang, C.Q., Sun, H.T., Gao, X.M., Ren, N., Sheng, Y.Y., Wang, Z., Zheng, Y., Wei, J.W., Zhang, K.L., Yu, X.X., *et al.* (2016). Interleukin-6 enhances cancer stemness and promotes metastasis of hepatocellular carcinoma via up-regulating osteopontin expression. Am J Cancer Res *6*, 1873-1889.
Wang, H., Yu, C., Gao, X., Welte, T., Muscarella, A.M., Tian, L., Zhao, H., Zhao, Z., Du, S., Tao, J., *et al.* (2015a). The osteogenic niche promotes early-stage bone colonization of disseminated breast cancer cells. Cancer Cell *27*, 193-210.
Wang, H., Zhang, C., Zhang, J., Kong, L., Zhu, H., and Yu, J. (2017). The prognosis analysis of different metastasis pattern in patients with different breast cancer subtypes: a SEER based study. Oncotarget *8*, 26368-26379.
Wang, N., Docherty, F.E., Brown, H.K., Reeves, K.J., Fowles, A.C., Ottewell, P.D., Dear, T.N., Holen, I., Croucher, P.I., and Eaton, C.L. (2014). Prostate cancer cells preferentially home to osteoblast-rich areas in the early stages of bone metastasis: evidence from in vivo models. J Bone Miner Res *29*, 2688-2696.
Wang, W., Yu, S., Zimmerman, G., Wang, Y., Myers, J., Yu, V.W., Huang, D., Huang, X., Shim, J., Huang, Y., *et al.* (2015b). Notch Receptor-Ligand Engagement Maintains Hematopoietic Stem Cell Quiescence and Niche Retention. Stem Cells *33*, 2280-2293.
Watson, C.J., and Khaled, W.T. (2008). Mammary development in the embryo and adult: a journey of morphogenesis and commitment. Development *135*, 995-1003.
Wegiel, B., Bjartell, A., Culig, Z., and Persson, J.L. (2008). Interleukin-6 activates PI3K/Akt pathway and regulates cyclin A1 to promote prostate cancer cell survival. Int J Cancer *122*, 1521-1529.

Wei, W., Jobling, W.A., Chen, W., Hahn, W.C., and Sedivy, J.M. (2003). Abolition of cyclin-dependent kinase inhibitor p16Ink4a and p21Cip1/Waf1 functions permits Ras-induced anchorage-independent growth in telomerase-immortalized human fibroblasts. Mol Cell Biol *23*, 2859-2870.
Weigelt, B., Peterse, J.L., and van 't Veer, L.J. (2005). Breast cancer metastasis: markers and models. Nat Rev Cancer *5*, 591-602.
Weiss, L. (1990). Metastatic inefficiency. Adv Cancer Res *54*, 159-211.
Weiss, L. (1992). Comments on hematogenous metastatic patterns in humans as revealed by autopsy. Clin Exp Metastasis *10*, 191-199.
Went, P., Vasei, M., Bubendorf, L., Terracciano, L., Tornillo, L., Riede, U., Kononen, J., Simon, R., Sauter, G., and Baeuerle, P.A. (2006). Frequent high-level expression of the immunotherapeutic target Ep-CAM in colon, stomach, prostate and lung cancers. Br J Cancer *94*, 128-135.
Werner-Klein, M., Scheitler, S., Hoffmann, M., Hodak, I., Dietz, K., Lehnert, P., Naimer, V., Polzer, B., Treitschke, S., Werno, C.*, et al.* (2018). Genetic alterations driving metastatic colony formation are acquired outside of the primary tumour in melanoma. Nat Commun *9*, 595.
Wiedswang, G., Borgen, E., Karesen, R., Kvalheim, G., Nesland, J.M., Qvist, H., Schlichting, E., Sauer, T., Janbu, J., Harbitz, T.*, et al.* (2003). Detection of isolated tumor cells in bone marrow is an independent prognostic factor in breast cancer. J Clin Oncol *21*, 3469-3478.
Williams, J.M., and Daniel, C.W. (1983). Mammary ductal elongation: differentiation of myoepithelium and basal lamina during branching morphogenesis. Dev Biol *97*, 274-290.
Woo, S.M., Kim, J., Han, H.W., Chae, J.I., Son, M.Y., Cho, S., Chung, H.M., Han, Y.M., and Kang, Y.K. (2009). Notch signaling is required for maintaining stem-cell features of neuroprogenitor cells derived from human embryonic stem cells. BMC Neurosci *10*, 97.
Wu, A., Dong, Q., Gao, H., Shi, Y., Chen, Y., Zhang, F., Bandyopadhyay, A., Wang, D., Gorena, K.M., Huang, C.*, et al.* (2016). Characterization of mammary epithelial stem/progenitor cells and their changes with aging in common marmosets. Sci Rep *6*, 32190.
Xu, S., and Neamati, N. (2013). gp130: a promising drug target for cancer therapy. Expert Opin Ther Targets *17*, 1303-1328.
Xu, Z., Robitaille, A.M., Berndt, J.D., Davidson, K.C., Fischer, K.A., Mathieu, J., Potter, J.C., Ruohola-Baker, H., and Moon, R.T. (2016). Wnt/beta-catenin signaling promotes self-renewal and inhibits the primed state transition in naive human embryonic stem cells. Proc Natl Acad Sci U S A *113*, E6382-E6390.
Yang, R., Masters, A.R., Fortner, K.A., Champagne, D.P., Yanguas-Casas, N., Silberger, D.J., Weaver, C.T., Haynes, L., and Rincon, M. (2016). IL-6 promotes the differentiation of a subset of naive CD8+ T cells into IL-21-producing B helper CD8+ T cells. J Exp Med *213*, 2281-2291.
Yin, T., and Li, L. (2006). The stem cell niches in bone. J Clin Invest *116*, 1195-1201.
Yoo, M.H., and Hatfield, D.L. (2008). The cancer stem cell theory: is it correct? Mol Cells *26*, 514-516.
Yook, J.Y., Kim, M.J., Son, M.J., Lee, S., Nam, Y., Han, Y.M., and Cho, Y.S. (2011). Combinatorial activin receptor-like kinase/Smad and basic fibroblast growth factor signals stimulate the differentiation of human embryonic stem cells into the cardiac lineage. Stem Cells Dev *20*, 1479-1490.
Yu, X., Zou, J., Ye, Z., Hammond, H., Chen, G., Tokunaga, A., Mali, P., Li, Y.M., Civin, C., Gaiano, N.*, et al.* (2008). Notch signaling activation in human embryonic stem cells is required for embryonic, but not trophoblastic, lineage commitment. Cell Stem Cell *2*, 461-471.
Yu, Z., Pestell, T.G., Lisanti, M.P., and Pestell, R.G. (2012). Cancer stem cells. Int J Biochem Cell Biol *44*, 2144-2151.
Zeng, Y.A., and Nusse, R. (2010). Wnt proteins are self-renewal factors for mammary stem cells and promote their long-term expansion in culture. Cell Stem Cell *6*, 568-577.
Zubeldia-Plazaola, A., Ametller, E., Mancino, M., Prats de Puig, M., Lopez-Plana, A., Guzman, F., Vinyals, L., Pastor-Arroyo, E.M., Almendro, V., Fuster, G.*, et al.* (2015). Comparison of methods for the isolation of human breast epithelial and myoepithelial cells. Front Cell Dev Biol *3*, 32.

7 Acknowledgement

Although at the end on every PhD project stands only one name, it can never be done by only one person. One finished PhD project is a success of the whole team. Everything is much easier with a good team. And I was one of lucky PhD candidates that had great people around me, which supported me on every step of my work.

Firstly I want to express my sincere gratitude to my advisor Prof. Dr. Christoph A. Klein for the possibility to work and study interesting and attractive topics, for the freedom and support he was continuously giving me in my work, and for his optimism in moments when this point where I am now looked so unreachable. His guidance helped me in all the time of research and writing of this thesis.

I am grateful to Prof. Dr. Frank Sprenger and Prof. Dr. Eugen Kerkhoff for their mentorship and advices during work.

I am grateful to Dr. Miodrag Gužvić, Dr. Courtney König, Dr. Elisabeth Schneider and Dr. Rezan Fahrioglu-Yamaci for useful comments, advices and discussions during work on my PhD thesis.

Every PhD student faces many problems on the beginning due to the lack of knowledge and related methodology. This period of learning is much easier with the help of more experienced colleagues. Therefore I owe endless gratitude to Dr. Hedayatollah Hosseini and Dr. Miodrag Guzvić for their help and advices that introduced me to the world of science.

Dr. Melanie Werner-Klein was great support and guide during the work on IL-6 project. She was an inexhaustible source of good advices and help with any problem I faced.

All technical assistants were always ready to help me and I learned a lot form them. Therefore I must mention Tom, Mani, Isa, Sandra Grunewald, Irene, Marietta, Theresa, Anthea and many others that were there in last years. Especially I want to thank Regina Heindl, Sandra Klaczek and Christian Reimelt, without them all the *in vivo* experiments could be hardly done.

I am grateful to all former and current members of AG Klein for provided help, useful comments and advices, support and positive atmosphere. Therefore, I want to thank to Nina, Mio, Heda, Christoph Irlbeck, Elisabeth, Rezan, Julia, Manjusha, Toby, and many others.

Franziska Durst was wonderful partner in the qPCR-project. She motivated me to continue when it was very difficult. She is a great example of a hard worker that I always have before my eyes.

I am happy to say that during this time I did not only acquire the knowledge about the topic of my research, but I also met great people that found the way to my heart and became very important to me. Besides mentioned Rezan, Elisabeth, Tom and others, special place in my heart found Verena, Basti

and Lini Lieb, and also Aleksandra Markiewitz. You all enriched my life and I am so happy for having you.

And the most important, I want to thank my family for the endless love and support.

Finally I want to dedicate this work and success to Milan, who never stop believing in me and encouraging me to keep going. Often he was caring for me more than I did for myself, and he did everything he could to make this journey easier to me. I am sure that I could not have come this far without your love, help, understanding and support.